SCUOLA
NORMALE
SUPERIORE

Classe di Scienze
PhD Thesis

The aging synapse: an integrated proteomic and transcriptomic analysis.

Candidate:
Cinzia Caterino

Supervisor:
Prof. Alessandro Cellerino

Academic Year 2018/19

Graphical abstract

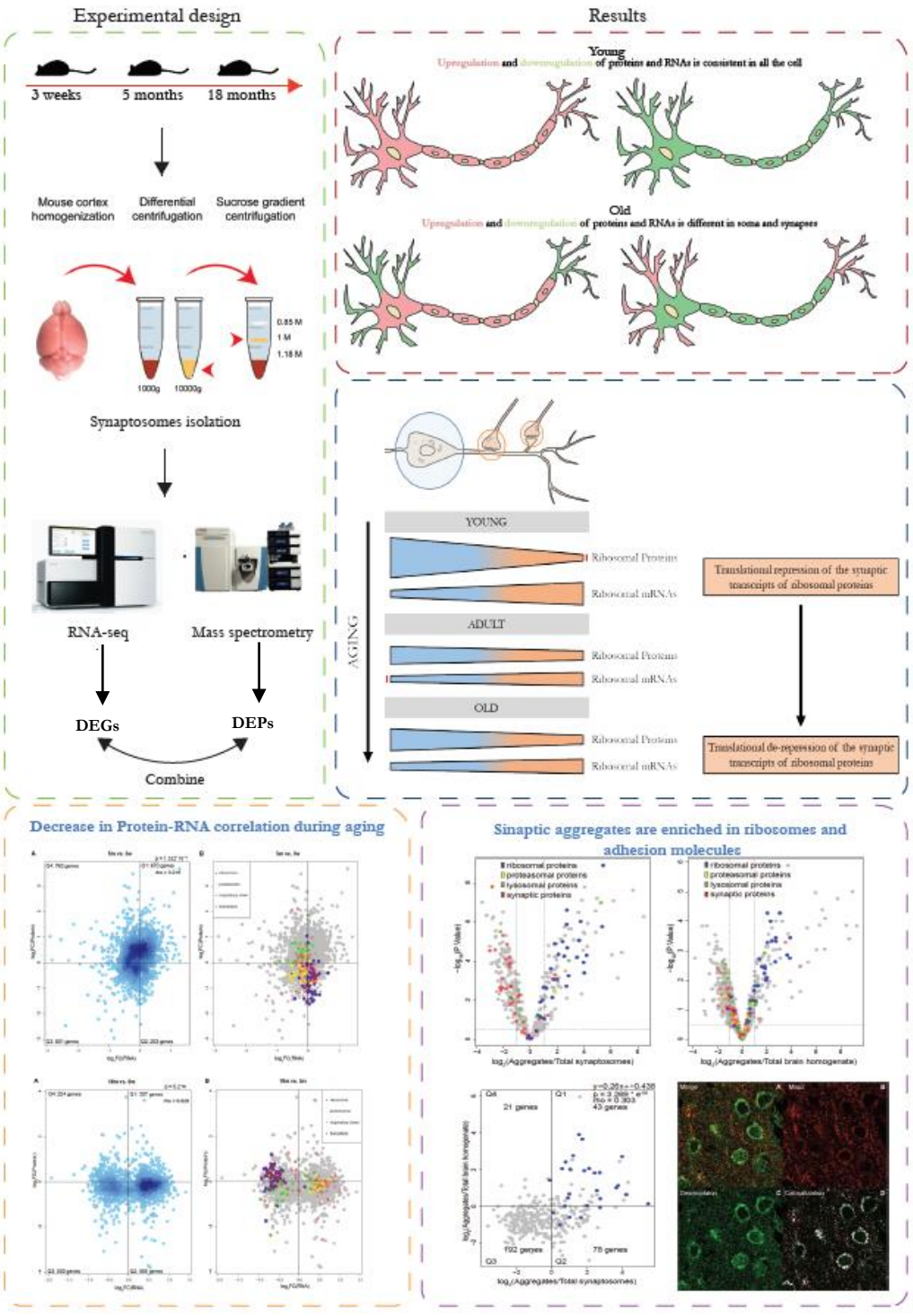

Abstract

An important hallmark of aging is the loss of proteostasis, which can lead to the formation of protein aggregates and mitochondrial dysfunction in neurons. Although it is well known that protein synthesis is finely regulated in the brain, especially at synapses, where mRNAs are locally translated in activity-dependent manner, little is known as to the changes in the synaptic proteome and transcriptome during aging. Therefore, this work aims to elucidate the relationship between transcriptome and proteome at soma and synaptic level during aging.

Cerebral cortices were isolated from 3 weeks-old mice, 5 months-old and 18 months-old mice and synaptosomal fraction was extracted by ultracentrifugation on discontinuous sucrose gradient. The fraction was then analyzed by Data Independent Analysis (DIA) Mass Spectrometry and the resulting data were analyzed using Spectronaut software. RNA was also extracted and analyzed by ribo-zero RNA-seq. Data were analyzed and combined with R software.

Proteomic and transcriptomic data analysis revealed that, in young animals, proteins and transcripts are correlated and synaptic regulation is driven by changes in the soma. During aging, there is a decoupling between transcripts and proteins and between somatic and synaptic compartments. For example, there is an increase of ribosomal proteins at synapses that is not mirrored by a concomitant increase at somatic level. Furthermore, soma-synapse gradient of ribosomal genes changes upon aging, i.e. ribosomal transcripts are less abundant and ribosomal proteins are more abundant in synaptic compartment of old mice with respect to younglings.

Mass spectrometry analysis of synaptic protein aggregates revealed that they are particularly rich in ribosomal proteins and also of some components of lysosomes and proteasome, suggesting that loss of proteostasis and inefficient degradation leads to aggregation of ribosomes in synaptic compartment. Strikingly, Desmoplakin, a structural constituent of desmosomes, was also highly abundant in synaptic aggregates. This study suggests that aging affects both the local translational machinery and the trafficking of transcripts and proteins.

Introduction

1. Synapses and synaptogenesis

Contact between neurons is established through structures called synapses. In general, there are two main types of synapses: electrical and chemical. Electrical synapses (neuronal gap junctions) function by the propagation of electrical impulses from one cell to another (and vice versa) via direct, physical contact. As a consequence, these synapses are characterized by a relatively simple organization of membrane structure and associated organelles and by a relatively lower plasticity(Zoidl & Dermietzel, 2002).

Chemical synapses convert electrical signals into chemical signals, which are then transmitted to the receiving neuronal partner and further converted again into electrical signals (Poggio & Koch, 1987). Therefore, chemical synapses use a broad range of neurotransmitters and neuropeptides for intercellular communication, in addition to a localized signal transduction machinery (Oswald Steward & Schuman, 2003). Cell–to-cell communication that occurs by chemical transmission is characterized by complex protein-driven molecular mechanisms of synthesis, delivery, storage, docking, fusion, neurotransmitter release and reuptake (Purves, 2004). In general, synapses are composed of three main constituents: a presynaptic component (presynaptic ending, axon terminal), a synaptic cleft, and a postsynaptic component (dendritic spines in excitatory neurons and dendrite shafts, cell bodies or axon initial segments in inhibitory neurons). The pre- and the postsynaptic membranes are uniquely distinguishable by visible densities along their corresponding plasma membranes. Together with the synaptic cleft, they are collectively referred to as the synapse (**Fig.1**). These elements are always wrapped by astrocytic processes that have important roles in key aspects of brain development and function, such as neuronal metabolism, synaptogenesis, homeostasis of the extracellular milieu, or cerebral microcirculation (Kettenmann & Ransom, 2013). Furthermore, it has recently been reported that astrocytes are able to discriminate the type of synapse they are in contact with, and influence synaptic transmission by means of Ca^{2+} currents. Therefore, we refer to this structure as to the "tripartite" synapse (Perea, Navarrete, & Araque, 2009). Typically, the presynaptic ending is characterized by the conspicuous presence of neurotransmitter-filled vesicles.

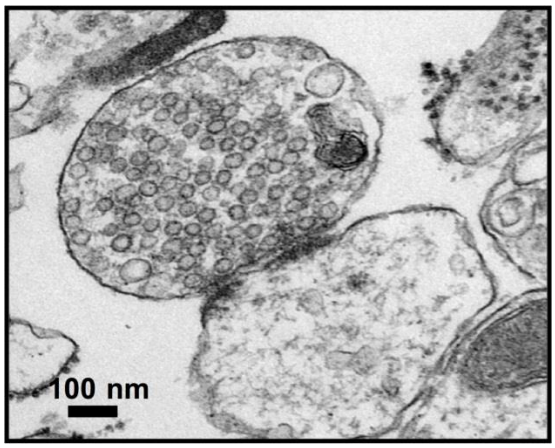

Figure 1. The image shows an isolated synapse from a brain sample before mass spectrometry analyses. The pre-synapse typically shows many vesicles containing neurotransmitters kept attached to the post-synapse (Z. Taoufiq, 2013).

Synapses in the brain are generally divided in two categories, depending from the densification of their presynaptic and postsynaptic elements (Gray, 1959). According to this characterization, type 1 synapses have an asymmetrical densification of the pre- and postsynaptic elements, are usually associated to small, round, clear synaptic vesicles and are mainly implicated in excitatory actions. On the other hand, type 2 synapses have a symmetrical densification of the two terminals, are associated with small, clear, flattened or pleiomorphic vesicles, and are mostly involved in inhibitory actions (**Fig.2**).

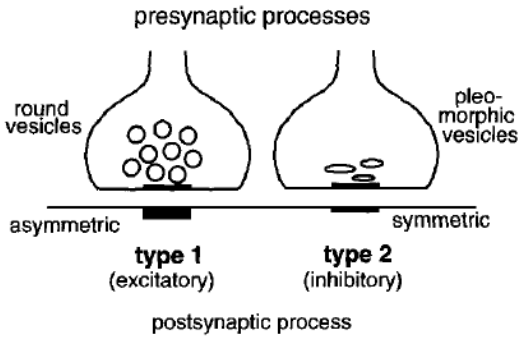

Figure 2. Classification of the chemical synapses in the brain. Type 1 synapses are mostly excitatory and show an asymmetry of the density of the terminals. Type 2 synapses are symmetrical and mostly inhibitory. Picture adapted from Shepherd, 2004.

In response to presynaptic membrane depolarization, neurotransmitters are released into the cleft following a rapid influx of Ca^{2+} ions in the presynaptic terminal. In particular, Ca^{2+} binds to

synaptotagmin which can then interact with the preassembled SNARE complex on the neurotransmitter vescicles. This interaction displaces complexin from the SNARE complex, bends the phospholipids, and opens the fusion pore (Tang et al., 2006). Neurotransmitter molecules bind their receptors on the postsynaptic membrane, leading to opening of ion channels that can result is either depolarization (excitation) or hyperpolarization (inhibition) of the postsynaptic terminal. The presynaptic terminal (bouton) also contains other organelles such as mitochondria, smooth endoplasmic reticulum, microtubules, and neurofilaments. The presynaptic membrane is variably populated by docking/fusion apparatus, ion channels, and other protein constituents. A 20–30 nM wide synaptic cleft separates the pre- and postsynaptic membranes and generally contains a dense plaque of intercellular material that includes microfilaments (Bai & Witzmann, 2007).

The postsynaptic membrane in excitatory synapses (type 1 synapses), is recognizable by a collection of dense material visible by electron microscopy on its cytoplasmic surface, the post-synaptic density (PSD) (Gray, 1959; Palay, 1956). This area is a specialization of the postsynaptic submembrane cytoskeleton, it is composed of granular/filamentous material, contains cisternae of smooth endoplasmic reticulum, and its existence seems to be dependent on the presence of the presynaptic ending. A subcellular fraction enriched in structures with PSD-like morphology has been shown to contain signal-transduction molecules thought to regulate receptor localization and function in the CNS (Kennedy, 2000). In particular, PSD of excitatory synapses is enriched in cytoskeletal proteins (actin, tubulin, fodrin and neurofilament proteins), signaling molecules, such as calcium-calmodulin-dependent protein kinase II (CaMKII), membrane receptors, such as NMDA and AMPA receptors, and the quaternary complex of Homer, Shank, GKAP and PSD-95, which are able to link the NMDA receptor complex and group I metabotropic glutamate receptors (mGluRs) (Okabe, 2007). Synaptic proteins are distributed as indicated in **Fig.3**.

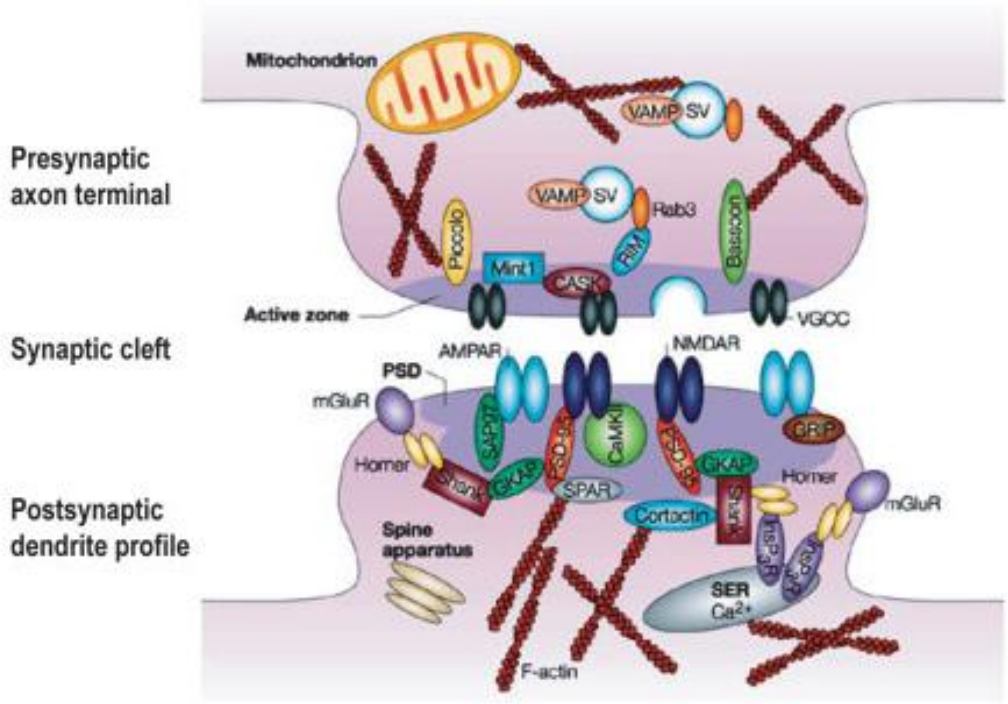

Figure 3. Distribution of synaptic proteins in an excitatory synapse. Picture adapted from Chiu & Cline (2010)

In mammals, synaptogenesis starts in the embryo and proceeds after birth, with rapid and specific changes of synapse numbers, synapse morphology and protein expression that can proceed throughout life (Meredith, 2015; Rice & Barone, 2000). In particular, synapse numbers in rodents rapidly increase in the first three weeks after birth (Rice & Barone, 2000), and the typical synaptic structure with normal sized synaptic vesicles and postsynaptic thickening can be observed at the end of the first postnatal week (Li, 2010). Synaptogenesis consists of biochemical and morphological changes in both the pre- and postsynaptic elements. Physiochemical compatibility of these elements and correct timing with competitive exclusion of inappropriate connections are essential for the formation of a specific network of connections (Jacobson & Jacobson, 1991). These developmental changes allow neurons to establish connections with appropriate partners, to prune the initial wiring of extensive synaptic connections into a more refined and restricted number of relatively stable synaptic contacts, and to tune the functional properties of synapses to prepare them for adult function and plasticity (Margeta & Shen, 2010). During synaptogenesis, target recognition cues, such as cadherins and integrins, guide the migrating neurons to specific layers of the cerebral cortex (Graus-Porta et al., 2001). To establish contact with its synaptic partner, the growing dendritic process follows then a variety of diffusible chemotropic factors (that can be attractive or repulsive) in its extracellular milieu (McAllister, 2002). On the other end, the postsynaptic neuron is not a passive receptor of the connection, but actively participates to the target recognition through its filopodia (Nimchinsky, Sabatini, & Svoboda, 2002). Upon synapse formation, NMDA receptor is recruited to

the nascent excitatory synapse (Barrow, 2009). Subsequent AMPA receptor recruitment makes the synapse functional and allows rapid synaptic transmission (Hall & Ghosh, 2008). It is generally accepted that in addition to these examples the synaptic proteome undergoes extensive developmental changes that underlie the progression of synaptogenesis and synapse maturation (Moczulska et al., 2014). On the other hand, dysregulated synaptic protein expression and disruption of timely interactions of proteins during development have been linked to impaired synaptic function in several disorders, such as autism, schizophrenia and several forms of mental retardation (Grant, 2012). Recently it has been shown that, receptors involved in the chemotropic response to recognition cues are tightly coupled to ribosomes and their activation triggers local translation in retinal ganglion cells. In particular, this coupling is achieved through RNA binding proteins (RBPs) which link mRNAs and ribosomes to these receptors. The RBPs that act as linkers are specific for each receptor (Koppers et al., 2019).

2. Synaptic plasticity and activity-dependent translation

It is important to recognize that the nervous system continues to remodel and change not just early in development but throughout the entire period of development (and even during adulthood) in response to environmental influences as well as genetically programmed events. This phenomenon is termed synaptic plasticity. As already mentioned in §1, the influx of Ca^{2+} triggered by presynaptic membrane depolarization, leads to the exocytosis of neurotransmitter-loaded synaptic vesicles. Since the number of vesicles docked to the presynaptic terminal is variable, there is a certain probability P that a given vesicle is released into the synaptic cleft (Korn & Faber, 1991). If P is high, the synapse will therefore exhibit depression, because the first action potential will exhaust the pool of available vesicles and the subsequent action potentials will evoke smaller effects. On the contrary, when P is small, the synapse may exhibit facilitation, because the first action potential will only cause a small number of vesicles to be released and, if the inter-stimulus interval is small enough, spikes in a train will trigger larger effects due to accumulation of synaptic Ca^{2+}(Thomson, 2000). Multiple forms of synaptic plasticity, such as Long-Term Potentiation (LTP) and Long-Term Depression (LTD) were observed in neocortex *in vivo* (Tsumoto & Suda, 1979). Interestingly, identical stimuli can trigger LTP or LTD and both mechanisms have been reported to be dependent on NMDA receptors activation in several brain areas (Hunt & Castillo, 2012): in the dentate gyrus, for example, the direction of NMDAR plasticity (e.g., LTP or LTD) appears to depend on the free Ca2+ concentration triggered by the induction protocol (Harney, Rowan, & Anwyl, 2006). It has been reported that LTP and LTD mechanisms are dependent on dendritic protein synthesis (Huber, Gallagher, Warren, & Bear, 2002). In particular, LTP can be divided in two phases: early LTP, which is traditionally elicited by a single weak tetanic stimulation, lasts less than 3 h and is unaffected by protein synthesis inhibitors (Frey, Krug, Brödemann, Reymann, & Matthies, 1989); by contrast, late LTP, typically induced by multiple tetanic stimuli, is both longer-lasting and dependent on new synthesis of new proteins in the dendrites (Huang, Nguyen, Abel, & Kandel, 1996). In fact, when isolated CA1 dendrites were treated with protein synthesis inhibitor anisomycin after a train of tetanic stimuli, a decline in LTP was observed (Cracco, Serrano, Moskowitz, Bergold, & Sacktor, 2005).

3. Synaptic ribosomes and ribosome profiling experiments

As already mentioned in §2, in order to achieve activity-dependent translation, ribosomes must be present at synaptic level. Ultrastructural studies demonstrated that ribosomes already populate immature dendritic spines in the hippocampus of very young animals (7 days-old rats), accumulating as polysomes within the stubby protrusion of the spine, in a ubiquitous fashion. The maturation of the synapses, between days 10 and 28, leads to a change in the shape of the spines and to a localization of polysomes at the base of the spine neck. Quantitatively, it was observed that the number of polysomes in each spine decreases between development and adulthood, as well as the number of spines itself, as shown in **Fig.4** (O. Steward & Falk, 1985).

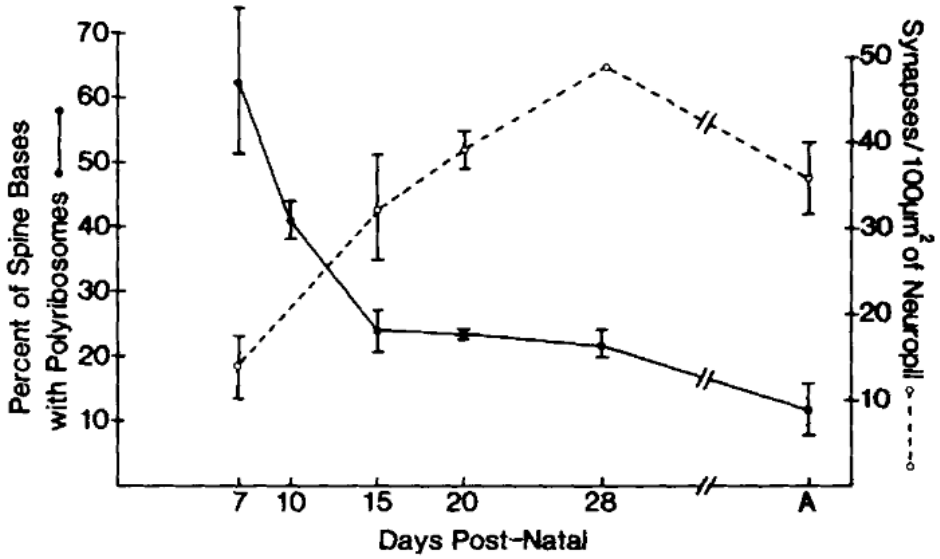

Figure 4. Relation between age (indicated as Days post-natal), number of spines in dentate gyrus and percent of polyribosomes located at the base of the spine in rats. Figure taken from O. Steward & Falk, 1985.

It was also hypothesized that synaptic polyribosomes could be involved in local translation (Koenig & Adams, 1982). Strikingly, it has recently been shown that monosomes are involved in synaptic translation in hippocampal neuropil and that the localization of mRNAs in synapses or somata and the association with monosomes is regulated by different 3'UTRs (Biever et al., 2019). Evidence that local protein synthesis is required for long-lasting synaptic plasticity was first provided by Kang and Schuman. They demonstrated that BDNF could induce LTP that was blocked by protein synthesis inhibitors even when pre- and postsynaptic pyramidal neurons were severed from their somas (Kang & Schuman, 1996). Afterwards, it was shown that other forms of synaptic plasticity require dendritic translation, such as mGluR-LTD (Huber, Kayser, & Bear, 2000). Furthermore, Cracco et al. showed that disruption of the rapamycin-sensitive signaling pathway interferes with the persistence of LTP in

isolated dendrites (Cracco et al., 2005). This is also supported by the observation that components of the translational machinery, such as ribosomes and tRNAs, as well as translation initiation and elongation factors (Sutton & Schuman, 2006), the RNA-induced silencing complex (RISC) and microRNAs (miRNAs; Schratt, 2009) are all present at the synapse. These findings suggest a local regulation of translation in an activity-dependent way that would allow each individual synapse of a given neuron to remodel its respective synaptic proteome through alterations in protein abundance and/or protein activity independently from neuronal soma (Hanus & Schuman, 2013). It has been shown that a group of developmental and adult brain disorders, including fragile X syndrome (FXS) and autism (Belmonte et al., 2004) are linked to abnormal changes in synaptic connectivity and plasticity due to defects in protein translation in dendrites. On these bases, a recent work by Schuman and coworkers was able to demonstrate that local translation is a characteristic of both pre- and postsynaptic elements (Hafner, Donlin-Asp, Leitch, Herzog, & Schuman, 2019). Furthermore, they were able to characterize the pool of mRNAs present and translated at synaptic level: these are mainly involved in synaptic function or related to mitochondria and ribosomes. Finally, they showed that local translation takes place also in inhibitory boutons and it is involved in different forms of synaptic plasticity, such as potentiation induced by neurotrophins (BDNF) and depression induced by the activation of metabotropic glutamate receptor 1 or 5 ($mGluR_{1/5}$) or by endocannabinoids (Hafner et al., 2019).

Synaptic activity triggers the active transport of mRNAs and their associated factors, such as RNA binding proteins (RBPs) or miRNAs from the cell body into dendrites (Doyle & Kiebler, 2011). Currently, there is little insight concerning the molecular dynamics of mRNA transport. The hypothesized model predicts that, upon transcription, trans-acting RBPs recognize and bind cis-acting localization elements (zipcodes), commonly located in the 3'-untranslated region (3'-UTR) of transcripts. One of the most noteworthy examples of differential 3'-UTR usage is Brain Derived Neurotrophic Factor (BDNF) mRNA. BDNF transcripts can be processed at two different polyadenylation sites, giving rise to two different isoforms, one with a long 3'-UTR (2.85 kbp) and one with a short 3'-UTR (0.35 kbp) (Liu, 2006, 2005). The two isoforms produce the same protein, but the short transcript is restricted to the soma, while the long transcript is transported to the dendrites (An, 2008). In general, before its export from the nucleus to the cytoplasm, pre-mRNA is processed to a mature form and transported through the nuclear pore complex (Le Hir, Gatfield, Izaurralde, & Moore, 2001). After its export, the RNA-protein complex undergoes maturation via the binding of additional factors, including RBPs, adaptors and/or motor proteins. This remodeling results in the packaging of the mRNA into functional transport ribonucleoprotein particles (RNPs; Hutten, Sharangdhar, & Kiebler, 2014). Once assembled, cytoplasmic RNPs are translocated along microtubules via motor proteins to synapses. However, it is not clear how messenger ribonucleoparticles (mRNPs) are recruited to and retained at specific, activated synapses for subsequent translation. It has been suggested that the local actin cytoskeleton and associated motor proteins anchor specific mRNAs at the synapse (Martin & Ephrussi, 2009). Learning and memory require local transport of mRNAs and de novo synthesis of proteins. As each form of synaptic activation may exert distinct characteristics, most likely via different signaling cascades involving distinct signaling receptors, different sets of proteins are required for translation in order to achieve the proper form of plasticity (Vanderklish & Edelman, 2005).

Local synaptic translation, finally, plays a role also in the biogenesis of structural components. In fact, it has been showed that β-catenin mRNA preferentially localizes to newly established presynaptic terminals and is locally translated. This protein leads to a reduction in the rate of synaptic vesicle release during development of functional boutons, thus allowing the correct formation of the synaptic contact (Taylor, Wu, Tai, & Schuman, 2013).

4. Synapse reduction during aging

Aging of the brain is associated with mild cognitive decline, which mainly affects declarative and working memory, the latter being mediated by the prefrontal cortex (PFC). Several studies have analyzed the aging of this brain area and have suggested that, rather than a loss of neurons, a reduction of spines takes place during aging. In particular, Duan et al.(2003) showed that in layer III of area 46 of monkeys PFC the dendritic length is not affected by aging, but in old animals the number of spines on apical dendrites was reduced by 43%, while the number of spines on basal dendrites is reduced by 27%. Another study in monkeys correlated synaptic loss in layers II/III of area 46 with aging, showing that after 20 years the greatest synaptic loss affects asymmetric synapses (**Fig.5**) (Peters, Sethares, & Luebke, 2008).

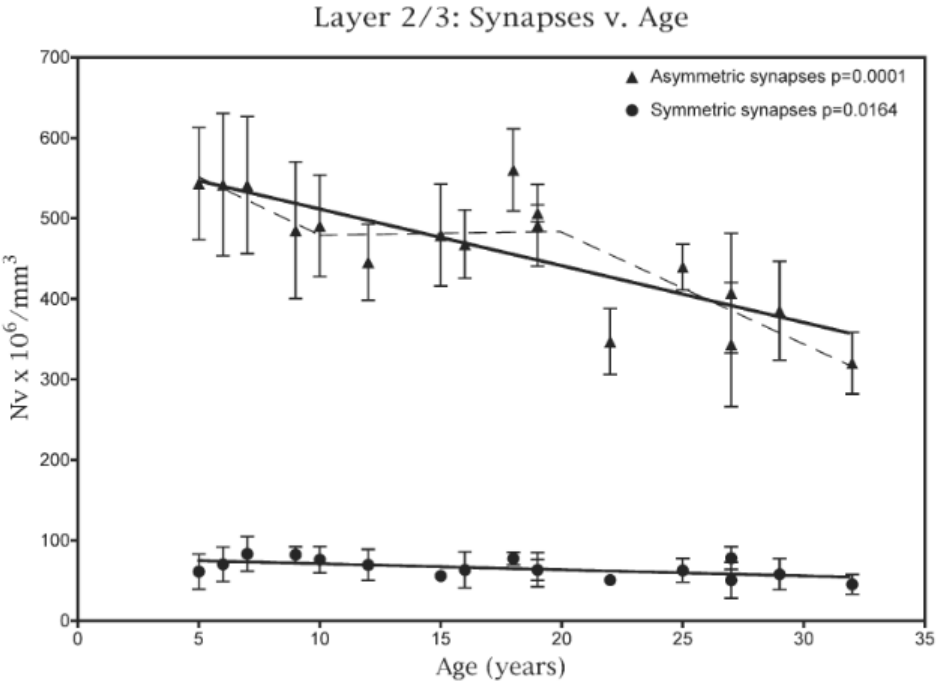

Figure 5. Age-dependent synaptic loss in layers II/III of area 46 of monkeys prefrontal cortex. Symmetric and asymmetric synapses are taken into account. Figure adapted from A. Peters et al.(2008).

In the same study, they showed an inverse correlation between Cognitive Impairment Index (CII) and asymmetric synapse number in layers II/III of area 46 (Peters et al., 2008), meaning that a decrease in synaptic density is associated to a higher cognitive impairment. A successive study (Dumitriu et al., 2010) demonstrated that the age-dependent synaptic reduction in area 46 of monkey PFC mostly affects thin spines, which are the most motile and plastic and seems to be associated with the acquisition of new memories. In particular, they found a strong correlation between the decrease in working memory function (measured with DNMS - delayed non-matching-to-sample – test) and the average volume of thin spines (rho = 0.97; **Fig.6**). For what concerns the other types of spines, such as the mushroom-shaped ones, they found no change upon aging. Finally, they observed that the thin spines that were left unmodified in old animals were larger than those present in young animals, suggesting a decreased functionality of these highly dynamic structures (Dumitriu et al., 2010).

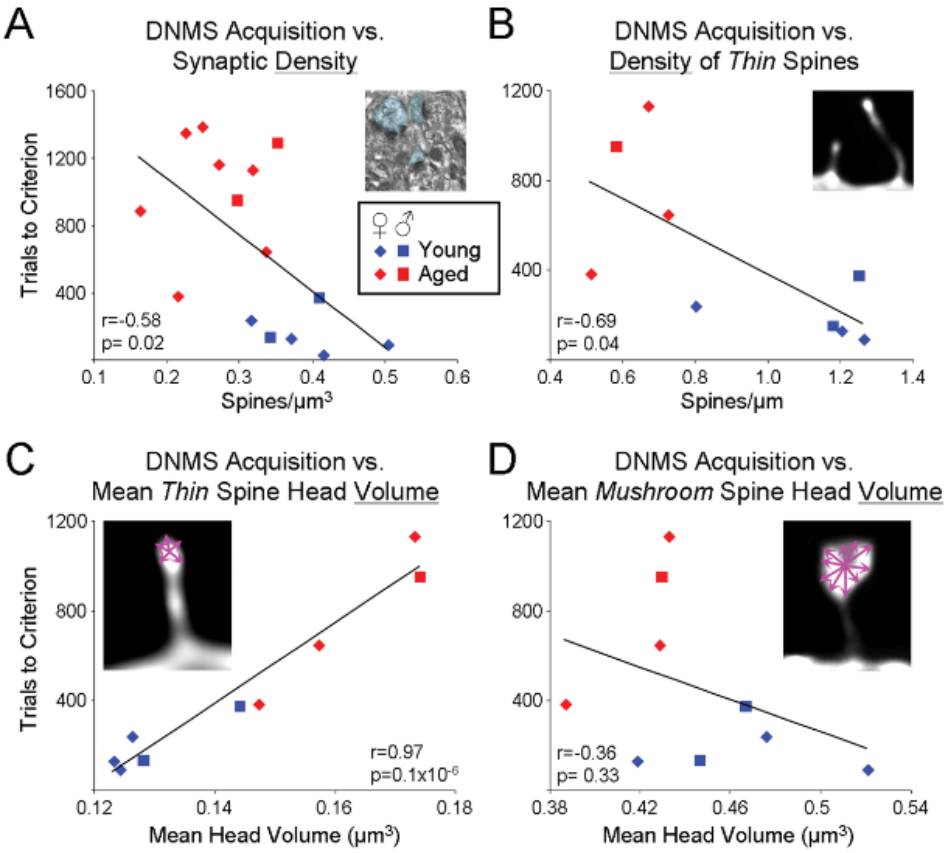

Figure 6. Cognitive performances significantly correlate with synaptic density and spine volume. **A)**Correlation of synaptic density with DNMS test in young and old animals. **B)** Correlation of thin spines density with DNMS test in young and old animals. **C)** Correlation of DNMS with thin spine head volume in young and old animals. **D)** Correlation between mushroom spine head volume and DNMS test scores in young and old animals. Picture adapted from Dumitriu et al. (2010).

In contrast with primate brain, mouse cortex exhibits an increase in bouton dynamics upon aging. In particular, en passant boutons seem to be formed and eliminated with a much higher frequency in old animals, thus impairing the acquisition of new memories connected with the stabilization of the synaptic contact (Grillo et al., 2013).

5. Synaptosomes as a research tool

The fundamental role of the synapse in neurotransmission and plasticity has fueled increasing efforts for the identification of synaptic protein and later RNAs, leading to the establishment of increasingly comprehensive mapping and profiling of the synaptic proteome and transcriptome. Sample complexity reduction strategies are required to facilitate meaningful applications of proteomic and transcriptomic analyses. The feasibility of protein enrichment by subcellular fractionation has been demonstrated through the analysis of the rat brain sub-proteomes of cytosolic, mitochondrial and microsomal fractions (Ori et al., 2015). Another well-established subcellular fractionation technique, synaptosomal isolation, has recently been applied in various proteomic studies, providing an enrichment of cellular components found at the synapse. By further fractionation the synaptosomes, it is possible to isolate specific synaptic regions, such as the vescicles.

The term "synaptosome" was first mentioned in a paper published in 1964 by Whittaker's group (Gray &Whittaker, 1962). The aim of the study was to explore the synaptic localization of several known and putative neurotransmitters and their synthesizing enzymes, and to subfractionate the disrupted synaptosomes to obtain homogeneous fractions of synaptic vesicles and other synaptic components(Whittaker, Michaelson, & Kirkland, 1964). Rather than organelles, synaptosomes are artificial, membranous sacs that contain synaptic components and are generated by subcellular fractionation of homogenized or ground-up nerve tissue, because the lipid bilayers naturally reseal together after the axon terminals are torn off by the physical shearing force of homogenization. Synaptosomes contain the complete presynaptic terminal, including mitochondria and synaptic vesicles, along with the postsynaptic membrane and the postsynaptic density (PSD). This typical morphology can be observed clearly via electron microscopy (**Fig.7**; Daniel, Malladi, Kettle, McCluskey, & Robinson, 2012). Roughly 40% of synaptosomal mass is composed of glial fragments (Biesemann et al., 2014) that most likely originate from the tripartite synapse.

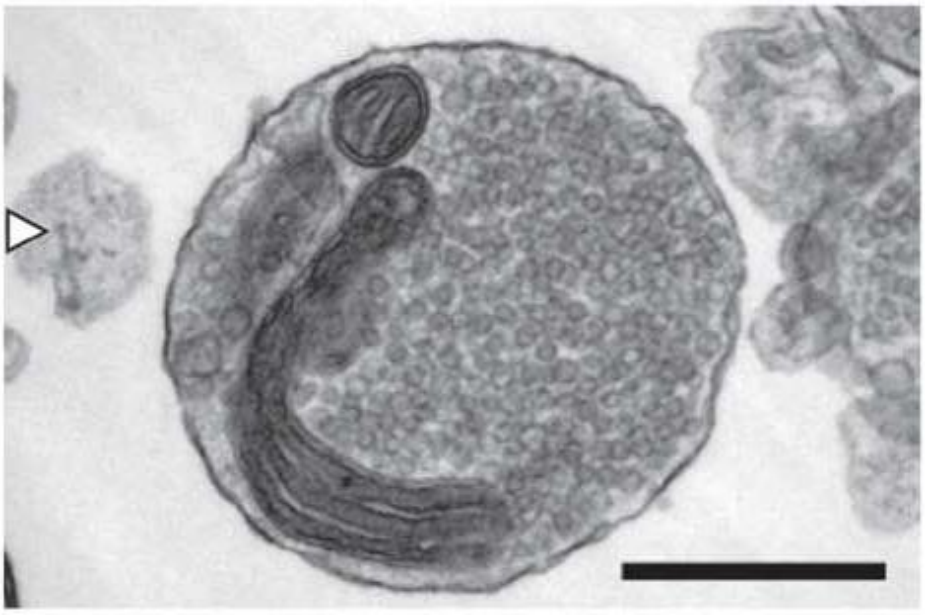

Figure 7. Synaptosomes were attached to PEI-coated 1.4-mm sapphire coverslips in 96-well plates by centrifugation in 30 μg/ml of synaptosomal protein in SET medium. Synaptosomes were then incubated in HBK at 30 °C for 15 min to facilitate recovery from low-temperature conditions. Synaptosomes were processed for electron microscopy and imaged. Scale bar 0.5μm. Figure from Daniel et al.(2012)

Synaptosome preparation is achievable with slightly different protocols all based on several differential centrifugation steps followed by sucrose (Gray &Whittaker, 1962; Whittaker et al., 1964), Ficoll/sucrose (Booth & Clark, 1978), or Percoll (Nagy & Delgado-Escueta, 1984) density-gradient ultracentrifugation, to enrich a crude synaptosomal fraction from their mitochondrial and microsomal contamination. Synaptosomes have been extensively used as research tool in both proteomic (Moczulska et al., 2014; Schrimpf et al., 2005) and transcriptomic studies (Chen et al., 2017) (cfr §7 and §9 for more details).

6. Proteomic analysis platforms

In the last decade, mass-spectrometry based methods have been developed to obtain global profiling of protein abundance in biological samples. When a global assessment of the total synaptosomal proteome is desired, a combination of several proteomic platforms should be used, as these have been shown to be complementary rather than alternative ways of measuring protein abundances in biological systems (Wu, Wang, Baek, & Shen, 2006). For the last 15 years, liquid chromatography-tandem mass spectrometry (LC-MS/MS)-based proteomics has provided broad detection and relative quantification of thousands of proteins across a variety of biological samples using a data-dependent acquisition (DDA) strategy (Bateman et al., 2014). In DDA, a subset of the most abundant ions reaching the mass spectrometer detector during an MS1 scan

are individually isolated and fragmented in sequential MS2 scans, and each MS2 scan can be analyzed with a database search algorithm (**Fig.8** - Mann, Hendrickson, & Pandey, 2002).

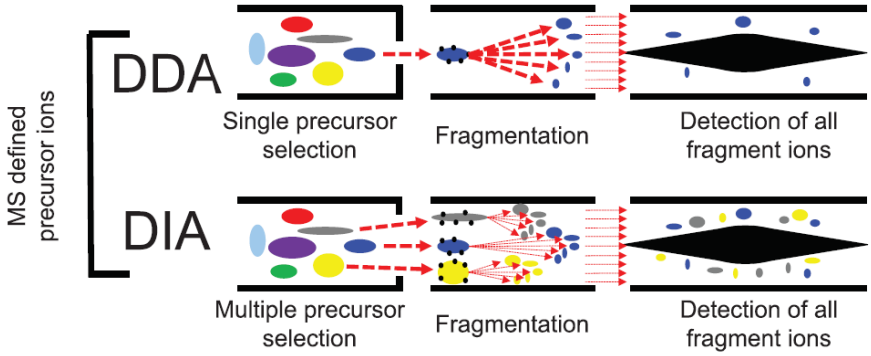

Figure 8. A cartoon schematic of how peptides are isolated, fragmented, and analyzed by a mass spectrometer working in data-dependent acquisition (DDA) or data-independent acquisition (DIA) modes. In DDA, single precursor ions are isolated, fragmented, and analyzed in an MS2 scan by the mass spectrometer. The precursor ions are then chosen by the instrument on the basis of abundance. DIA is different from DDA in that all precursor ions within a selected mass range are isolated, fragmented, and analyzed in a single MS2 scan. Picture adapted from Hu, Noble, & Wolf-Yadlin, (2016).

DDA typically can quantify a few thousand of proteins from cells or tissue homogenates. Unfortunately, irreproducibility and imprecision are fundamental to DDA's design; if too many peptide species co-elute and appear in a single MS1 scan, then DDA stochastically samples only the most abundant peptides and misses the rest. This approach diminishes reproducibility and prevents the measurement of low-abundance peptides (Venable, Dong, Wohlschlegel, Dillin, & Yates, 2004). Additionally, to survey as many peptides as possible, DDA deliberately samples each peptide species only once or twice, preventing precise absolute quantification that requires multiple measurements per peptide (Hu et al., 2016). DIA repeatedly samples the same peptides for more precise quantification; it differs from DDA by dispensing with the isolation of individual peptide species and instead repeatedly selecting mixtures of peptide species within large, pre-specified mass ranges for MS2 scans. DIA is therefore guaranteed to sample all peptides within the selected mass ranges, allowing for the identification of all sufficiently abundant peptides within them if the resulting spectra are properly interpreted (Bilbao et al., 2015). Proper interpretation of DIA data is currently problematic because the complex MS2 scans contain mixtures of peptides and therefore are more difficult to analyze. Fortunately, recent developments in bioinformatics software have adequately overcome this DIA issue, so that DIA now closely matches DDA in the number of peptide identifications while still allowing precise quantification of most of them. Quantification relies on comparing DIA spectra to sets of annotated and refined peptide-MS2 spectrum matches from DDA experiments called spectral libraries that show accurate,

empirically determined fragmentation patterns for each peptide in the library. However, DIA is currently more imprecise, compared to other MS acquisition modalities, to measure very low-abundance peptides, likely because their signals are dwarfed by those from abundant co-eluting peptides (Hu et al., 2016).

In this work I followed the pipeline illustrated in **Fig.9**. Proteins were precipitated, digested, separated by Ultra Performance Liquid Chromatography and analyzed by Mass spectrometry. The peaks were then analyzed with Pulsar software for library creation and then quantified with Spectronaut.

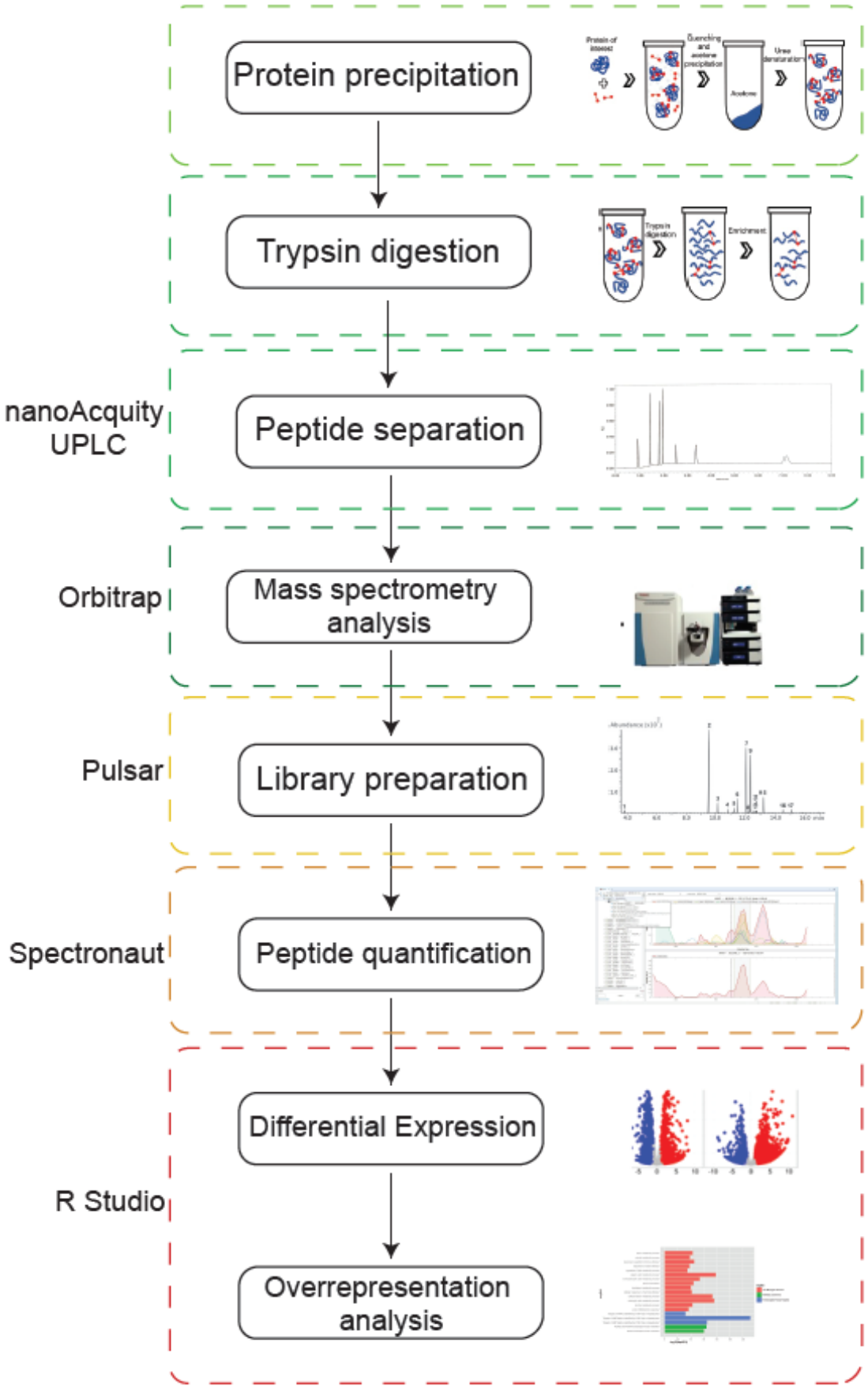
Protein precipitation
Trypsin digestion
nanoAcquity UPLC
Peptide separation
Orbitrap
Mass spectrometry analysis
Pulsar
Library preparation
Spectronaut
Peptide quantification
R Studio
Differential Expression
Overrepresentation analysis

Figure 9. Proteomics pipeline. Proteins are precipitated using acetone, then trypsinized, separated by UPLC and analyzed by MS/MS. Libraries are created using Pulsar and peaks are quantified using Spectronaut. Then differential expression analysis and overrepresentation analysis are run using R studio.

7. Synaptosome proteomics

The application of Mass Spectrometry (MS) methods represented a major breakthrough in the identification of proteins present in the synapse. Previous proteomic analyses of synaptosomal samples revealed a high complexity of its proteome (Filiou et al., 2010; McClatchy, Liao, Lee, Park, & Yates, 2012). In Filiou's paper Isoelectric Focalization (IEF) was coupled with LC-MS/MS to obtain a comprehensive analysis of murine synaptosome proteome and phosphoproteome. With this technique, they identified 2980 unique proteins with two or more peptides, including 118 phosphoproteins (Filiou et al., 2010). McClatchy *et al.*, instead, used Metabolic^{15}N labeling and Multidimensional Protein Identification Technology (MudPIT) to analyze three rat brain regions (cortex, hippocampus and cerebellum) at four different time points (p1, p10, p20, p45) (**Fig.10**). They identified 167429 peptides and found 3081 statistically significant changes during development and 1896 statistically significant changes between brain regions (McClatchy et al., 2012).

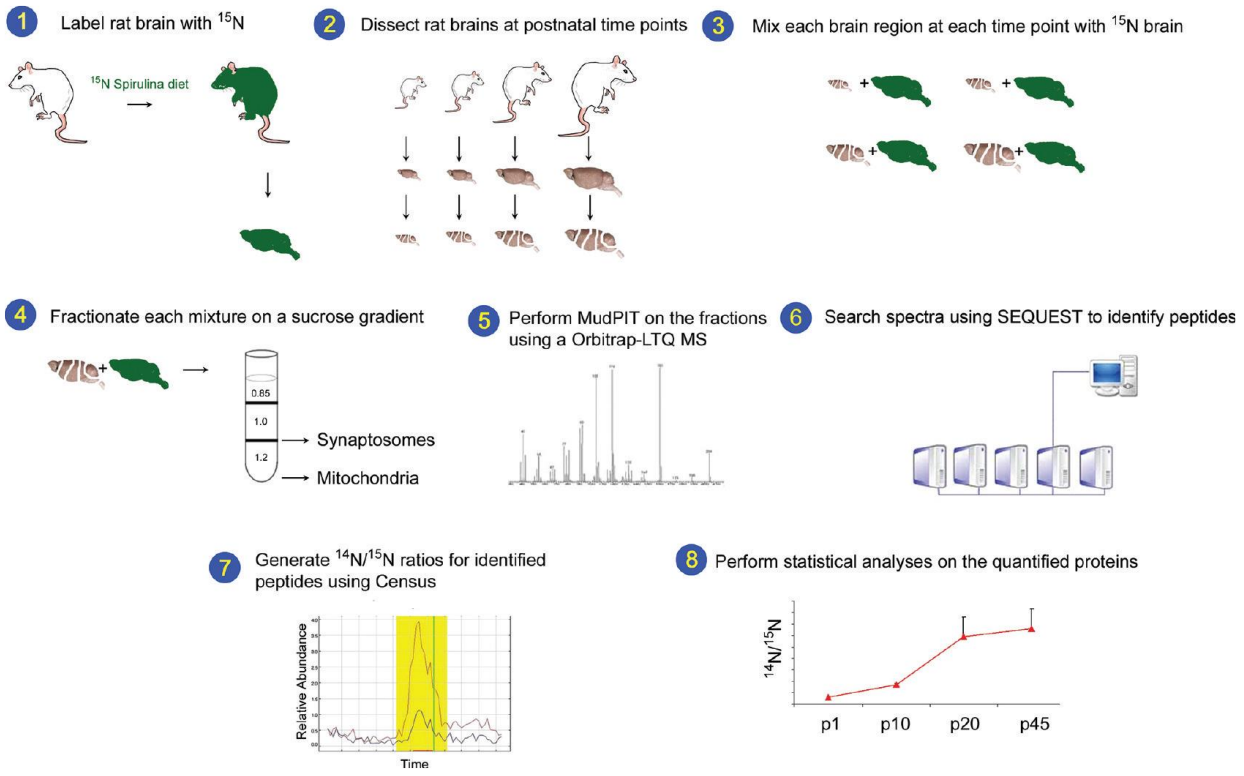

Figure 10. Graphical abstract from McClatchy et al. (2012). Rats were labeled with 15N, and the 15N-labeled p45 brains (green) were removed and homogenized **(1)**. The hippocampus, cortex, and cerebellum were dissected from unlabeled (14N) rats at p1, p10, p20, and p45 **(2)**. The 15N total brain homogenate was mixed 1:1(w/w) with each of the14N brain regions **(3)**. The synaptosomal and mitochondrial fractions were isolated

from each mixture using a discontinuous sucrose gradient **(4)**. Each fraction was analyzed by MudPIT on an LTQ-Orbitrap hybrid mass spectrometer (MS) **(5)**. The MS data was searched with SEQUEST to identify the peptides and subsequent proteins in each fraction **(6)**. Census calculated the 14N /15N ratios for the identified peptides. An example of the Census output with the 14N (red line) and the corresponding 15N (blue line) peptide abundances is shown. The y-axis is relative abundance and the x-axis is time **(7)**. Statistical analyses were performed on the average 14N /15N protein ratios. The 14N /15N ratios for the protein synaptophysin from the synaptosomal fraction in the cortex are shown **(8)**.

Finally, Moczulska et al. (2014) used an improved variant of MudPIT to quantitatively analyze changes in the synaptic proteome during development of the mouse brain. They quantified the developmental expression level of 3422 proteins during early postnatal development from adolescence (3 weeks) to early adulthood (8 weeks) (Moczulska et al., 2014; **Fig.11**).

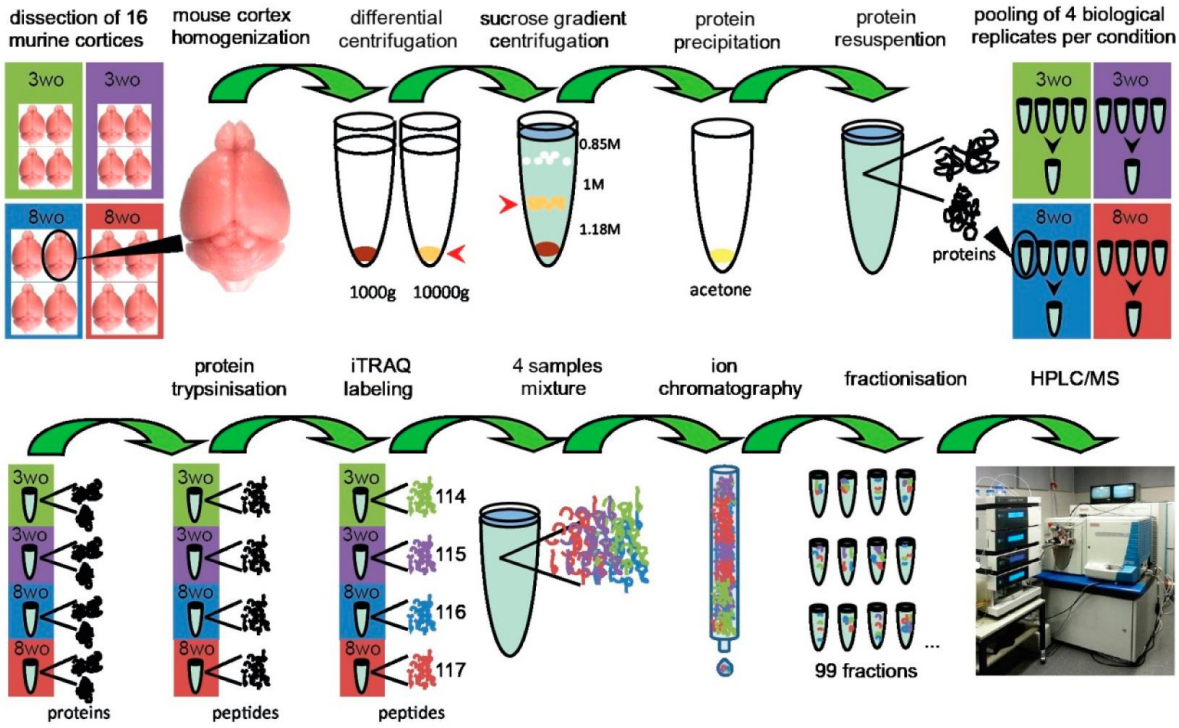

Figure 11. Graphical abstract from Moczulska et al. Sample preparation and experimental workflow incorporating high-resolution strong cation exchange. Mouse cerebral cortex from 16 animals was isolated, homogenized, and differentially centrifuged at 1000 g and 10000 g. The pellet obtained after 10000g centrifugation was redissolved and layered on a discontinuous sucrose gradient. The synaptosomal fraction was collected from the 1.18 M/1 M interface, and proteins were subsequently precipitated by cold acetone. The protein concentration was measured, and four pools (two young and two adult) were obtained by combining an equal amount of protein from individual synaptosomal preparations of four brains of identical age. The four protein samples were trypsinized and labeled with one of the four iTRAQ reagents. Subsequently, labeled samples were mixed, followed by off-line separation using strong cation exchange (SCX) chromatography. SCX fractions were analyzed by HPLC−MS using a 3 h gradient on a high-resolution nano HPLC system that was coupled online to a Velos Orbitrap mass spectrometer. Proteome Discoverer was used

for peptide identification, protein inference was accomplished according to maximum parsimony principle, and quantification was based on iTRAQ reporter ion intensities.

8. Transcriptomics analysis platforms

Transcriptomics platforms are able to provide a snapshot of a given condition, allowing the sequencing of a representative sample of all RNAs found in a tissue in a certain time point. The first attempt to obtain the transcriptome profile of human brain resulted in only 609 mRNA sequences (Adams et al., 1991). From that time, technology advancement provided high throughput platforms capable of identifying thousands of transcripts, and transcriptomes of disease states, tissues and also single cells are routinely generated (Sandberg, 2014). Before performing RNA sequencing, it is necessary to extract RNA from tissues or cells. This is usually achieved treating samples with chaotropic salts and then isolating RNA from other macromolecules such as DNA and proteins (Chomczynski & Sacchi, 1987). After RNA purification, it is necessary to remove ribosomal RNA (rRNA), which accounts for 80% of total RNA in a sample: rRNA removal strategies are usually based on affinity capture of rRNA (RiboZero techniques) or selective enrichment of mRNAs (polyA+ enrichment) (Zhao et al., 2014). Normally, for an RNA-seq experiment, a combination of high-throughput sequencing methodology and computational data analysis is used. Since the RNA molecule is converted to cDNA prior sequencing, high-throughput sequencing platforms for RNA-seq are basically the same as those for DNA sequencing (summarized in **Fig.12**).

Platform (Manufacturer)	Commercial release	Typical read length	Maximum throughput per run	Single read accuracy	RNA-Seq runs deposited in the NCBI SRA (Oct 2016)
454 (Roche, Basel, Switzerland)	2005	700 bp	0.7 Gbp	99.9%	3548
Illumina (Illumina, San Diego, CA, USA)	2006	50–300 bp	900 Gbp	99.9%	362903
SOLiD (Thermo Fisher Scientific, Waltham, MA, USA)	2008	50 bp	320 Gbp	99.9%	7032
Ion Torrent (Thermo Fisher Scientific, Waltham, MA, USA)	2010	400 bp	30 Gbp	98%	1953
PacBio (Pacbio, Menlo Park, CA, USA)	2011	10,000 bp	2 Gbp	87%	160

NCBI, National Center for Biotechnology Information; SRA, Sequence Read Archive; RNA-Seq, RNA sequencing.

Figure 12. Sequencing technology platforms commonly used for RNA-seq. Picture adapted from Lowe, Shirley, Bleackley, Dolan, & Shafee (2017).

The length of the sequence generated by these platforms is usually around 100bp, but can vary from 30 to 10000 nucleotides (**Fig.11**). The standard pipeline of an RNA-seq experiment consists in the fragmentation of the RNA specimen, followed by its conversion in a cDNA molecule, which is then sequenced. The sequences are then quality controlled, aligned to a reference genome to obtain a quantitation of the abundance of each transcript (Lowe et al., 2017) and then analyzed for differential

expression using R studio. In this work, I performed RNA-seq according to the standard pipeline described above, as illustrated in **Fig.13**.

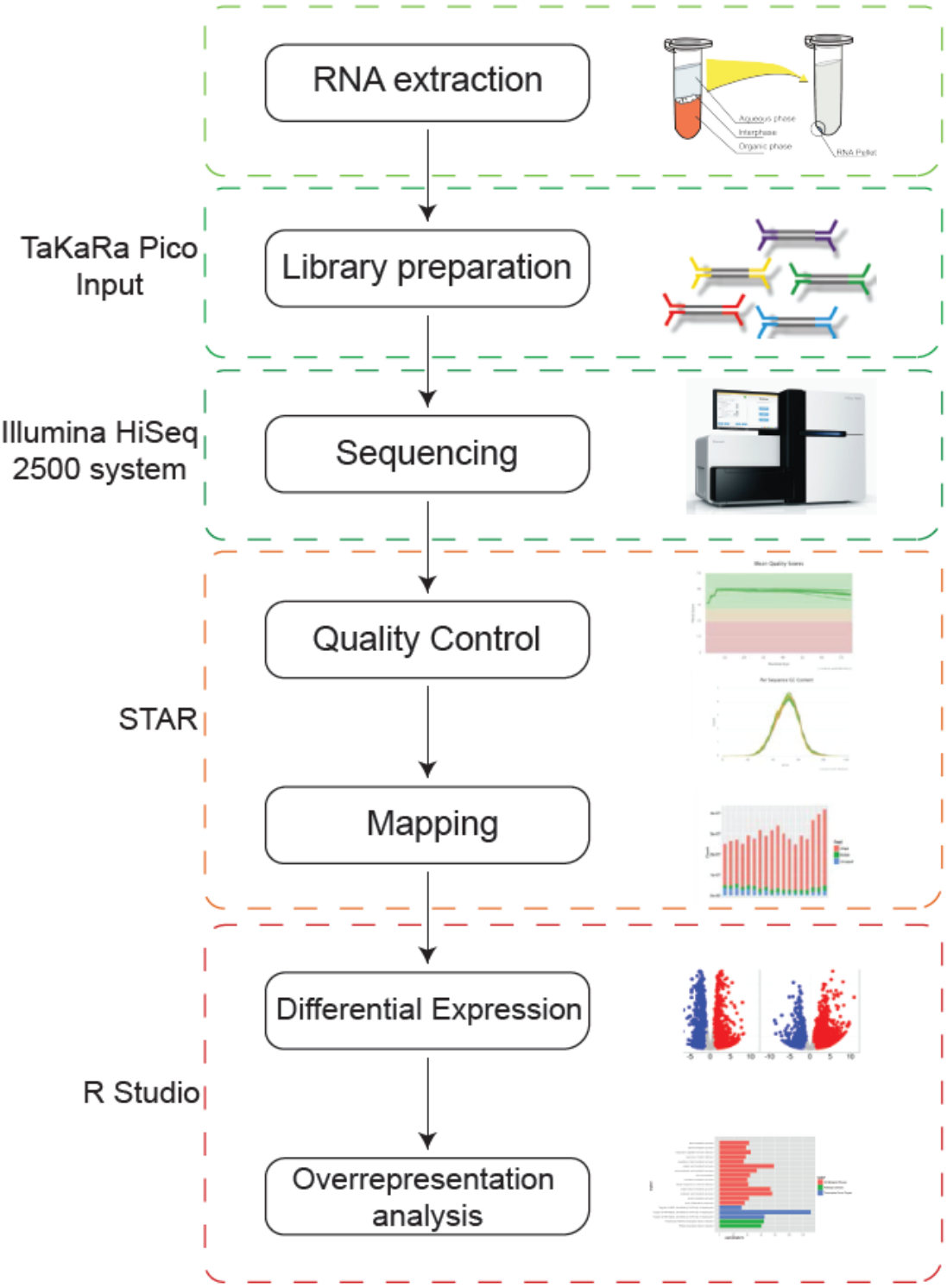

Figure 13. Summary of RNA-sequencing. The mature transcripts are extracted from an organism, fragmented and converted into cDNA. Libraries are prepared using TaKaRa Pico system, then cDNA is sequenced using Illumina technology. The sequences are quality controlled and aligned to a reference genome using STAR software. Finally they are analyzed *in silico*using R studio.

9. Synaptosome transcriptomics

The application of high throughput sequencing platforms to synaptosome preparations is a relatively new field of analysis. Williams *et al.* applied microarray analysis to synaptoneurosomes isolated from the prefrontal cortex dissected *post mortem* from patients with Alzheimer's disease at different stages. They were able to reveal early expression change in neuroplasticity genes, including those regulated and translated at the synapse(Williams et al., 2009). In Cajigas et al., the 454 sequencing technology was used to identify the full complement of mRNAs present in synaptic regions. They focused their attention on the CA1 area of the rat hippocampus and identified 2,550 mRNAs that are associated with the dendrites and/or axons in the hippocampal neuropil (Cajigas et al., 2012; **Fig.14**)

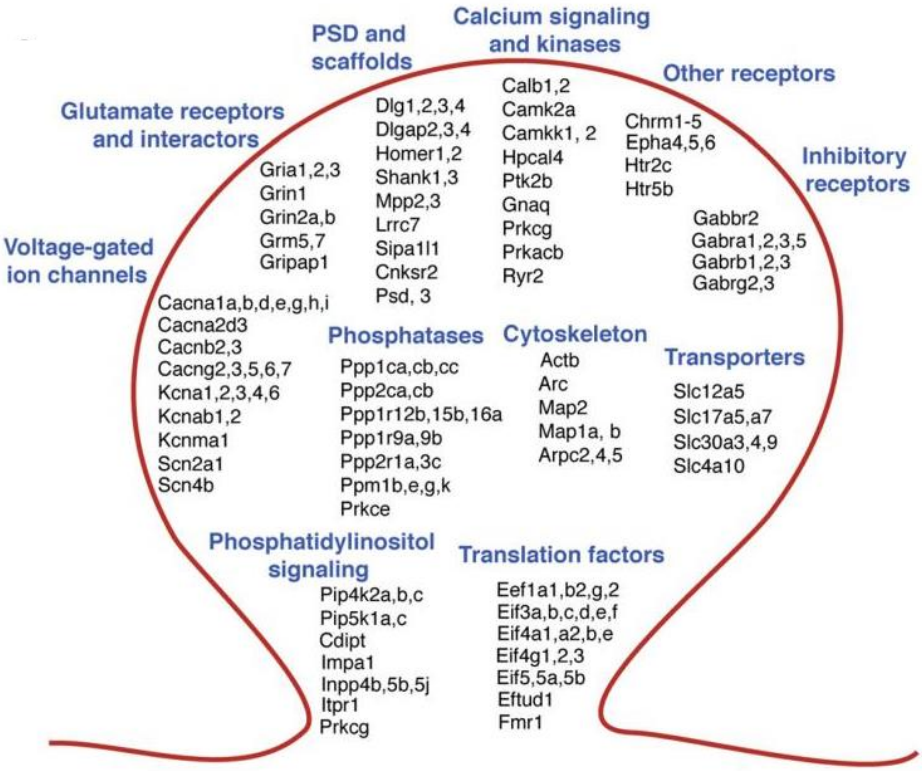

Figure 14. Main synaptic transcript families identified by microarrays performed on the CA1 neuropil. Picture adapted from Cajigas et al. (2012)

A recently published paper presented, for the first time, a comparative analysis of the synaptosome transcriptome in aging mouse brain. The authors show that, along with changes in expression of genes contributing to biological pathways related to neurite guidance and synaptosomal physiology, a vast number of novel, unannotated lincRNAs is also affected within local synaptic environment as a result of aging (Chen et al., 2017). In the work by Zappulo et al.(2017), a comprehensive analysis of synaptic transcriptome and proteome is provided. The authors used cultured neurons and

mechanically separated neurites from somata and performed on the two fractions RNA-sequencing, proteomic analysis and also quantified mRNA translation rates by ribosome profiling a protein synthesis by stable isotope labelling aminoacids in cell culture (SILAC) (Zappulo et al., 2017). They identified 661 proteins and 18111 protein-coding transcripts enriched in neurites. Among the latter they identified transcripts known to be synaptically localized and also transcripts encoding mitochondrial proteins. Using Ribo-seq and pulsed SILAC, they were able to confirm the translation of 242 proteins in soma and neurites. Interestingly, they identified some RNA binding proteins (RBPs) in neurites, which are associated mainly with translational control, RNA stability and spicing and some conserved RBP binding motifs in neurite-localized mRNAs. In this way they were able to divide neuritic proteins in three main classes: those that are translated locally, those that are mainly transported from soma to neurites and those with intermediate characteristics. To the latter class belong proteins whose synthesis has a partial contribution from the transported corresponding mRNA(**Fig.15**).

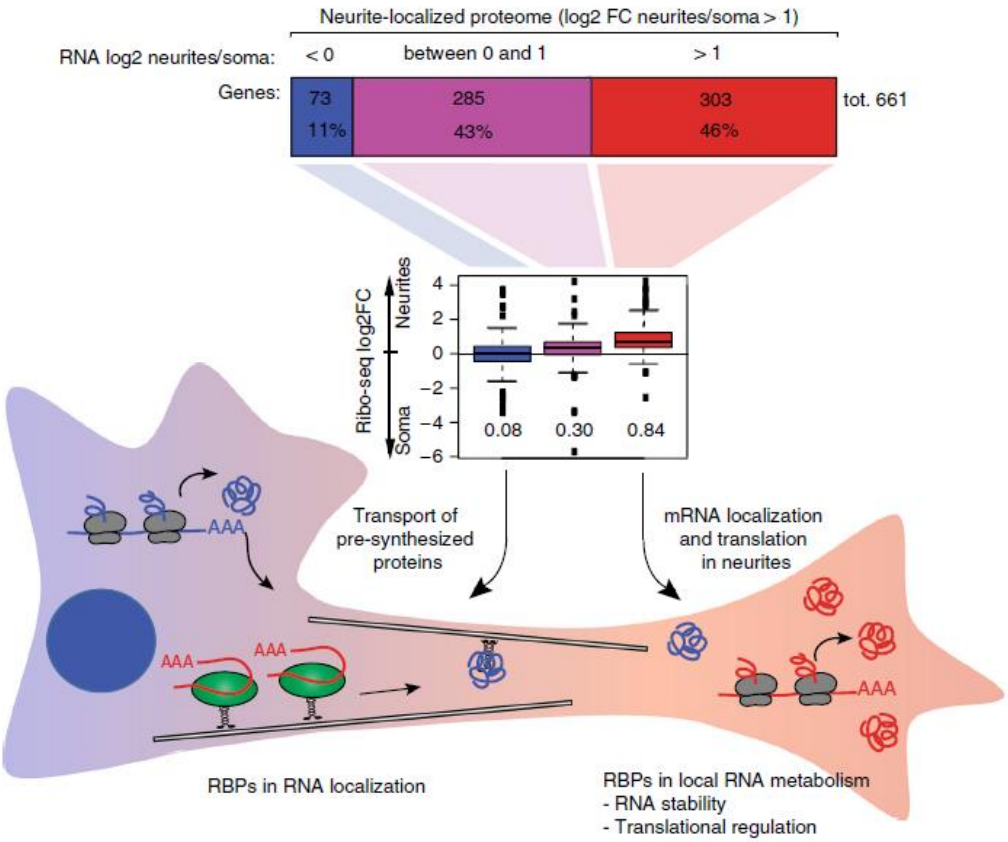

Figure 15. Proteins localized to neurites were divided in three groups according to the relative synaptic abundance of the corresponding mRNA: proteins that are localized to the neurites but don't have significant contribution from the corresponding mRNA are indicated in blue, neurite-localized proteins that have a partial contribution of the corresponding mRNA are indicated in purple, neurite-localized proteins whose

mRNA is also localized in neurites are indicated in red. As expected, the latter group of transcripts is also the more enriched in the ribo-seq experiment (middle panel). Picture adapted from Zappulo et al. (2017).

Ouwenga et al.(2017) applied TRAP (Translating Ribosome Affinity Purification) to a percoll-purified synaptoneurosomal fraction of mouse prefrontal cortex. With this approach, they were able to obtain a list of local translation candidates containing not only known synaptic proteins, but also novel candidates, such as *Brsk1*. Furthermore, they analyzed 3'UTRs and 5'UTRs of synaptically translated transcripts and found a high heterogeneity of regulatory sequences, such as G quartets and strong polyA signals (Ouwenga et al., 2017). Finally,Middleton, Eberwine, & Kim (2019) used single cell RNA sequencing to analyze transcript composition of mechanically dissected neurites and somata. They were able to provide a catalogue of constitutive dendritic transcripts (consDend) related to synaptic functions and cytoskeleton. Interestingly, they also identified a set of differentially expressed dendritic transcripts (deDend), whose function was mainly related to translation and mitochondrial activity. Furthermore, the same work identified some secondary structures in the 3'UTR, including two hairpin structures derived from B1 and B2 SINE elements, which appear to mediate the localization of the transcripts to the dendrites. In line with the abovementioned work of Zappulo, they postulated that, rather than the differential expression of Dendritic Targeting Elements (DTEs), neuritic mRNAs achieve their localization using tissue-specific RBPs(Middleton et al., 2019).

10. Protein aggregation

Protein aggregation is a phenomenon in which misfolded protein, that are not in the conformation required for their functionality, form large multimeric complexes or interact inappropriately with other cellular components impairing cell viability (Stefani & Dobson, 2003). Some diseases, called misfolding diseases, arise when a specific protein fails to fold correctly (Thomas, Qu, & Pedersen, 1995). Considerable attention is nowadays focused on a group of misfolding diseases called amyloidosis. In these diseases, specific peptides or proteins fail to fold or to remain correctly folded and then aggregate so as to give rise to 'amyloid' deposits in tissue (Stefani & Dobson, 2003). Amyloid structures can be recognized because they possess specific biochemical properties, due to a characteristic structure, constituted of highly organized β-sheets (Jiménez et al., 1999). Amyloidoses include a range of sporadic, familial or transmissible degenerative diseases, some of which affect the brain and the central nervous system (e.g. Alzheimer's and Creutzfeldt-Jakob diseases)(Dobson, Swoboda, Joniau, & Weissman, 2001).

Newly synthesized proteins fold into their native structure, which represents a local minimum of free energy. During the folding process, though, the polypeptide might assume some intermediate conformations which are characterized by a lower energy state than the native state, such as that of the amyloid fibril (Jahn & Radford, 2008; **Fig.16**).

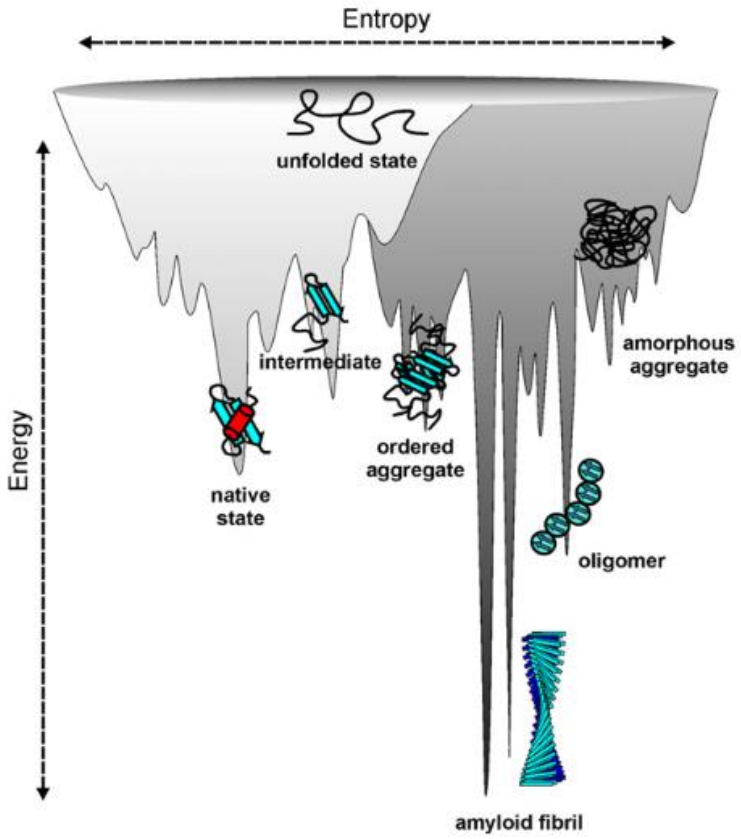

Figure 16. llustration of a combined energy landscape for protein folding and aggregation, showing the multitude of conformational states available to a polypeptide chain. Picture adapted from Jahn & Radford (2008).

Protein misfolding that leads to aggregation can arise as a consequence of age, environmental stress, chemical modifications, destabilising mutations or lack of oligomeric assembly partners (O'Connell, Zhao, Ellington, & Marcotte, 2012; Vendruscolo, 2012). In fact, loss of proteome balance during aging, was recently analyzed in *Caenorhabditis elegans* (Reis-Rodrigues et al., 2012; Walther et al., 2015). Reis-Rodrigues et al.(2012) analyzed SDS-insoluble aggregates and found a notable enrichment for proteins encoding ribosomal subunits and, in general, for proteins related to translation, growth, cofactor metabolic process, determination of adult lifespan and respiratory chain (Reis-Rodrigues et al., 2012). In Walther's work, the authors used SILAC in order to label and identify proteins at different time points and observed a change in stoichiometry of different proteins which may underlie an impairment of proteostasis. Furthermore, they analyzed protein aggregates and observed that the most soluble proteins were also the most abundant and those that contributed more to the aggregation in aged animals. They also observed that long-lived *daf-2* mutants sequestered toxic proteins into aggregates, while *hsf-1* mutants accumulated more soluble proteins. Therefore, they hypothesized that protein aggregation might be the combined result of the general proteostasis impairement and of an attempt of the cell to sequester toxic proteins from the cytoplasm (Walther et al., 2015).

11. Aim of the thesis

In the scenario described above, a comparison between synaptic transcriptome and proteome at different ages seems to be lacking. Therefore, the aim of this work is to analyze, for the first time, the composition of synaptic proteome and transcriptome in mouse brain aging. To achieve this, I isolated synaptosomes from 3 weeks-, 5 months- and 18 months-old cortices and performed RNA-sequencing and Data-Independent Acquisition proteomics. These three time points span the three main stages of the brain: in fact at 3 weeks synaptogenesis is still ongoing, although the brain is already formed; at 5 months the mouse is considered young adult and this is an intermediate time point between development and aging. Some studies have found age-related deficits in contextual memory when comparing young (3–6-months-old) and aged (16–18-months-old) C57BL/6 mice (Fukushima et al., 2008; Peleg et al., 2010), therefore we picked this age as last time point in which cognitive decline starts. Furthermore, to shed some light in synaptic protein aggregation, synaptic aggregates were isolated from old mouse cortex optimizing a recently published protocol (Reis-Rodrigues et al., 2012), in order to perform proteomic analysis.

Results

1.Validation of synaptosomal enrichment by western blot and qPCR.

Synaptosomes were extracted from brains of 4 young (3 weeks old), 4 adult (5 months old) and 4 old (18 month old) male mice (n=12). The quality of enrichment for the synaptosomal fractions was initially assessed by Western blotting analysis using antibodies against glutamate receptor ionotropic NMDA 2B (NMDAR2B), a known postsynaptic protein (Hussain *et al.* 2016), Histone H3 (H3) and Tubulin. **Fig.17A** depicts a representative immunoblot showing enrichment of NMDAR2B and depletion of H3 in synaptosomal fractions. **Fig.17B-C** report the quantification of H3 and NMDAR2B in the different fractions.

RNA was extracted from synaptosomes. Expression of the following transcriptsthat were detected as enriched in hippocampal neurites by Cajigas (Cajigas, 2012) was measured by qPCR: Calcium/calmodulin-dependent protein kinase type II alpha chain (CAMKIIα), discs large homolog 4 (Dlg4), Glutamate Ionotropic Receptor AMPA Type Subunit 1 (Gria1) and Activity-regulated cytoskeleton-associated protein (Arc)(**Fig.17D-G**). Expression levels were normalized with respect toH3f3b, coding for the histonic protein 3, a transcript reported to be enriched in the somatic compartment (Cajigas, 2012). Since there was no significative difference between the three age groups, the data from the 12 animals were combined during the quantification of Western blot and qPCR.

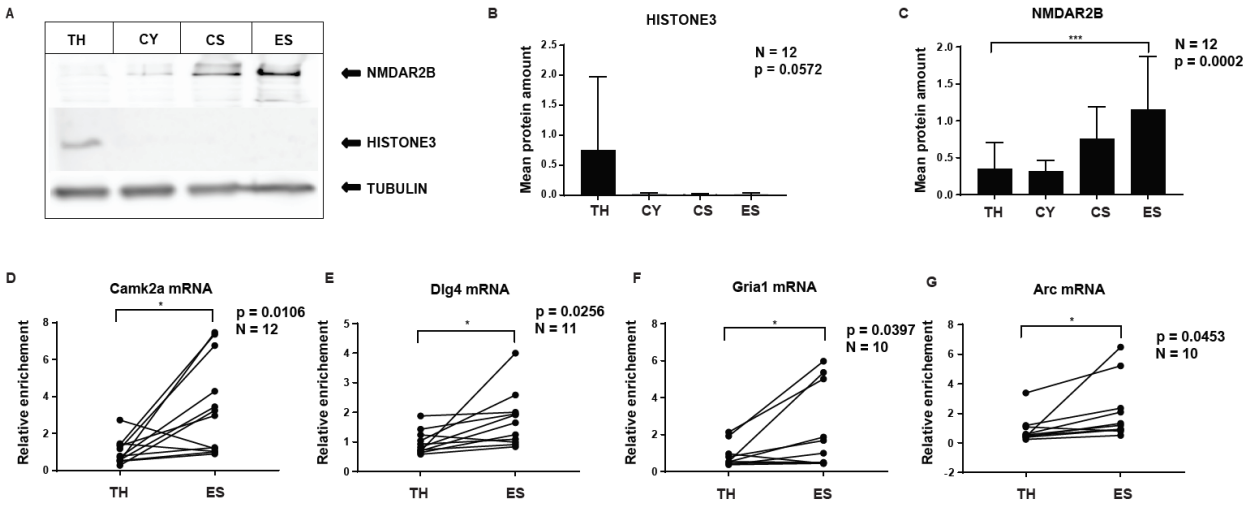

Figure 17. Enrichment of canonical synaptic protein and transcripts. **A)** Example of Western blot on subcellular fractions derived from an old mouse. TH = Total Homogenate, CY = Cytosol, CS = Crude Synaptosomes, ES = Enriched Synaptosomes. **B)** Quantification of Histone3 protein amount in each subcellular fraction. Statistical significance calculated with One-way ANOVA test. Tubulin was used as loading control. Since no significant difference was detected between the age groups the data from all the animals were combined for the quantification. N = 12. TH = Total Homogenate, CY = Cytosol, CS = Crude Synaptosomes, ES = Enriched Synaptosomes. **C)** Quantification of NMDAR2B protein amount in each

subcellular fraction. Statistical significance calculated with One-way ANOVA test. Tubulin was used as loading control. N = 12. TH = Total Homogenate, CY = Cytosol, CS = Crude Synaptosomes, ES = Enriched Synaptosomes. **D-G)** qPCR on synaptically-enriched transcripts. The expression values are normalized on *H3F3B*, coding for the histonic protein 3 B. Lines connect fractions derived from the same samples. Total homogenate (TH) and enriched synaptosomes (ES) were compared. Statistical significance was calculated with paired Student's t-test. Since no significant difference was detected between the age groups the data from all the animals were combined for the quantification. N = 12. **D)** *Camk2a* mRNA. **E)** *Dlg4*mRNA. **F)** *Gria1*mRNA. **G)** *Arc* mRNA.

After passing this initial quality control, global expression profiles of transcripts in the total homogenate and in the synaptosomal fraction were obtained using RNA-seq (Performed by the transcriptomic facility of Fritz Lipmann Institute in Jena) with Ribozero depletion of ribosomal RNAs (Petrova, Garcia-Alcalde, Zampaloni, & Sauer, 2017). Reads were aligned to the reference *Mus musculus* genome (GRCm38.85) using Tophat software and assigned to specific genes. Since this technique does not enrich specifically for messenger RNAs and primary transcripts are not depleted, a moderate percentage of reads mapping to intronic sequences is expected. Notably, the percentage of intronic reads was much smaller in the synaptosomal fraction (**Fig.18**), consistent with notion that this fraction contains mature RNAs transported from the cell body. A total of 32978 (19097coding) and 27905 (17911 coding) transcripts were detected with at least one read in the total homogenate and synaptosomal fraction, respectively.

Protein abundances were quantified by mass-spectrometry based proteomics and data independent acquisition (Performed by the proteomic facility of Fritz Lipmann Institute in Jena). A total of 4083 and 3221 proteins were detected with non-null peptide absolute intensity in the total homogenates and synaptosomal fraction, respectively. The percentage of proteins for which also the corresponding transcript was detected is 77% in total homogenate (N = 3176) and 98% in synaptosomes (N = 3168).

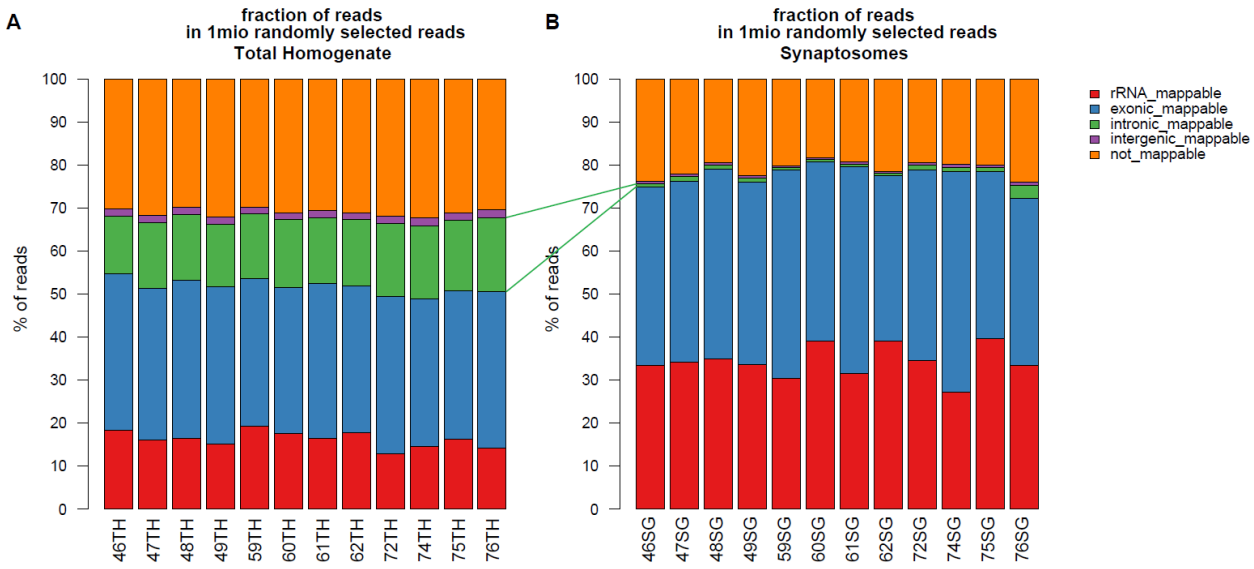

Figure 18. Fraction of reads mapping on intergenic region (purple), exonic regions (blue), intronic regions (green), ribosomal RNA (rRNA) genes (red) in total homogenate (**A**) and synaptosomes (**B**). Unmappable reads are indicated in orange.

For each transcript and protein expressed in both fractions, an enrichment score in the synaptosomes was calculated (N = 3149). For each time point, genes belonging to gene sets synapse (GO:0045202) and nucleus (GO:0005634) were selected (Nuclear genes = 987 and synaptic genes = 346 in young animals; nuclear genes= 789 and synaptic genes = 337 in adult animals; nuclear genes = 925 and synaptic genes = 331 in old animals). Interestingly, the number of nuclear genes detected from transcriptomic and proteomic analysis is lower in adult animals than in young and old animals. Probability distribution functions of the enrichment scores of the abovementioned genes were estimated by kernel density and visualized as density plots. **Fig.19A-C** illustrate the enrichment of transcripts coding for synaptic proteins and the depletion of transcripts coding for nuclear proteins and **Fig.19D-F** illustrate the enrichment of synaptic proteins and the depletion of nuclear proteins for each of the three age steps separately.

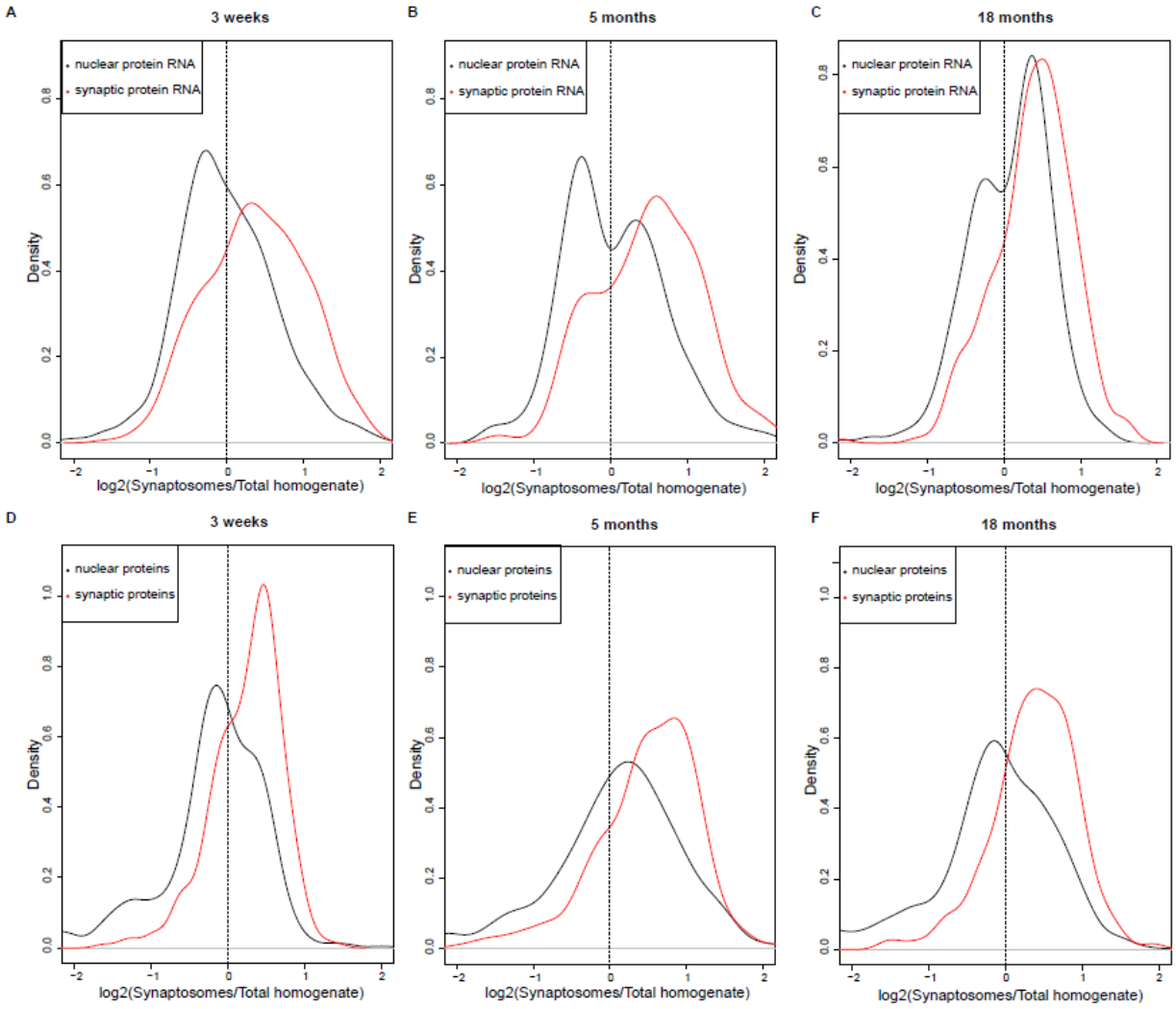

Figure 19. Global enrichment of synaptic proteins and transcripts in the synaptosomes of three age groups. **A-C)** Gaussian kernel density plot of transcript enrichment. Synaptosomal fold change is reported in logarithmic scale on the x axis, while the y axis shows the estimated probability density functions. Black line refers to proteins belonging to the GO category nucleus (GO:0005634) and red line to the GO category synapse (GO:0045202) are depicted in red. **A)**young animals, **B)** adult animals **C)** Old animals. **D-E)** Gaussian kernel density plot of protein enrichment. Synaptosomal fold change is reported in logarithmic scale on the x axis, while the y axis shows the estimated probability density functions. Black line refers to proteins belonging to the GO category nucleus (GO:0005634) and red line to the GO category synapse (GO:0045202) are depicted in red. **D)**young animals, **E)** adult animals **F)** Old animals.

2. Comparison of synaptosomal transcript enrichment with published datasets.

My RNA-seq data were compared with three recently published datasets. Ouwenga et al.(2017) used a Translating Ribosome Affinity Purification (TRAP) approach to identify transcripts specifically translated in neuronal processes in cerebral cortex (**Fig.20A**). A highly-significant correlation was detected providing an independent demonstration that our samples are enriched for synapses and that synaptic transcripts can be reliably identified. The fact that the correlation of our data was

particularly high with the TRAP dataset (rho = 0.723, p value < $2.2*10^{-16}$calculated with Spearman's correlation), suggests that most of the transcripts I detected are actively translated. Zappulo et al. (2017) used neurons differentiated from mouse embryonic stem cells to analyze protein and RNA expression and translation rates in mechanically isolated cell bodies and neurites. They also analysed translation rates of synaptic transcripts by means of Ribo-seq and stable isotope labeling with amino acids in cell culture (SILAC) experiments. Finally, Middleton, Eberwine, & Kim(2019) used primary mouse hippocampal neurons from E18 embryos in which cell bodies and dendrites were mechanically separated using a micropipette. They performed single-cell RNA amplification and sequencing (aRNA) and identified a subset of highly conserved dendritic transcripts. These data were compared with synaptosomal enrichment of either transcripts or proteins I obtained from my preparations, combining the data from all three age groups (N=12) (**Tab.1**). In the case of Zappulo *et al.* dataset, the correlation is lower than in the previous comparison (rho = 0.208 for proteins, p value = 0.007 and rho = 0.068 for transcripts, p value < $7.68*10^{-7}$ calculated with Spearman's correlation). It should be noticed, however, that I analysed synaptic proteome and transcriptome from cerebral cortex of adult animals, while Zappulo et al.(2017) used an *in vitro* differentiation model of only six days that generates embryonic neurons of uncertain regional identity. Finally, it is noteworthy that I found a high correlation of our data with highly conserved dendritic transcripts from Middleton et al.(2019)(rho = 0.523, p value = $1.11*10^{-9}$ calculated with Spearman's correlation) (**Fig.20D**), further corroborating the strong synaptic content of my synaptosomal enrichment.

Table 1. Datasets correlated with proteomic and transcriptomic data.

Study	Tissue	Age	Data	Our dataset	N. of matching entries
Ouwenga et al., 2017	mouse cortex	3 weeks	TRAP-seq RNA-seq	Ribo-zero RNA-seq	3527
Zappulo et al., 2017	mESC derived neurons	DIV6	Stranded total RNA-seq	Ribo-zero RNA-seq	5135
Zappulo et al., 2017	mESC derived neurons	DIV6	LFQ proteomic	LFQ proteomic	167
Middleton et al., 2019	Primary hippocampal neurons	E18	single-cell RNA amplification and sequencing	Ribo-zero RNA-seq	529

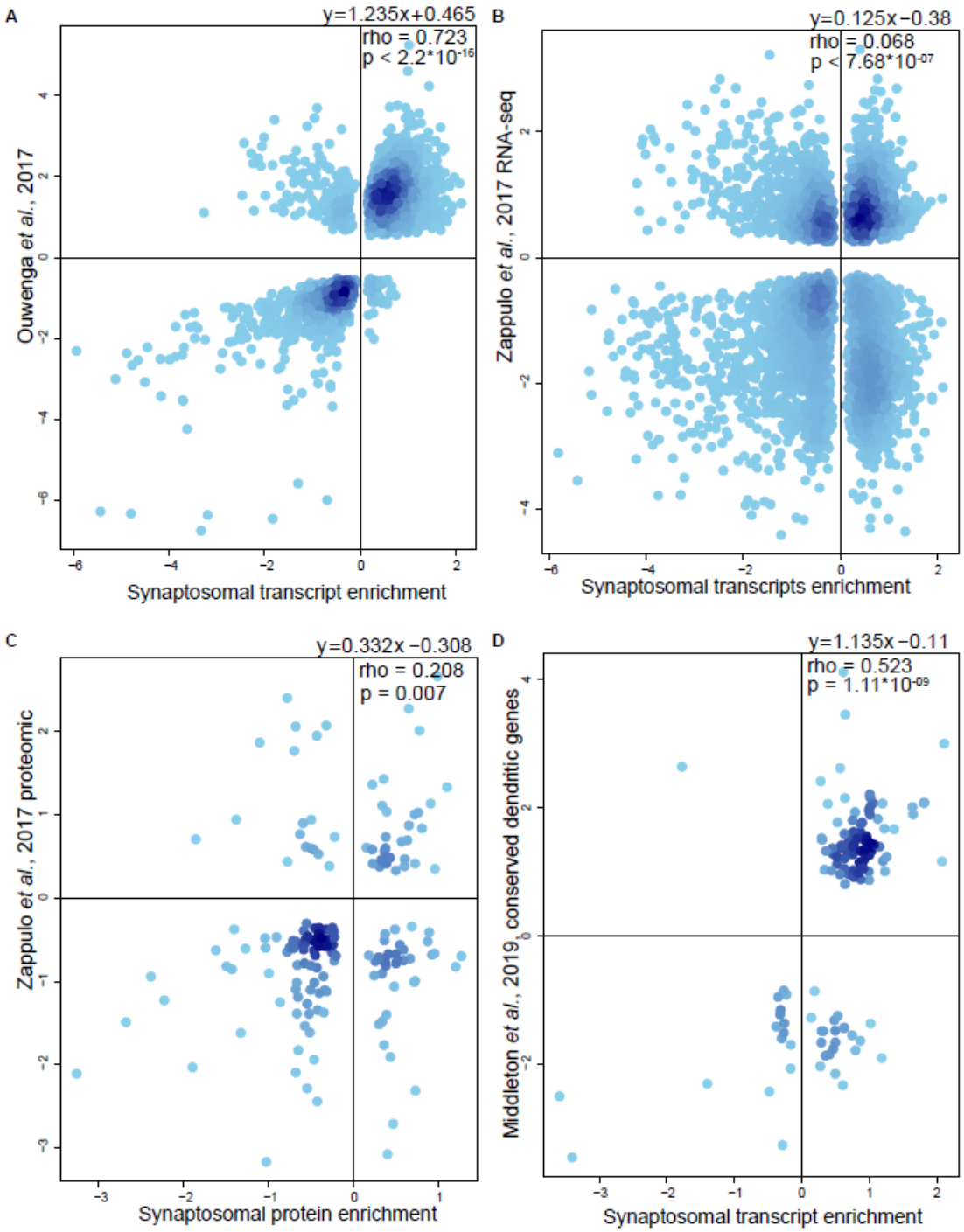

Figure 20. Comparison of synaptosomal enrichment of transcripts or proteins with published datasets. Enrichment is expressed as fold change synaptosomal fraction vs. total homogenate in logarithmic scale. Correlation was computed as using Spearman's correlation coefficient and reported in the upper right corner of the plot, together with its p value. The best linear fit of the data equation is reported on the upper right part of the plot. **A)** Comparison with the dataset of Translating Ribosome Affinity Purification from cortical neuronal processes of Ouwenga et al. (2017). **B)** Comparison with neurite-enriched transcripts of embryonic neurons from Zappulo et al. (2017). **C)** Comparison with neurite-enriched proteins of embryonic neurons

from Zappulo et al. (2017). **D)** Comparison with conserved dendritic transcripts identified in Middleton et al. (2019).

3. Comparison of synaptosomal enrichment in transcriptome and proteome.

Genes were selected that: i) are detected also at the protein level and ii) are differentially expressed (in either direction) between synaptosomal fraction and total homogenate when p-values for differential expression at the protein and transcript level are combined in a meta-analysis (Fisher's method) (Lury & Fisher, 1972) in young animals. This selection left 3149 pairs of matched proteins and transcripts. Synaptosomal enrichment at protein and transcript level of these is plotted as scatter plot in **Fig.21**. The first quadrant of this plot contains proteins that show synaptic enrichment also at the transcript level. Examples of proteins belonging to this group are the presynaptic protein Bassoon and the postsynaptic proteins Calcium/calmodulin-dependent protein kinase type II alpha chain (CAMKIIα), discs large homolog 4 (Dlg4) and Glutamate Ionotropic Receptor AMPA Type Subunit 1 (Gria1). The overrepresented GO categories within this gene set are reported in **Fig.22B** and clearly correspond to terms related to synapses and neuronal processes. The third quadrant contains genes that show somatic enrichment both at protein and transcript level, the overrepresented GO categories within this gene set are reported in **Fig.22C** and clearly correspond to terms related to nuclear proteins, as expected. The second and the fourth quadrants are interesting, as they contain genes whose corresponding proteins and transcripts show opposite directions of enrichment. The second quadrant contains synaptically-depleted proteins whose transcripts are enriched in the synaptosome. The overrepresented GO categories of this gene set are represented in **Fig.22D** and correspond mainly to organelles such as the mitochondrion or the ribosome but also to extracellular matrix and – surprisingly – to spliceosome. These likely correspond to transcripts that are translationally repressed or proteins whose half-life is shorter in the synapses. The fourth quadrant contains enriched proteins coded by depleted transcript. These proteins are possibly synthesized at somatic level and transported to the neuronal processes. The overrepresented GO categories of this gene set are represented in **Fig.22A.** These are enriched for term related to lytic vacuoles and vescicle components that are involved in soma-processes trafficking or in synaptic vescicle trafficking, such as dynamin family proteins, Syntaxin 12 (Stx12) and the synaptosomal associated protein 25 (Snap25).

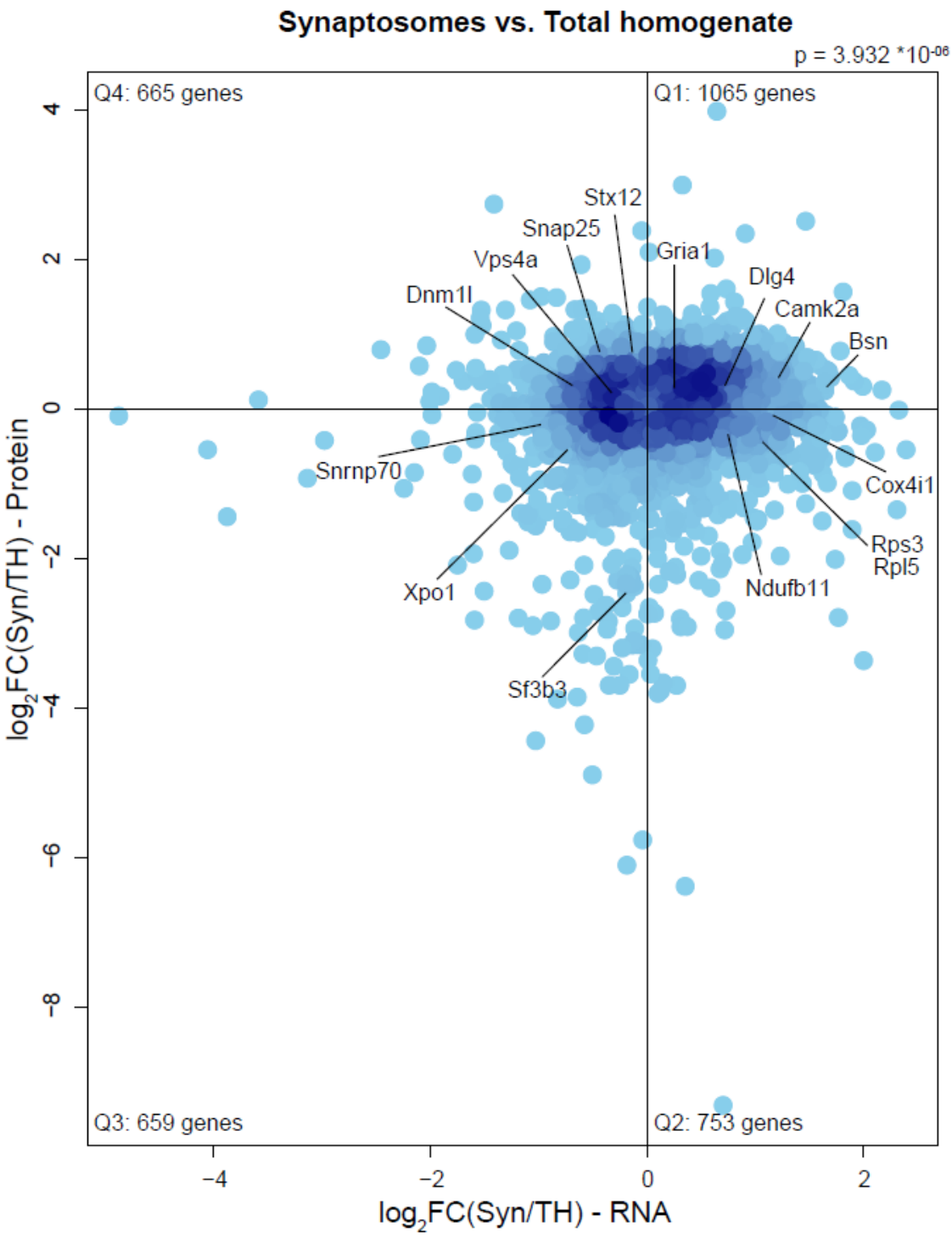

Figure 21. Comparison of synaptosomal enrichment in proteome and transcriptome. Proteins and RNAs enrichment are plotted as log of the ratio synaptosome vs. total homogenate. Quadrants were named clockwise, starting from the upper right one. The distribution of genes in each quadrant is not uniform according to Fisher's exact test ($p = 3.932*10^{-06}$). Protein and RNA fold changes were correlated using Spearman's correlation ($rho = 0.107$, $p = 1.675*10^{-9}$). TH = Total homogenate, Syn = Synaptosomes.

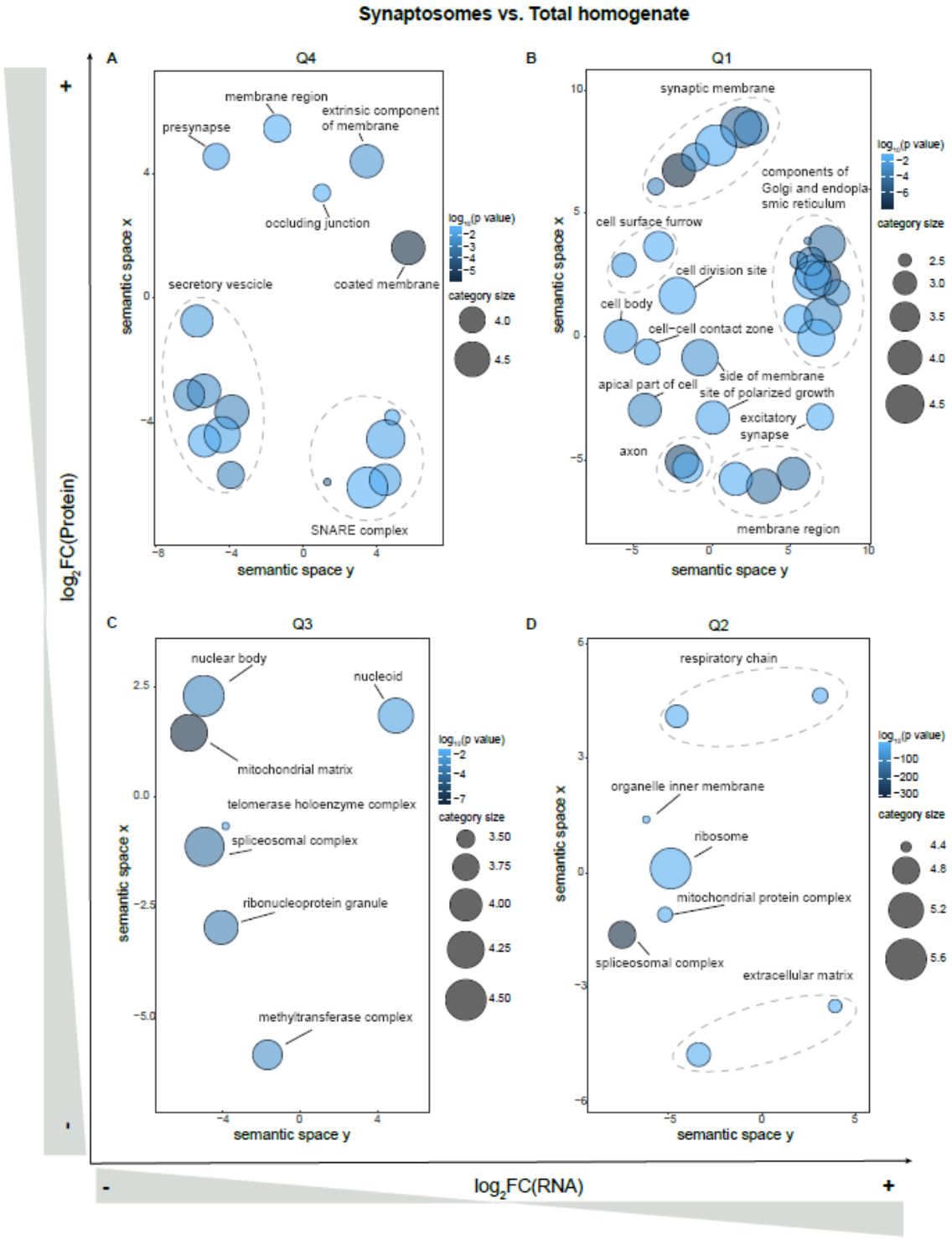

Figure 22. Overrepresentation of Cellular Component Gene Ontology terms in the four quadrants of **Fig.21**. Similar terms are clustered together based on their semantic similarity using the REVIGO algorithm, and are colored according to $\log_{10}$(p value). **A)** Genes showing synaptosomal enrichment of protein and depletion of transcript. **B)** Genes showing synaptosomal enrichment of both protein and transcript. **C)** Genes showing

synaptosomal depletion of both protein and transcript. **D)** Genes showing synaptosomal depletion of protein and enrichment of transcript.

To obtain indirect evidence that transcripts in the second quadrant of **Fig.21** (i.e. transcript enriched and protein depleted) are translationally repressed, I used the Zappulo et al.(2017) dataset as reference. I chose this dataset and not that from Ouwenga et al. (2017) because in the work by Zappulo et al., the authors quantified translation rates by Ribo-seq and protein synthesis rates by SILAC in isolated neurites as compared to isolated soma, whereas in the work by Ouwenga et al. the informations regarding proteins synthesis are not provided. Probability distribution functions of translation and protein synthesis rates were estimated by Gaussian kernel density and are reported as density plots in **Fig.23A,B**. Both translation rate and protein synthesis rate were lower for genes of the second quadrant as compared to genes of the first quadrant ($p < 2.2*10^{-16}$ and $p = 0.02$, respectively, estimated by Wilcoxon Test).

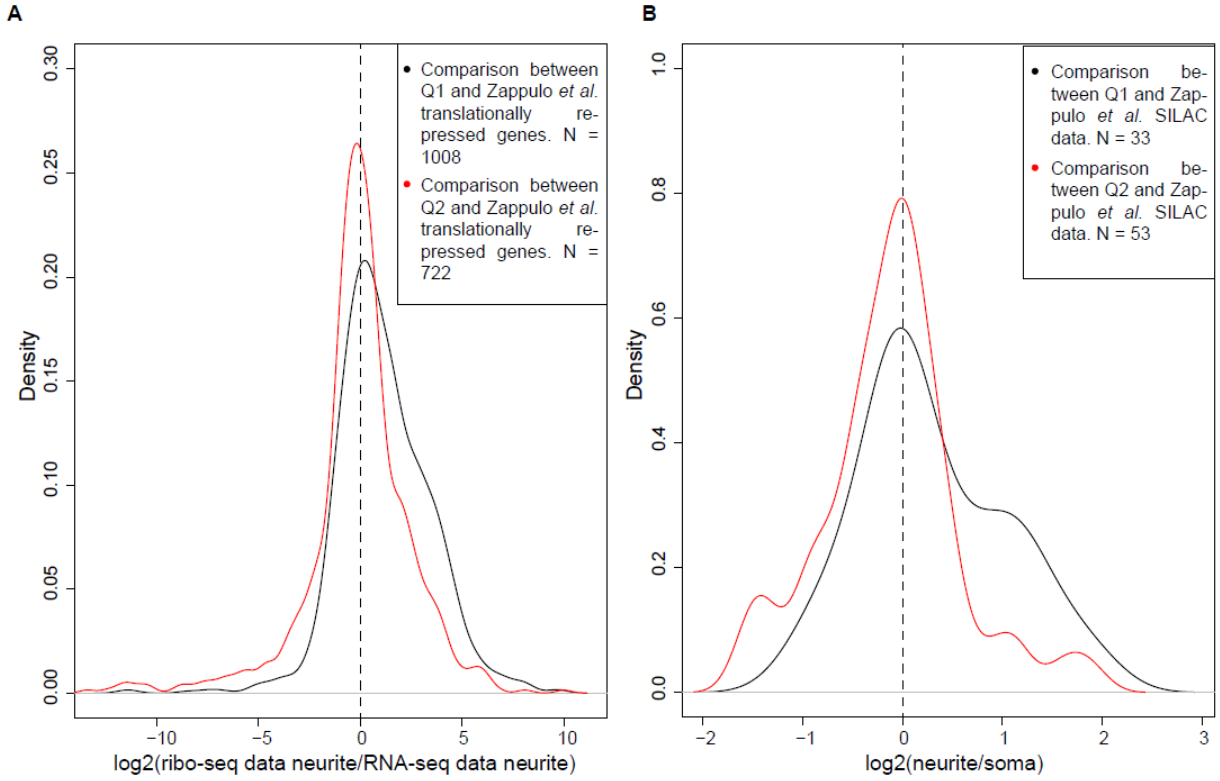

Figure 23. Rates of translation and protein synthesis for transcripts in quadrants 1 and 2 of **Fig.21** .**A)** Probability density plot of the translation rates of transcripts belonging to quadrant 1 (black line) and 2 (red line). The samples are independent according to Wilcoxon Test ($p < 2.2*10^{-16}$). **B)** Probability density plot of the protein synthesis rates of transcripts belonging to quadrant 1 (black line) and 2 (red line). The samples are independent according to Wilcoxon Test ($p = 0.02$).

As shown in **Fig.22C**, this quadrant is enriched for genes coding for ribosomal and mitochondrial proteins. To better visualize this relationship, I highlighted in the plot of **Fig.21** genes belonging to the GO categories translation (GO:0006412), ribosomes (GO:0005840) and respiratory chain (GO:0070469) and synapse (GO:0045202) (**Fig.24A**) and I obtained translational rates in the neurites for these genes from Zappulo et al. and plotted these as probability density plots (**Fig.24B**). It is apparent that translation is higher for synaptic transcripts, which are all actively translated at synaptic level as compared to genes belonging to ribosome, translation and respiratory chain categories. It is of particular note that transcripts coding for the translational machinery are enriched but translationally repressed at synaptic level.

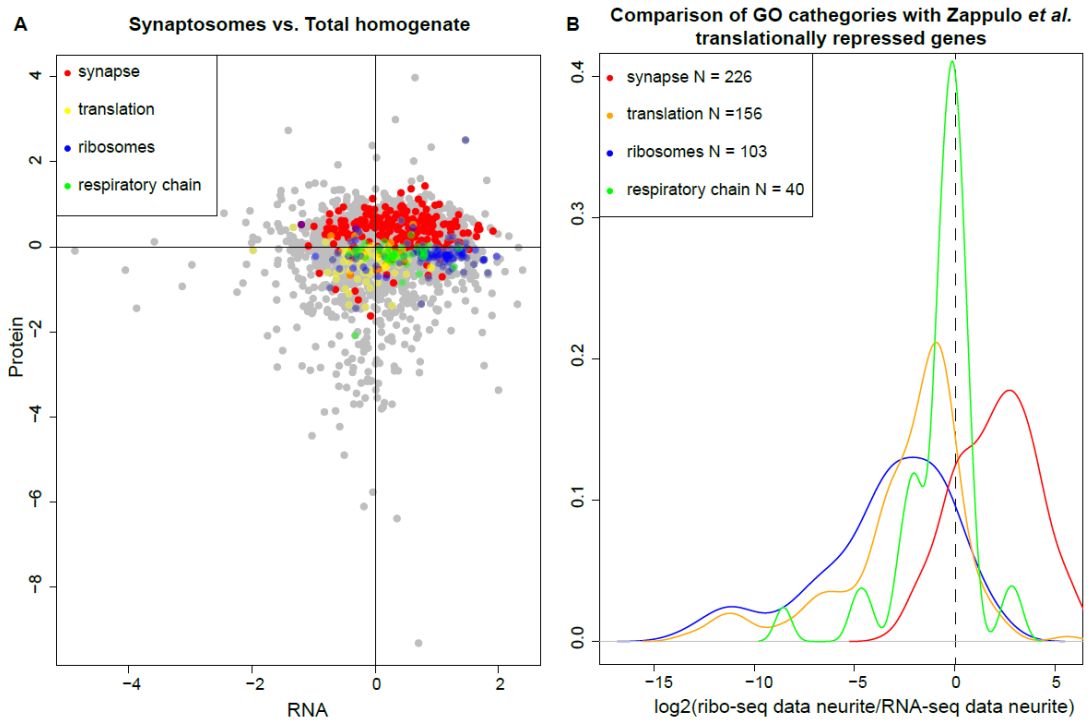

Figure 24. Comparison of synaptosomal enrichment in proteome and transcriptome for selected GO terms in young animals. **A)** Proteins and RNAs were divided in four quadrants according to their fold change. Genes belonging to specific Gene Ontology (GO) terms were highlighted in different colors, red = synapses, yellow = translation, blue = ribosome, green = respiratory chain as indicated also in the legend. **B)** Probability density plot of the translation rates of transcripts belonging to the different terms. Samples are non-identical according to Kruskal-Wallis Test ($p < 2.2*10^{-16}$).

The comparison between proteome and transcriptome of synaptosomes and total homogenate was repeated using the same procedure for the other two time points, yielding, respectively, 2726 and 3055 pairs of matched proteins and transcripts in adult and old animals (**Fig. 25A** depicts data coming from adult animals and **Fig.26A** refers to data coming from old animals). I also highlighted in the plots of **Fig.25A**and **26A** genes belonging to the GO categories translation (GO:0006412),

ribosomes (GO:0005840), respiratory chain (GO:0070469) and synapse (GO:0045202)(**Fig.25B** and **Fig.26B**).

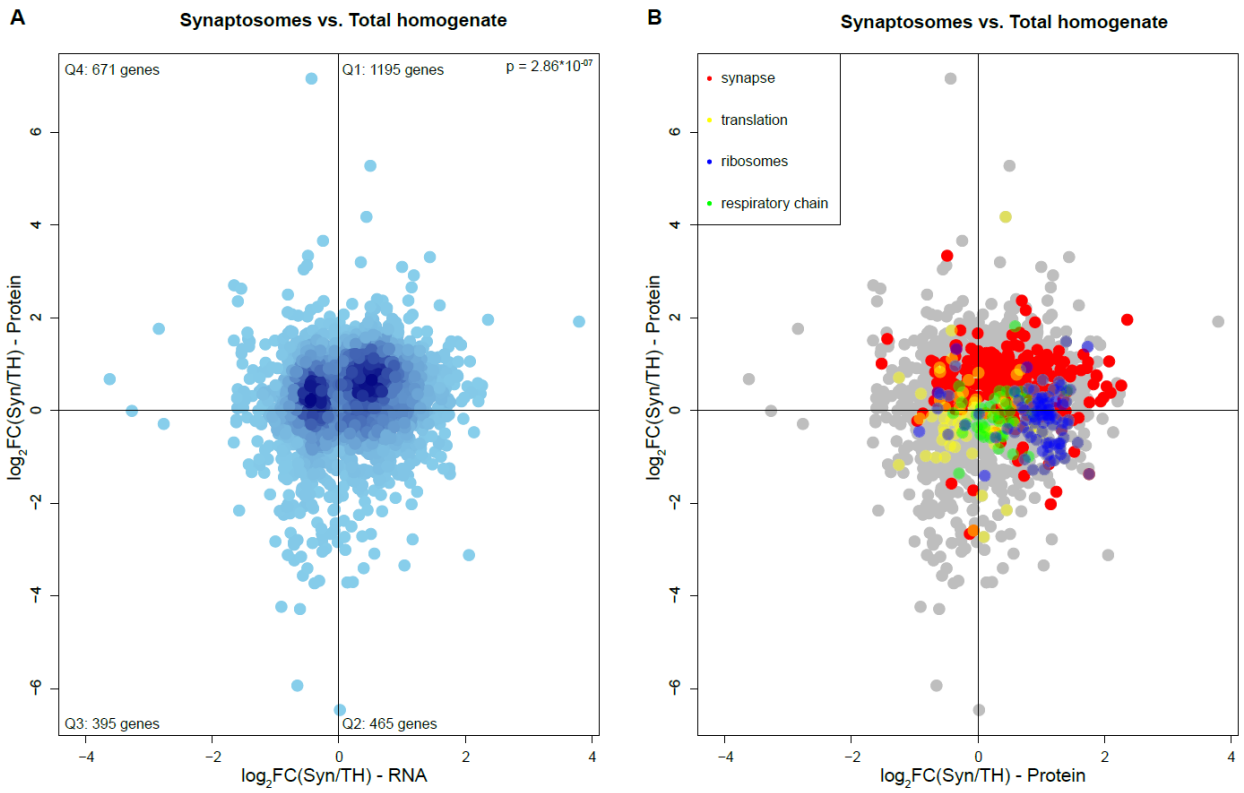

Figure 25. Comparison of synaptosomal enrichment in proteome and transcriptome in adult animals. **A)** Proteins and RNAs enrichment are plotted as log of the ratio synaptosome vs. total homogenate. Quadrants were named clockwise, starting from the upper right one. The distribution of genes in each quadrant is not uniform according to Fisher's exact test ($p = 2.86*10^{-07}$). Protein and RNA fold changes were correlated using Spearman's correlation (rho = 0.141, $p = 1.342*10^{-13}$). **B)** Genes belonging to specific Gene Ontology (GO) terms were highlighted in different colors, red = synapses, yellow = translation, blue = ribosome, green = respiratory chain as indicated also in the legend. TH = Total homogenate, Syn = Synaptosomes.

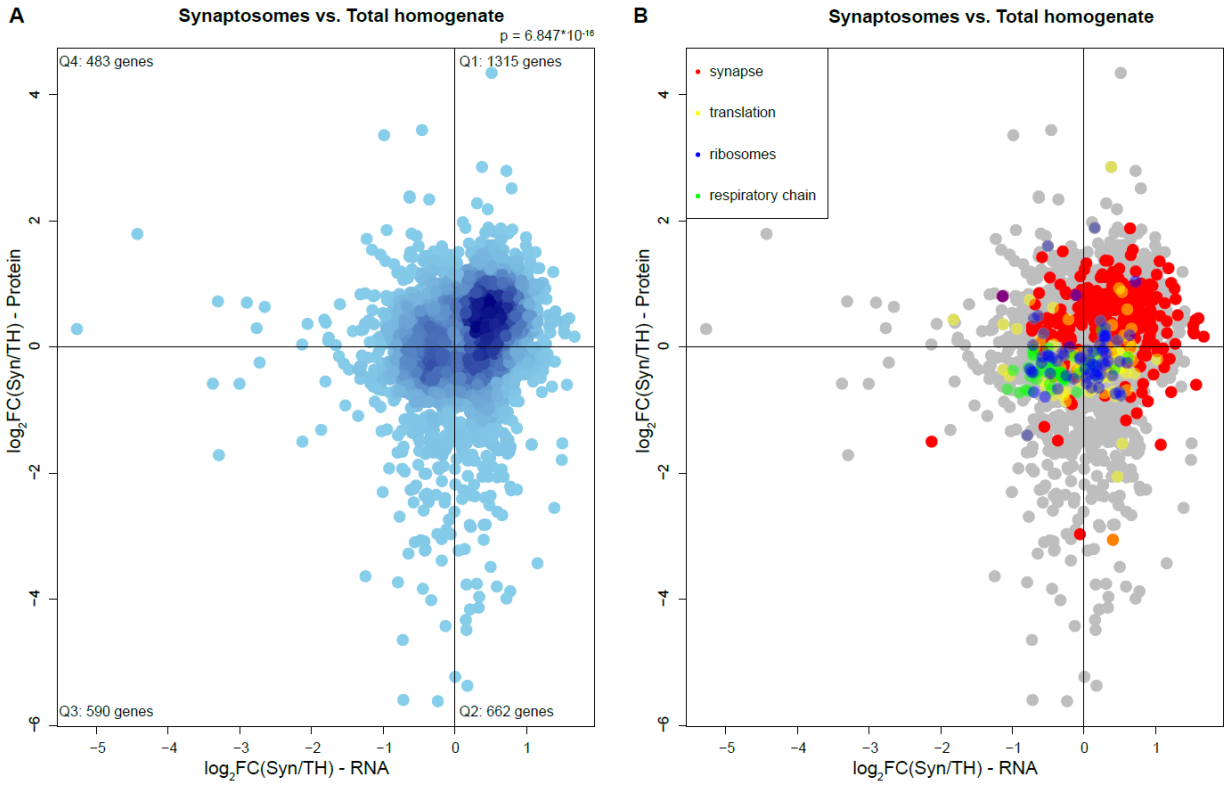

Figure 26. Comparison of synaptosomal enrichment in proteome and transcriptome in old animals. **A)** Proteins and RNAs enrichment are plotted as log of the ratio synaptosome vs. total homogenate. Quadrants were named clockwise, starting from the upper right one. The distribution of genes in each quadrant is not uniform according to Fisher's exact test ($p = 6.847*10^{-16}$). Protein and RNA fold changes were correlated using Spearman's correlation ($rho = 0.270$, $p < 2.2*10^{-16}$). **B)** Genes belonging to specific Gene Ontology (GO) terms were highlighted in different colors, red = synapses, yellow = translation, blue = ribosome, green = respiratory chain as indicated also in the legend.TH = Total homogenate, Syn = Synaptosomes.

The overrepresented GO categories within the gene sets depicted in **Fig.25A** and **26A** are reported in **Fig.27** (referring to adult animals) and **Fig.28** (referring to old animals). During aging, there is no substantial change in the genes enriched at synaptic level. The most relevant changes in GO categories affect genes that are enriched at transcript but not protein level in synaptosomes (located in the second quadrant). I could observe that in young animals there was an overrepresentation of categories related to spliceosome, both in quadrants 2 and 3 (**Fig.22C-D**); in adult and old animals these categories are overrepresented only in the 3rd quadrant (**Fig.27C, 28C**). GO categories related to ribosomes and respiratory chain are on the other hand overrepresented in the 2nd quadrant in young and adult animals (**Fig.22D, 27D**), but not in old animals (**Fig.28D**). At 18 months, in fact, respiratory chain GO category is overrepresented in Q3 (**Fig.28C**).

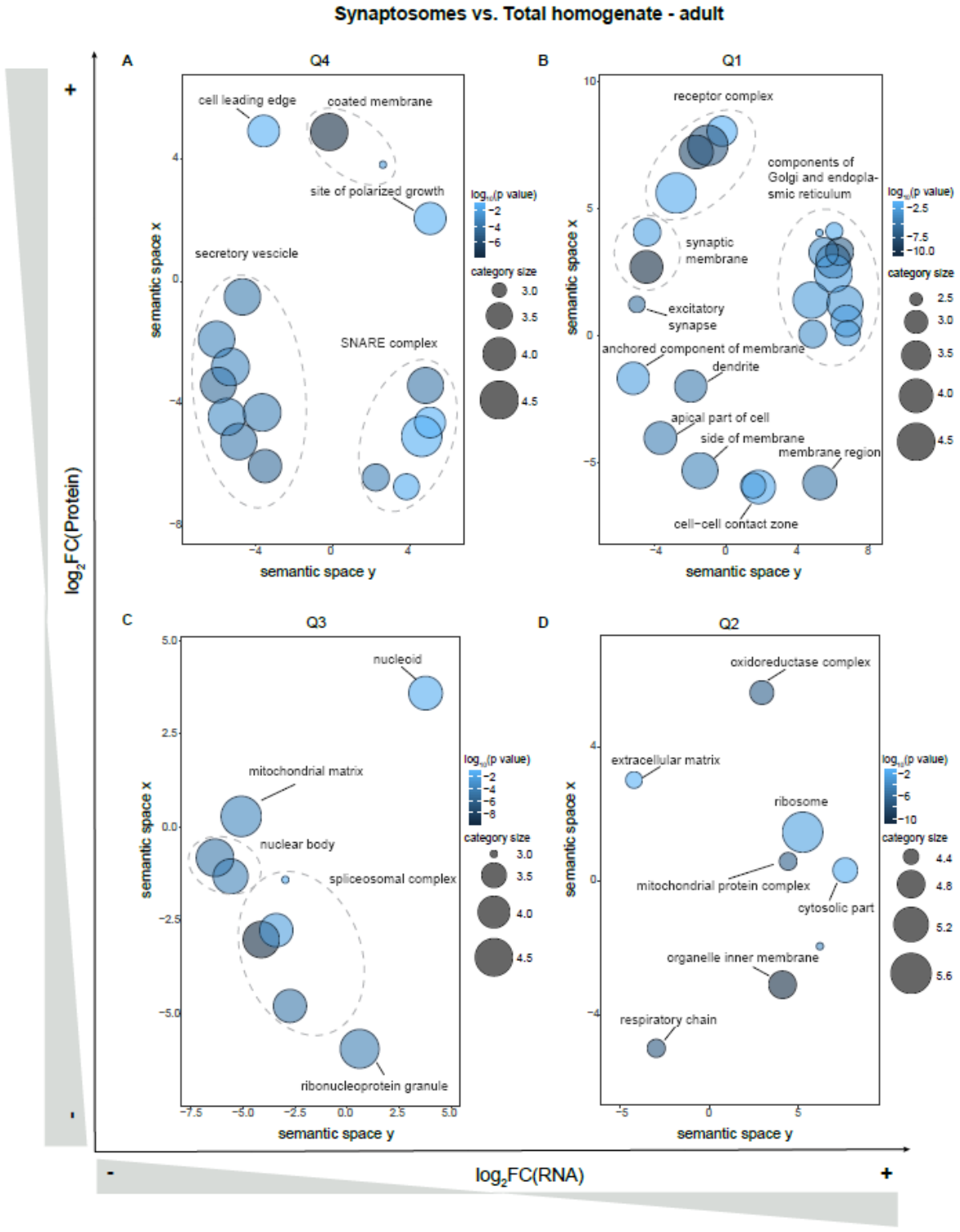

Figure 27. Overrepresentation of Cellular Component Gene Ontology terms in the four quadrants of **Fig.25A** (adult animals). Similar terms are clustered together based on teir semantic similarity using the REVIGO algorithm, and are colored according to $\log_{10}$(p value). **A)** Genes showing synaptosomal enrichment of protein and depletion of transcript. **B)** Genes showing synaptosomal enrichment of both protein and transcript. **C)** Genes showing synaptosomal depletion of both protein and transcript. **D)** Genes showing synaptosomal depletion of protein and enrichment of transcript.

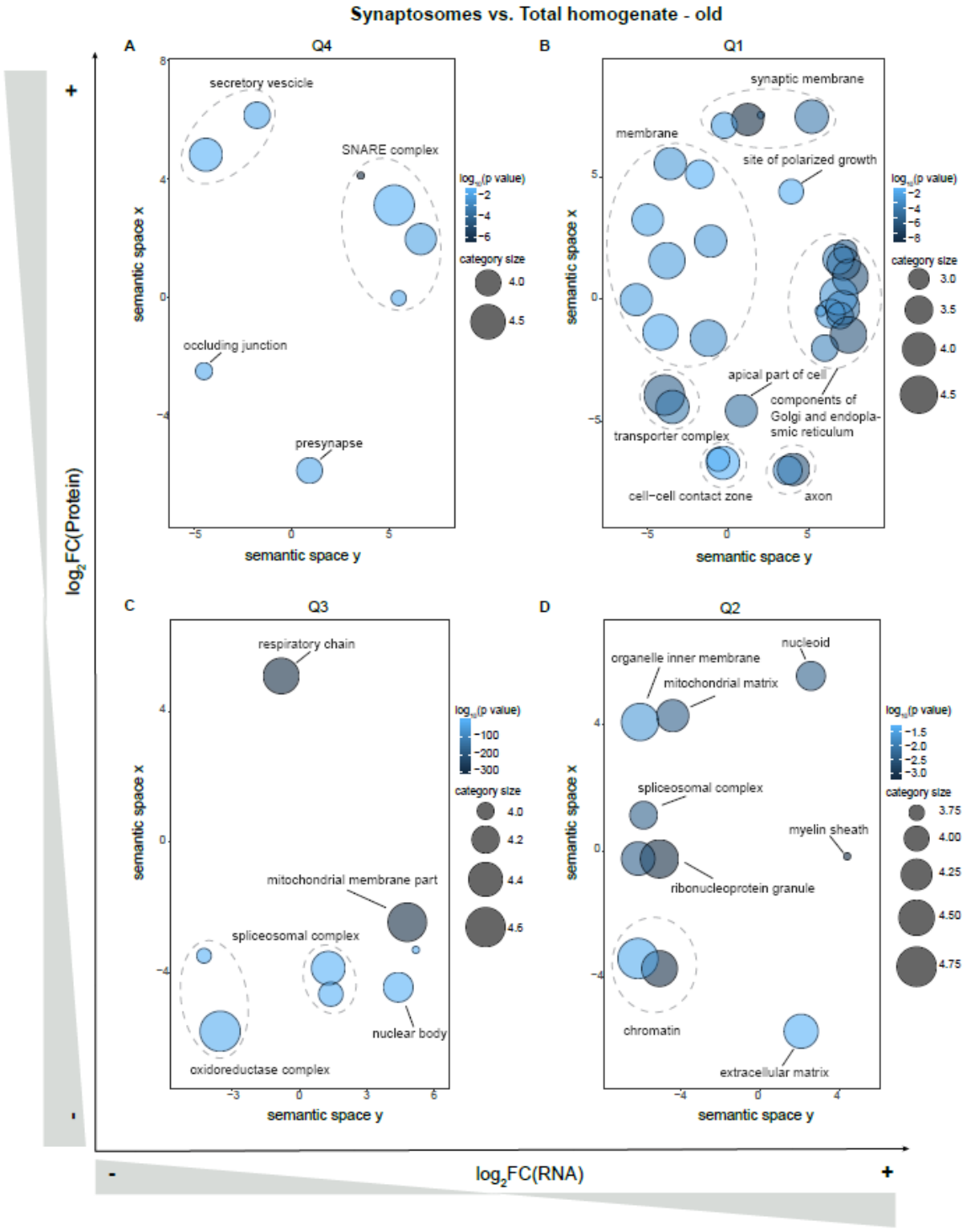

Figure 28. Overrepresentation of Cellular Component Gene Ontology terms in the four quadrants of **Fig.26A** (old animals). Similar terms are clustered together based on their semantic similarity using the REVIGO algorithm, and are colored according to $\log_{10}$(p value). **A)** Genes showing synaptosomal enrichment of protein and depletion of transcript. **B)** Genes showing synaptosomal enrichment of both protein and transcript. **C)** Genes showing synaptosomal depletion of both protein and transcript. **D)** Genes showing synaptosomal depletion of protein and enrichment of transcript.

The presence of ribosomes in synaptic terminals has been extensively reported (see for example Ainsley, Drane, Jacobs, Kittelberger, & Reijmers, 2014 and Hafner, Donlin-Asp, Leitch, Herzog, & Schuman, 2019). I was able to confirm this finding in cortical layers II-III by means of immunofluorescence (**Fig.29**) of ribosomal large subunit (Ribosomal protein 10a – RPL10a) combined with a marker of neuronal processes (Microtubule associated protein 2 – MAP2). As it can be appreciated in **Fig.29**, ribosomes are mainly located in the soma, but some ribosomal particles are also evident in neuronal processes (as indicated by the white arrows)

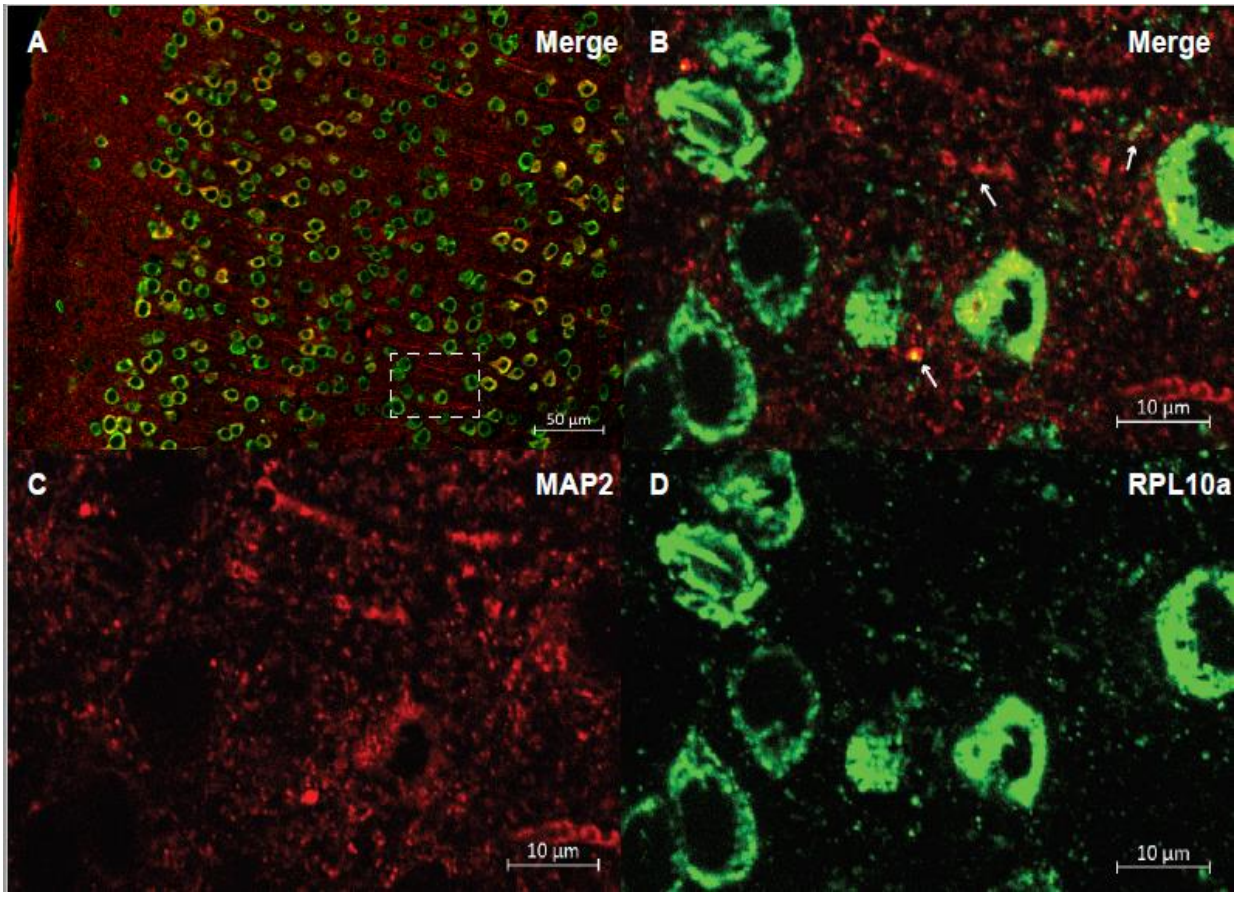

Figure 29. Immunofluorescence of an old (18 months-old) cortex (layers II-III). Immunoreactivity for ribosomal protein 10a (RPL10a) is visualized with green fluorophore, while immunoreactivity for Microtubule associated protein 2 (MAP2) is visualized with a red fluorophore. **A)** Merge 20X magnification; **B)** Merge 63X magnification of the dashed square; **C)**MAP2; **D)** RPL10a. Some instances of colocalization are shown by white arrows.

I was also able to observe, in the same area, the juxtaposition of ribosomal RNA (rRNA) 18S and the presynaptic element, combining the staining for rRNA (Y10b antibody) with the vescicular glutamate transporter 1 (VGLUT1) as a marker of presynaptic terminal (**Fig.30**).

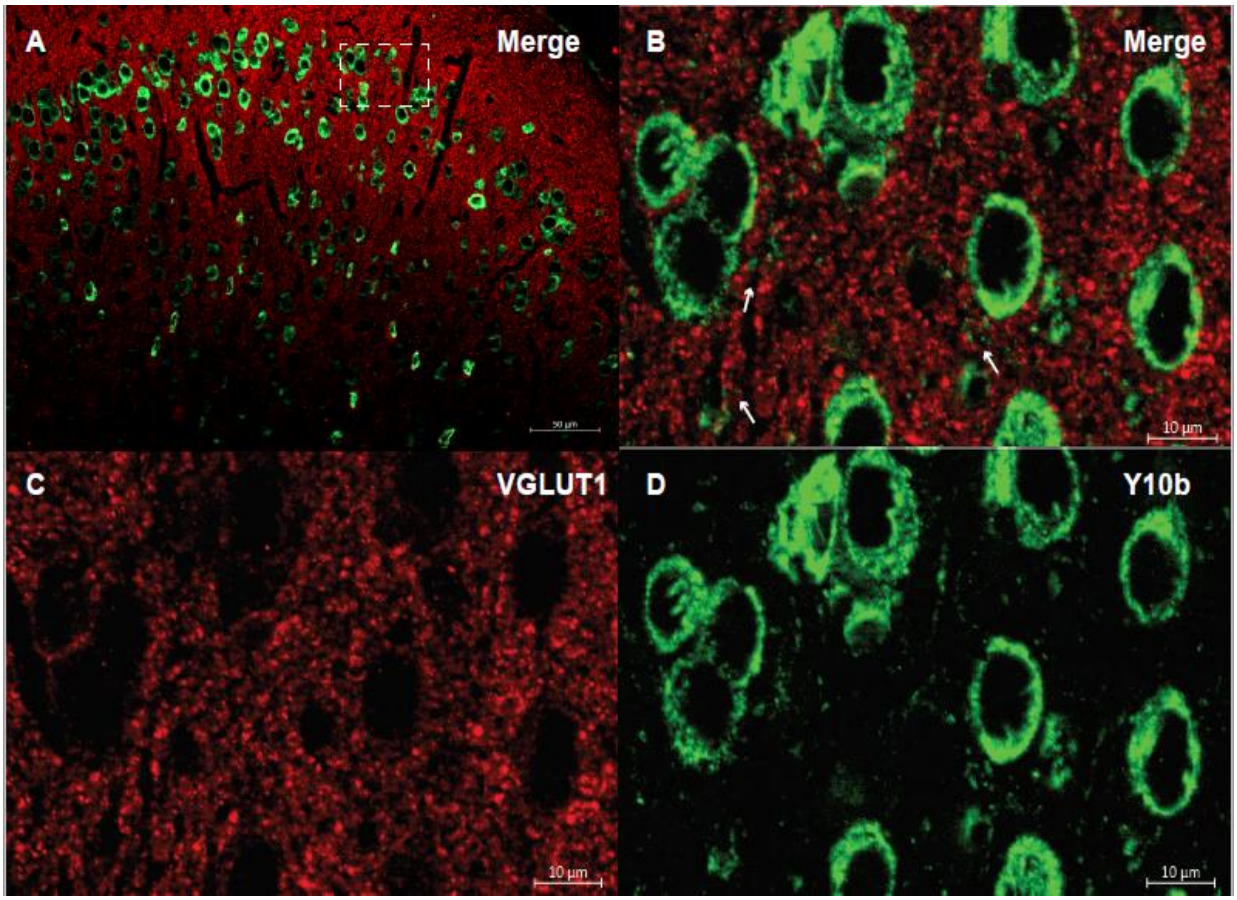

Figure 30. Immunofluorescence of an old (18 months-old) cortex (layers II-III). Immunoreactivity for Vesicular glutamate transporter (VGLUT1) is visualized with red fluorophore, while immunoreactivity for Y10b is visualized with a green fluorophore. **A)** Merge 20X magnification; **B)** Merge 63X magnification of the dashed square; **C)** VGLUT1; **D)** Y10b. Some instances of colocalization are shown by white arrows.

Finally, I could support the notion that synaptic ribosomes are fully assembled, combining the stainings of ribosomal protein (RPL10a) and RNA (Y10b) and observing their almost total colocalization not only in somata, but also in processes (**Fig.31**). The white arrows in **Fig.31** indicate the colocalization of ribosomal proteins and RNAs outside the somatic compartment.

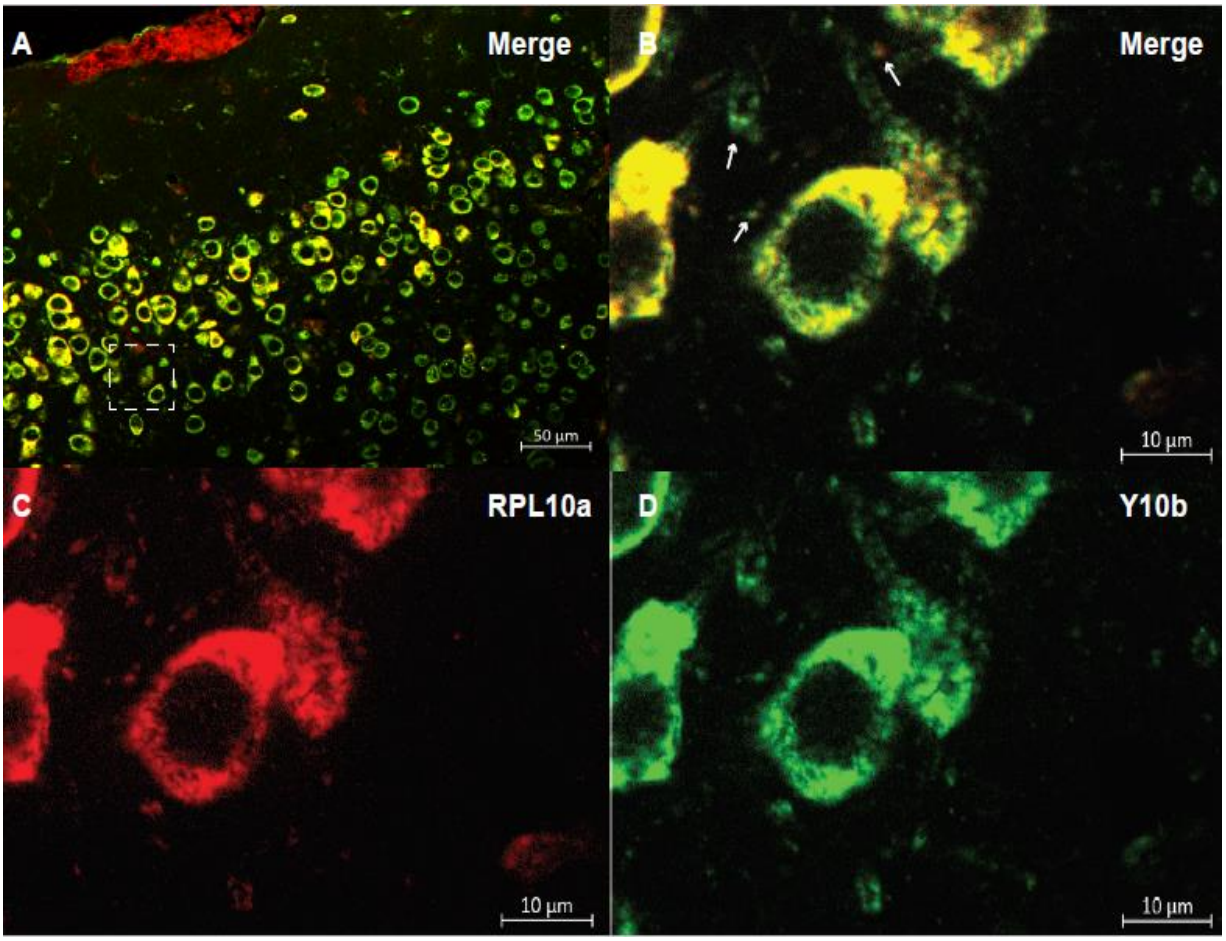

Figure 31. Immunofluorescence of an old (18 months-old) cortex (layers II-III). Immunoreactivity for ribosomal protein 10a (RPL10a) is visualized with red fluorophore, while immunoreactivity for Y10b is visualized with a red fluorophore. **A)** Merge 20X magnification; **B)** Merge 63X magnification of the dashed square; **C)** RPL10a; **D)** Y10b. Some instances of colocalization are shown by white arrows.

4. Non coding RNAs in synaptic compartment

Some non-coding RNAs (ncRNAs) are reported to be particularly enriched in synapses (Rybak-Wolf et al., 2014; Chen et al., 2017). In my dataset, I detected 26431 genes differentially expressed between synaptic and somatic compartment, 35% of which are annotated as ncRNAs (9397 genes). In particular, 10871 transcripts, out of which 827 are annotated as ncRNAs, were significantly enriched in synaptosomes. I compared these with You et al.(2015), Ouwenga et al.(2017) and Zappulo et al.(2017) datasets (**Fig.32**). You and coworkers performed Ribo-zero RNA-seq from total hippocampus somata and neuropil of 5 weeks-old mice hippocampus to analyse circular RNAs (circRNAs) in both compartments. They showed that circRNAs are significantly more enriched in neuropil compartment (You et al., 2015). When comparing our dataset with You et al., I found 51 ncRNA significantly enriched in synapses in both datasets. Only 9 ncRNA with a significant synaptic localization were detected in the comparison with Ouwenga et al. TRAP-seq dataset, this low number is expected since Ouwenga et al. sequencing was highly enriched for ribosome-bound

transcripts. Finally, I found 289 non-coding genes significantly enriched in synaptic compartment in both our dataset and Zappulo et al. dataset. To confirm that ncRNAs significantly enriched in synaptic compartment (N = 827) are translationally repressed, I used the Zappulo et al. dataset and, as control, protein coding RNAs that are significantly enriched in synaptosomes (N = 4083). Probability distribution functions of translation rates were estimated by Gaussian kernel density and are reported as density plots in **Fig.32D**. The very low translation rate confirms that transcript annotated as ncRNAs are not associated to ribosomes ($p < 2.2*10^{-16}$ calculated with Wilcoxon test).

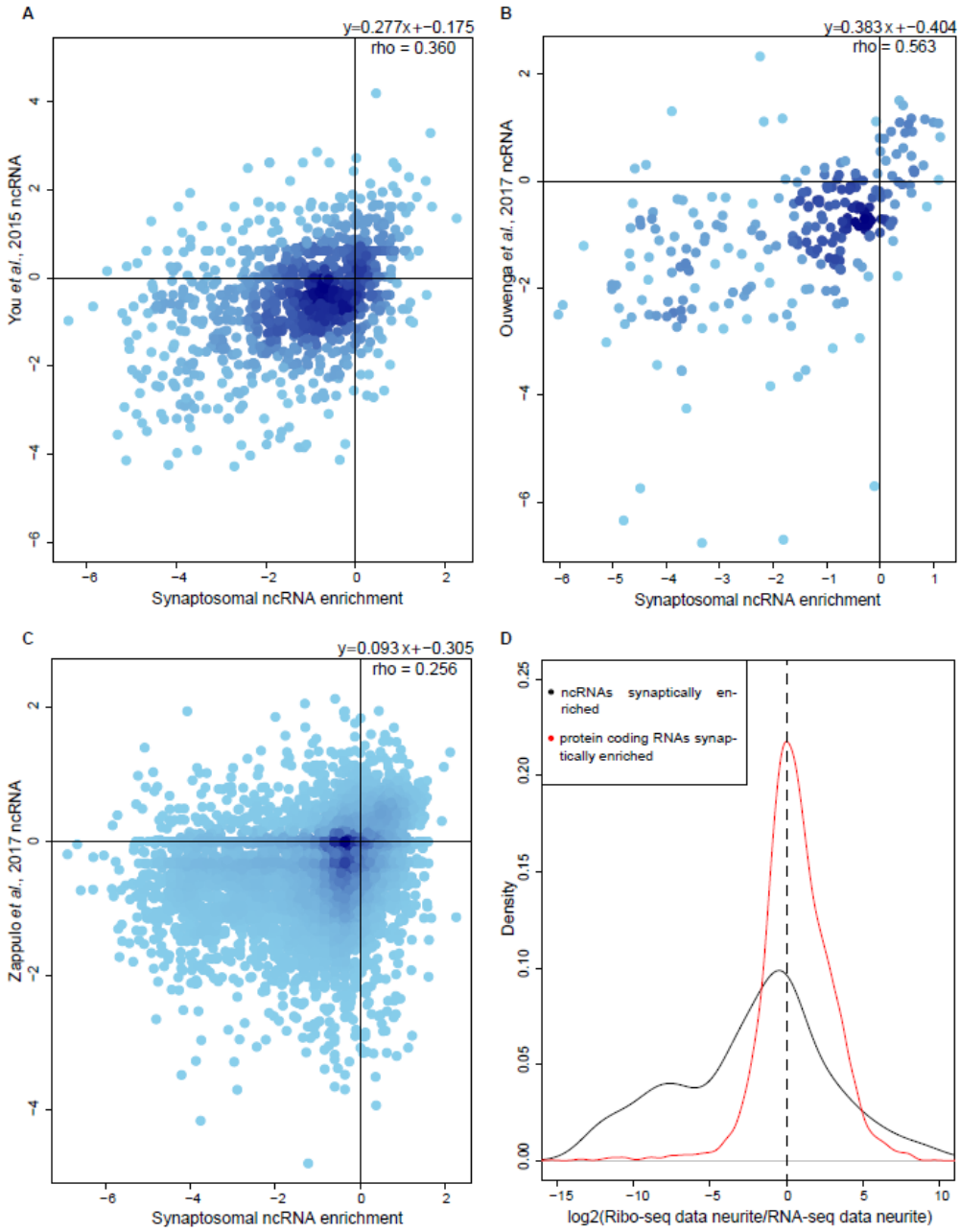

Figure 32. Comparison of synaptosomal enrichment of ncRNAs with published datasets. Enrichment is expressed as fold change synaptosomal fraction vs. total homogenate in logarithmic scale. Correlation was computed as using Spearman's correlation coefficient and reported in the upper right corner of the plot. The

best linear fit of the data equation is reported on the upper right part of the plot. **A)** Comparison with the dataset hippocampal synaptosomal transcript enrichment of You et al. (2015) dataset. **B)** Comparison with the dataset of Translating Ribosome Affinity Purification from cortical neuronal processes of Ouwenga et al., (2017). **C)** Comparison with neurite-enriched transcripts of embryonic neurons from Zappulo et al. (2017). D) Probability density plot of ncRNAs (black line) and protein coding RNAs (red line) synaptically enriched. Samples are non-identical according to Wilcoxon Test ($p < 2.2*10^{-16}$).

I validated three lncRNA highly enriched in synaptosomes by means of qPCR, Gm34838 (Fold Change = 2.63, p value = 0.03), Gm10925 (Fold Change = 1.19, p value = $1.95*10^{-5}$), Gm13340 (Fold Change = 1.10, p value = 0.0001) (**Fig.33**).

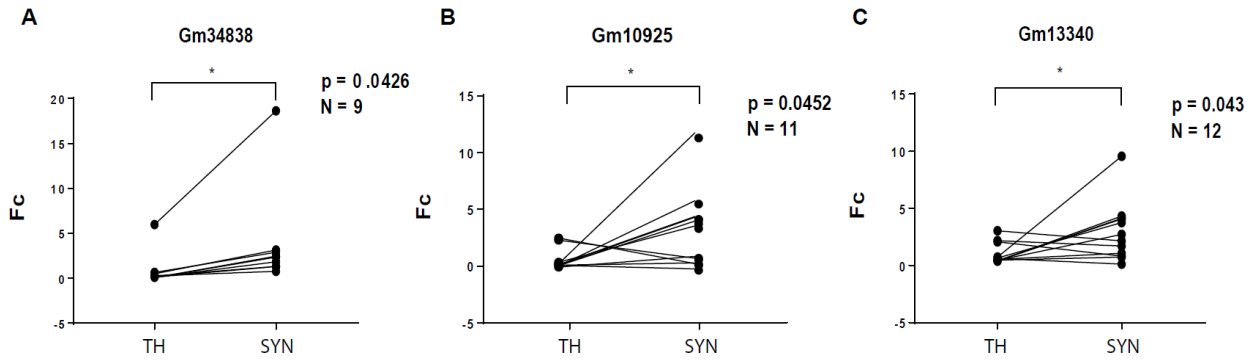

Figure 33. qPCR on synaptically-enriched lncRNAs. The expression values are normalized on *H3F3B*, coding for the histonic protein 3 B. Lines connect fractions derived from the same samples. Total homogenate (TH) and enriched synaptosomes (SYN) were compared. Statistical significance was calculated with paired Student's t-test. **A)** Gm34838 RNA, N = 9; **B)** Gm10925 RNA, N = 11; **C)** Gm13340 RNA, N = 12.

5. Protein stoichiometry analysis in synaptic and somatic compartment

To evaluate whether some protein complexes show different stoichiometry in somatic and synaptic compartment, I applied a previously published analysis method (Ori et al., 2015) to the proteomic dataset. In particular, individual proteome-wide profiles were median-centered, followed by outlier removal; subsequently, the proteomic profiles were restricted to the proteins annotated to be part of protein complexes. Finally an additional complex-wise normalization procedure was performed. First, relative abundances of proteins were calculated with respect to their mean across all conditions. As a next step, the abundance value of each protein was corrected by subtracting the mean relative abundance of the rest of the complex members. This method identifies proteins that are significant up- or down-regulated with respect to the other members of the complex. Among the proteins most affected with respect to the complex, I observed an overrepresentation of complexes involved in spliceosome and mRNA binding at synaptic level (**Tab.2**).

Table 2. The ten proteins most up-regulated in synaptosomes with respect to the other protein complex members

LogFC	adj.P.Val	Protein ID	Protein complex
4.27804	0.000262	Snrpa1	Spliceosome-U2
3.998296	3.26E-05	Hist2h2ab	Nucleosomal protein complex
2.865905	0.000128	Gatad2b	NuRD complex
2.467181	2.61E-05	Nup85	Nuclear pore complex (NPC)
2.463538	0.003391	Hist1h1a	Emerin regulatory complex
2.423403	6.11E-05	Snrpd2	Survival of motor neuron (SMN) complex;
2.31378	2.61E-05	Strap	Survival of motor neuron (SMN) complex
2.16952	7.15E-05	Lsm8	Spliceosome-LSm; emerin C25; emerin C52
2.01389	0.000842	Htatsf1	Spliceosome-A
1.938849	8.65E-06	Ipo4	H3.3 com

6. Global effects of age on protein and transcript composition

In order to visualize the spatial distribution of total homogenate and synaptosomal samples of different ages, I performed Principal Component Analysis (PCA), selecting as features genes that were significantly regulated during adulthood or aging (**Fig.34 A-D**). Furthermore, I correlated each total homogenate and synaptosomes sample with the others, both at RNA and protein level, using Spearman's correlation, and visualized correlation coefficients by means of a heatmap (**Fig.35 A-D**).

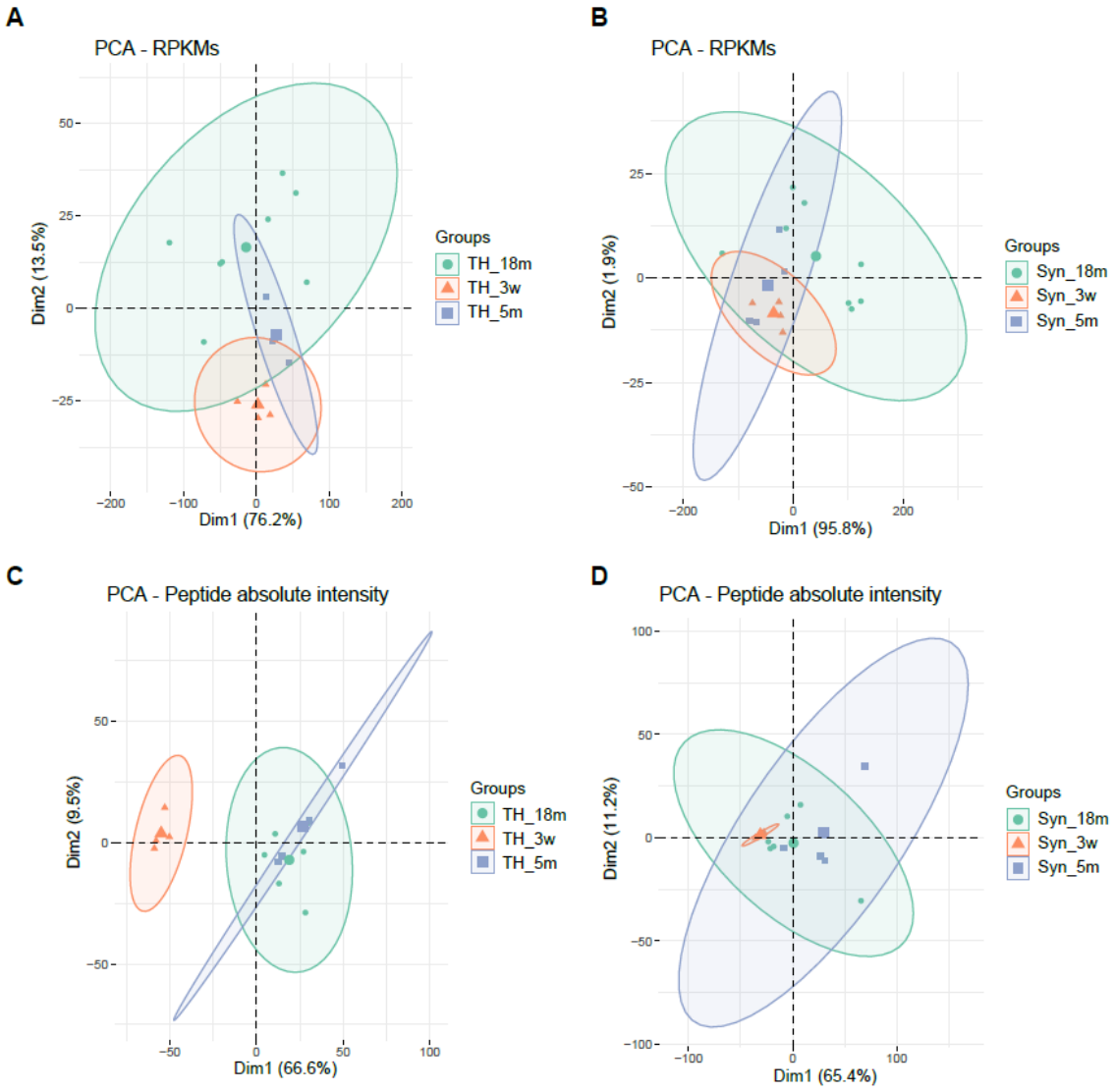

Figure 34. Principal component Analysis (PCA) of RNA Total homogenates (**A**) and Synaptosomes (**B**) and of protein Total homogenates (**C**) and Synaptosomes (**D**). Samples grouped by condition. The bigger dot in the middle of each group indicates the centroid, while the ellipse indicates the dispersion of each group. TH = Total Homogenate, Syn = Synaptosomes.

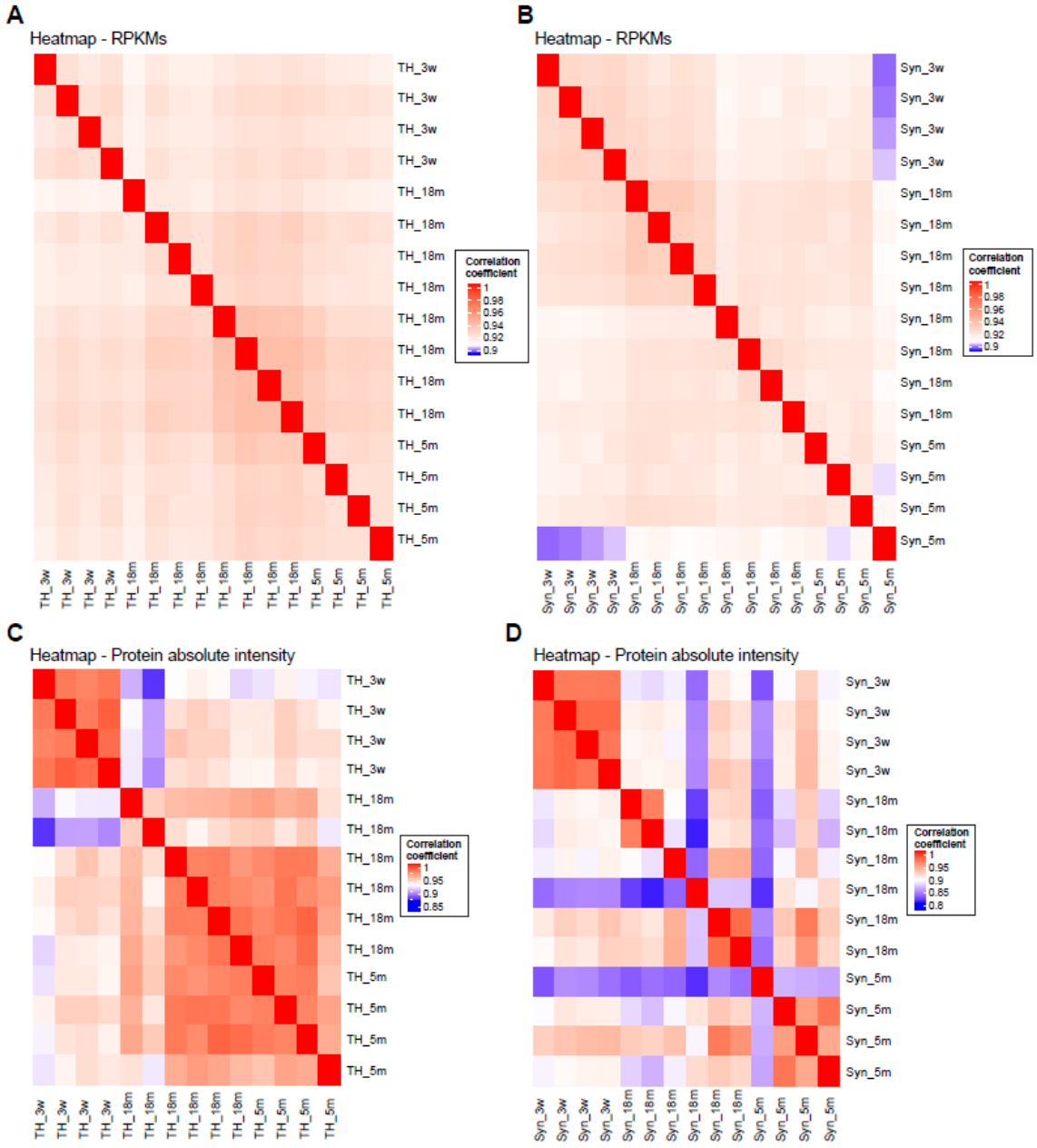

Figure 35. Heatmap of Spearman's correlation between RNA of Total homogenates (**A**) and Synaptosomes (**B**) and protein of Total homogenates (**C**) and Synaptosomes (**D**). Samples are clustered according to their condition. Color code on the right indicates Spearman's correlation coefficient. TH = Total homogenate, Syn = Synaptosomes.

I observed a clear separation between the ages at RNA level. This separation becomes less evident at protein level, this could represent a biological phenomenon suggesting a more homogeneous protein composition across the ages or could be due to the much lower depth of the data generated by proteomic as opposed to transcriptomic.

7. RNA-protein correlation is affected by age

To gain insights in the relationship between transcript and protein abundance, I performed Spearman's correlation between RNA Reads Per Kilobase Million (RPKMs) and correspondent protein absolute intensities (N=2449) for each time point both for total homogenate and synaptosomes. I detected a significant higher correlation in total homogenate as opposed to synaptosomes ($p=0.0002$ evaluated by two-way ANOVA), likely due to transport of some proteins from the soma. I also observed a decrease in correlation as a function of age ($p < 0.0001$ evaluated by two-way ANOVA) (**Fig.36**) indicating age-dependent decoupling between protein and transcript as previously observed in primate total brain homogenate (Wei et al., 2015).

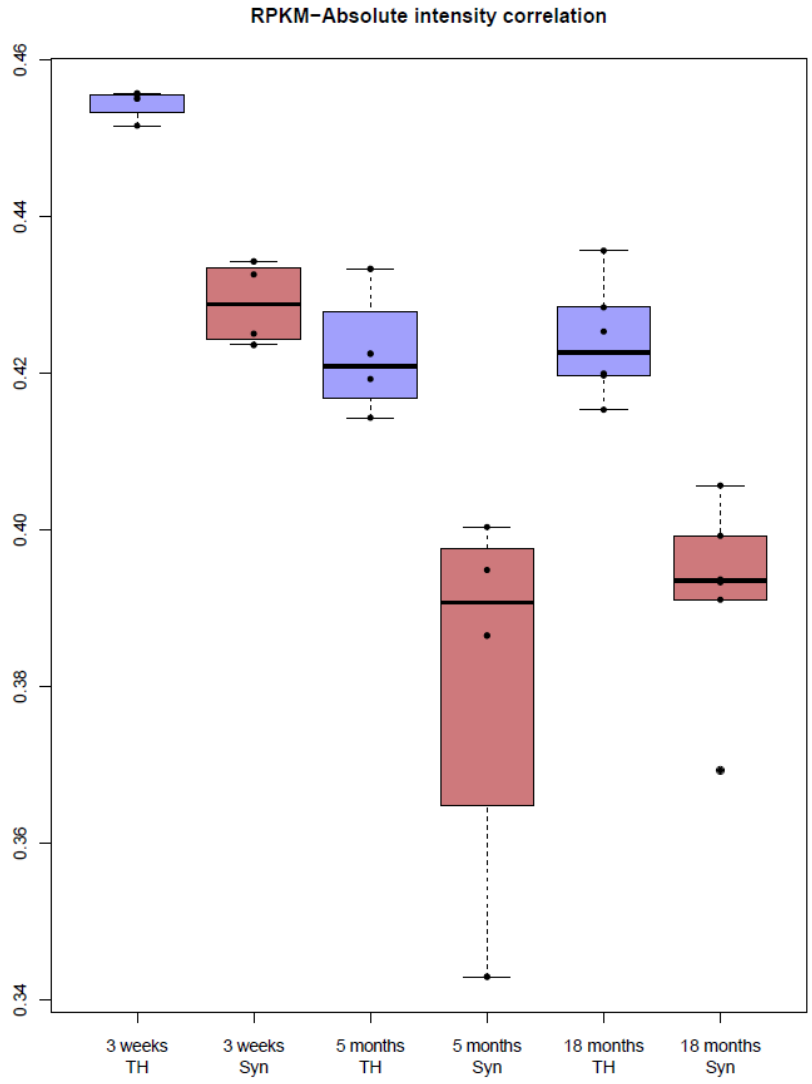

Figure 36. Box plot of the correlation between RNA RPKMs and protein absolute intensities in total homogenate (TH) samples, colored in blue and synaptosomal (Syn) samples, colored in red, at 3 weeks, 5 months and 18 months. Differences between conditions were evaluated by two-way ANOVA.

8. Correlation of proteins and RNAs with age in Total Homogenate

To analyze the behavior of transcripts during aging in total cortical homogenate, I calculated Spearman's correlation of RNA Reads Per Kilobase Million (RPKMs) with age for each gene, as indicated in **Fig.37**. Rho coefficients were calculated for every gene and analyzed using Generally Applicable Gene Enrichment (GAGE) (Luo, Friedman, Shedden, Hankenson, & Woolf, 2009) to obtain Gene Ontology categories enriched for genes whose expression is positively- or negatively correlated with age (**Fig.38**)

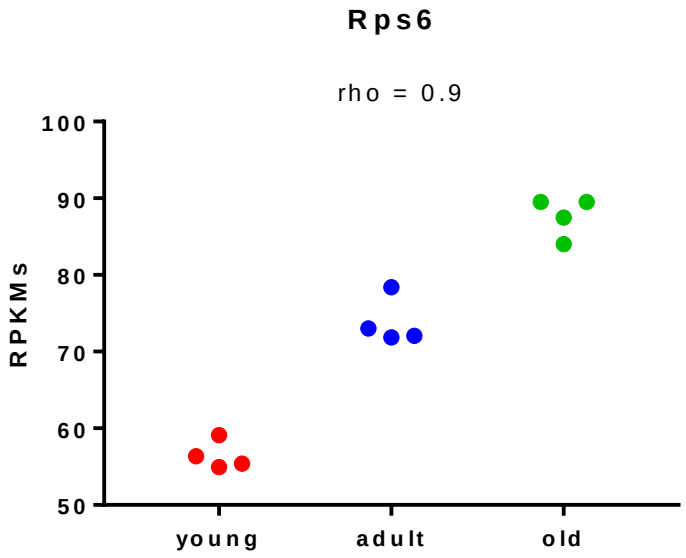

Figure 37.RPKM value of each sample was plotted as a function of age and Spearman's rho coefficient was calculated.

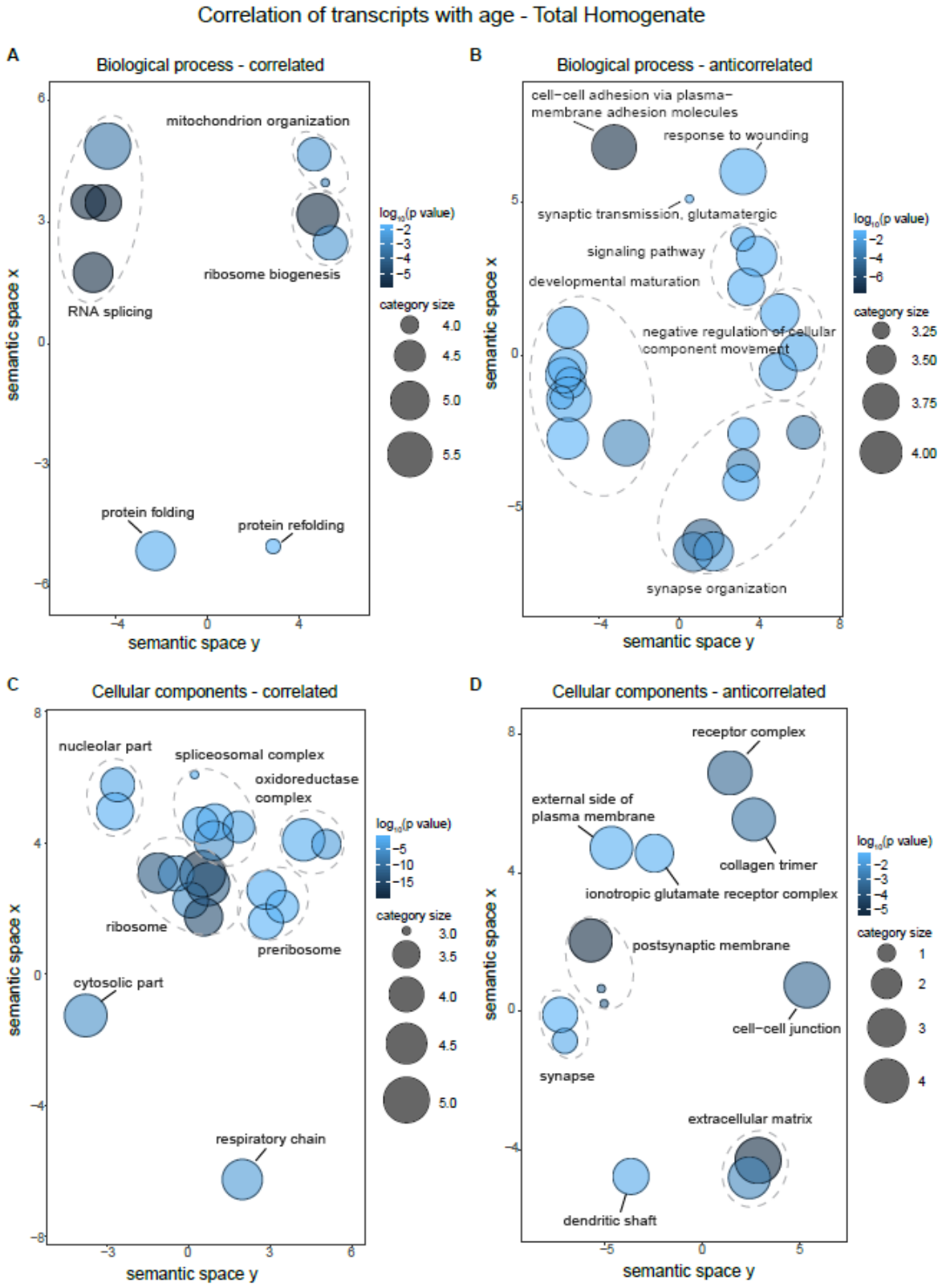

Figure 38. Gene Ontology categories of correlation of transcripts with age. Similar terms are clustered together based on their semantic similarity using the REVIGO algorithm, and are colored according to $\log_{10}$(p value). **A)** Biological process of transcripts positively correlated with age in total homogenate. **B)** Biological

process of transcripts negatively correlated with age in total homogenate. **C)** Cellular components of transcripts positively correlated with age in total homogenate. **D)** Cellular components of transcripts negatively correlated with age in total homogenate.

Transcripts that are upregulated upon aging, or, in other words, have a positive correlation with aging in total homogenate are related to splicing and ribosomes. Transcripts negatively correlated with aging are related to synaptic function. Spearman's correlation was calculated also using protein absolute intensities for each gene, as indicated in **Fig.39**. Then rho values of all the genes were analyzed by GAGE. The results are reported in **Fig.40**.

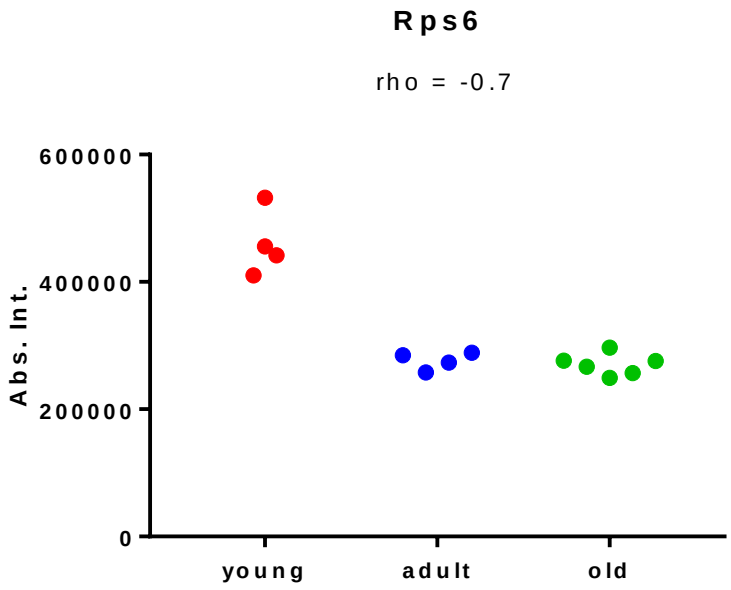

Figure 39. Absolute intensity value of each sample was plotted as a function of age and Spearman's rho coefficient was calculated.

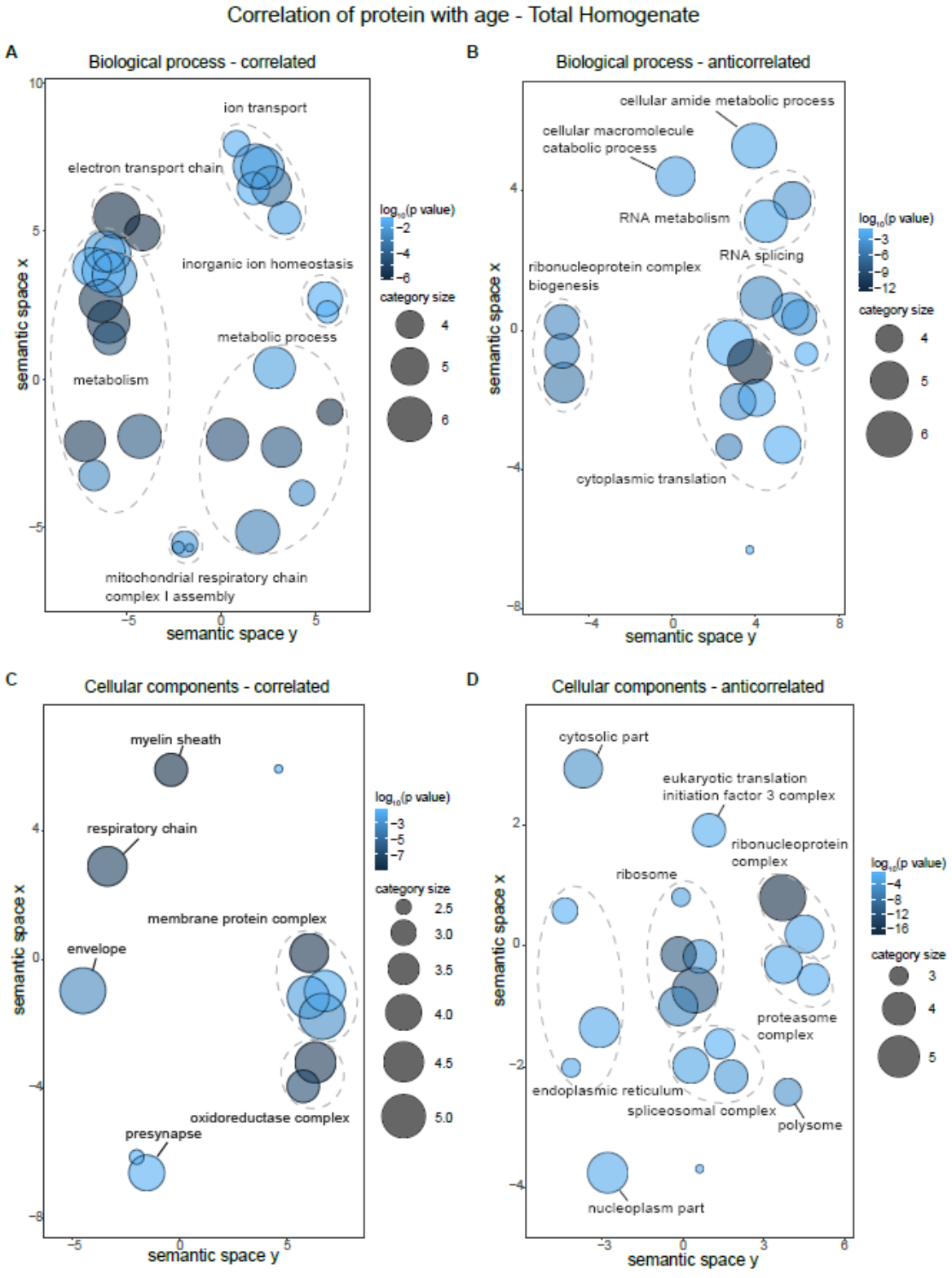

Figure 40. Gene Ontology categories of correlation of proteins with age.Similar terms are clustered together based on their semantic similarity using the REVIGO algorithm, and are colored according to $\log_{10}$(p value). **A)** Biological process of proteins positively correlated with age in total homogenate. **B)** Biological process of proteins negatively correlated with age in total homogenate. **C)** Cellular components of proteins positively

correlated with age in total homogenate. **D)** Cellular components of proteins negatively correlated with age in total homogenate. Plots obtained using ReviGO algorhytm (Supek *et al.*, 2011).

Remarkably, proteins have an opposite behavior as compared to transcripts. In this case, in fact, I observed a positive correlation with age for proteins related to synaptic components and a negative correlation with aging for proteins related to ribosomes and splicing. The same result was observed also in *Nothobranchius furzeri* (Sacramento et al., 2019)

9. Correlation of proteins and RNAs with age in Synaptosomes

I then computed the correlation of synaptic transcripts (expressed in RPKMs) with age using Spearman's correlation. I performed Generally Applicable Gene Enrichment (GAGE) (Luo et al., 2009) to obtain Gene Ontology categories positively- or negatively correlated with age (**Fig.41**).

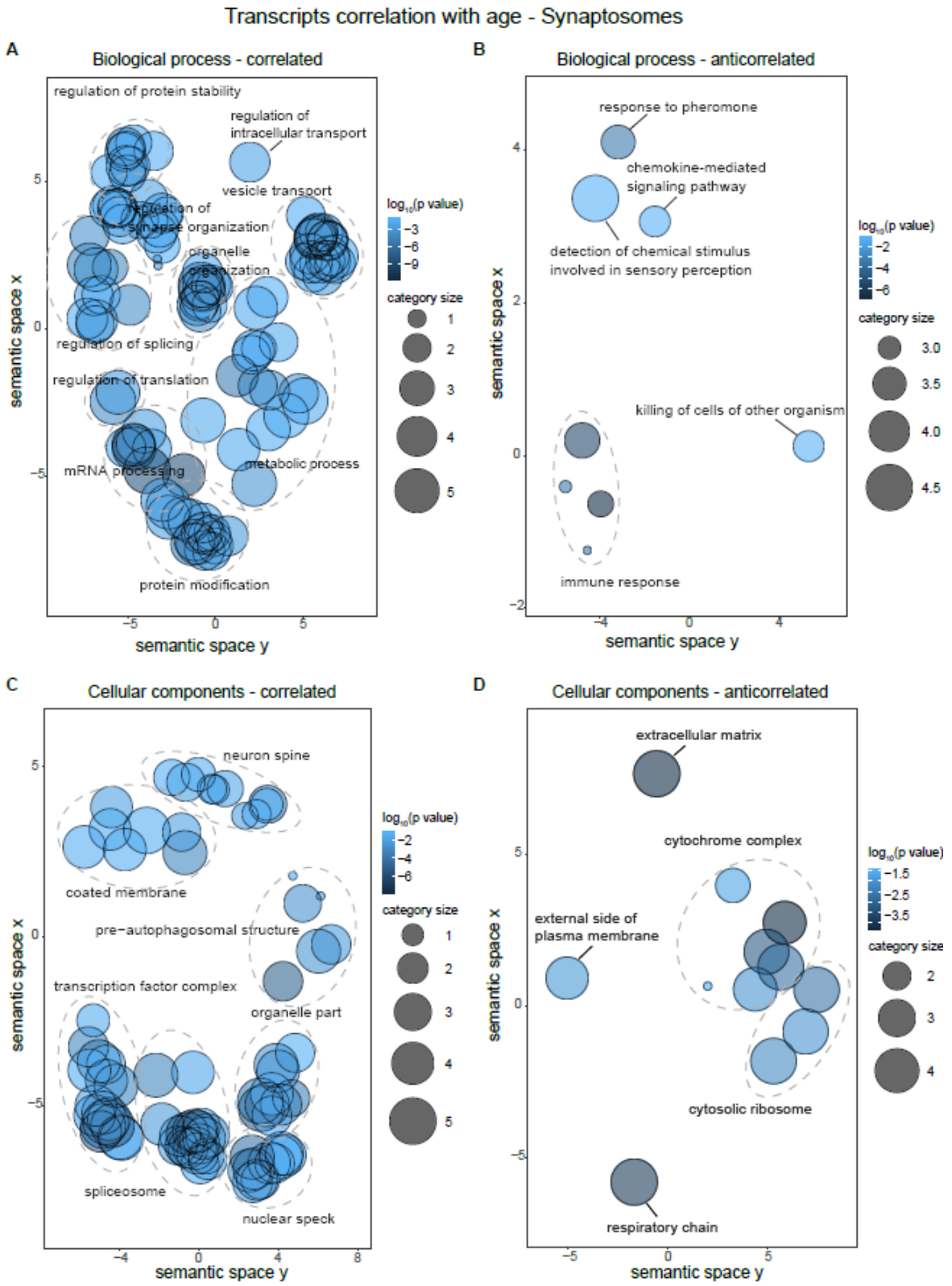

Figure 41. Gene Ontology categories of correlation of synaptic transcripts with age. Similar terms are clustered together based on their semantic similarity using the REVIGO algorithm, and are colored according to $\log_{10}$(p value). **A)** Biological process of transcripts positively correlated with age in synaptosomes. **B)**

Biological process of transcripts negatively correlated with age in synaptosomes. **C)** Cellular components of transcripts positively correlated with age in synaptosomes. **D)** Cellular components of transcripts negatively correlated with age in synaptosomes.

At synaptic level I observed that transcripts belonging to synaptic components are positively correlated with age, whilst in total homogenate they were negatively correlated with age (**Fig.38D** and **41C**). On the other hand, transcripts related to ribosomal genes are negatively correlated with age in synapse, while they were positively correlated with age in total homogenate (**Fig.38C** and**41D**), therefore the relative synaptic enrichment level for these genes decreases upon aging. The same process was repeated using protein absolute intensities (**Fig.42**), but in this case, I found no biological process categories significantly correlated with aging.

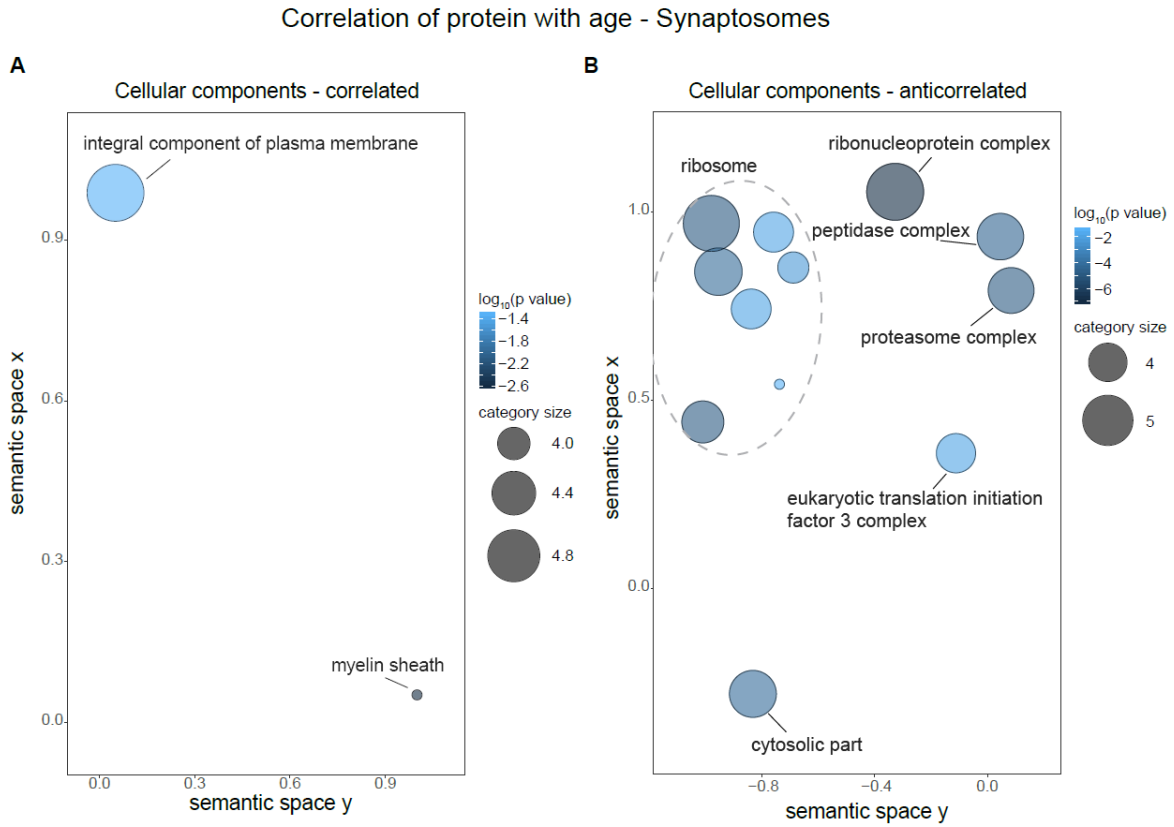

Figure 42. Gene Ontology categories of correlation of synaptic proteins with age. Similar terms are clustered together based on their semantic similarity using the REVIGO algorithm, and are colored according to $\log_{10}$(p value). **A)** Cellular components of proteins positively correlated with age in synaptosomes. **B)** Cellular components of proteins negatively correlated with age in synaptosomes.

As in total homogenate, I observed that proteins related to ribosome are negatively correlated with age in synaptosomes. Interestingly, I also noticed that proteins related to proteasome are negatively correlated with age at synaptic level.

10. Synaptic gradient of proteins and transcripts is affected by age

I analyzed whether the soma-synapse gradient of transcript or protein is affected by age. For each sample, the ratio between normalized counts in synaptosomal fraction and total homogenate was calculated for each transcript and these values were then correlated with age. This process yielded 2917 genes whose enrichment significantly correlated with age (p value < 0.05). These genes were analyzed using Generally Applicable Gene Enrichment (GAGE) (Luo et al., 2009) to obtain Gene Ontology categories enriched in members positively- or negatively-correlated with age in synaptosomes (**Fig.43**). I observed that categories related to mitochondria and respiratory chain have a positive correlation with age (**Fig.43A**), while categories related to ribosomes have a negative correlation with age (**Fig.43B**).

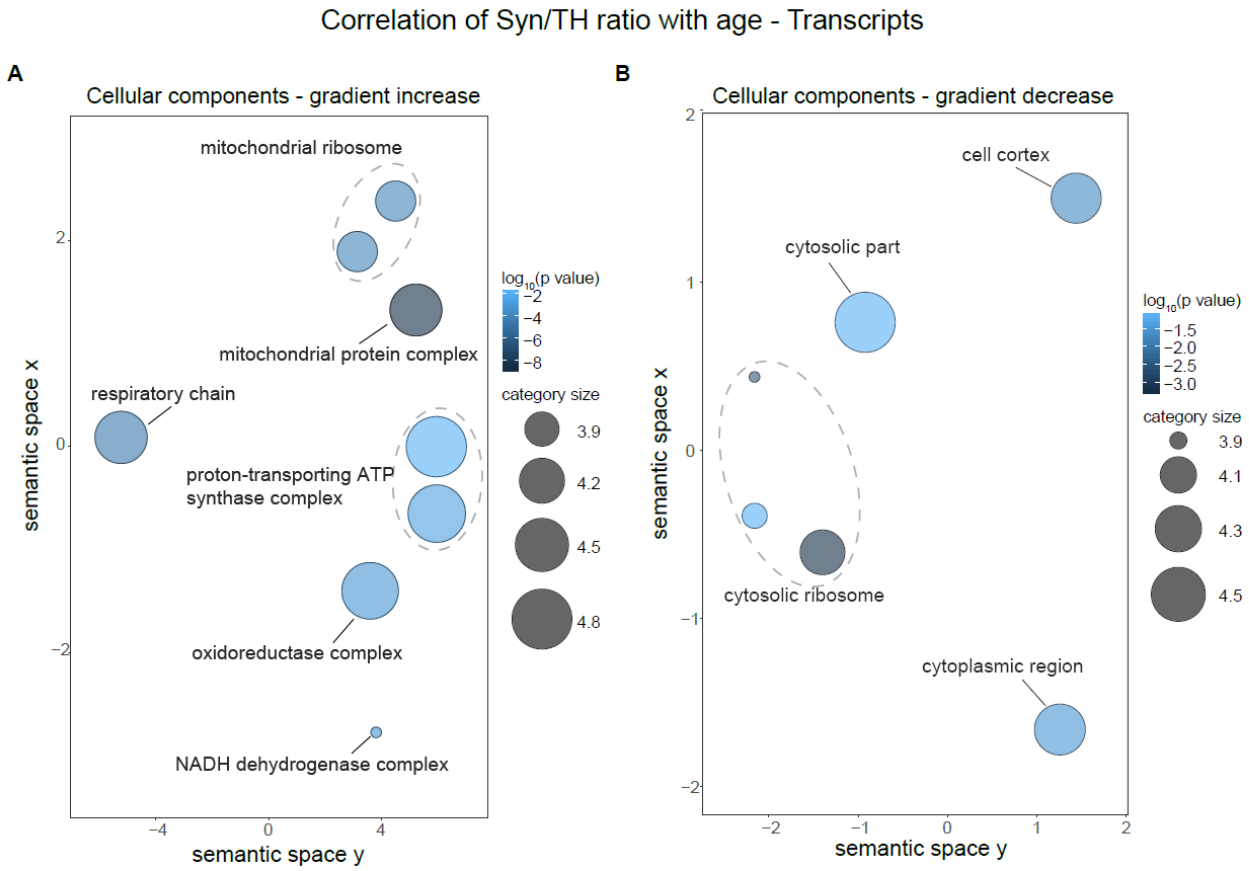

Figure 43. Gene Ontology categories of correlation of the ratio between synaptosomes and total homogenate with age at transcript level. Similar terms are clustered together based on their semantic similarity using the

REVIGO algorithm, and are colored according to $\log_{10}$(p value). **A)** Cellular components of transcripts showing positive gradient to synapses with aging. **B)** Cellular components of transcripts whose gradient to synaptic compartment decreases with aging. TH = Total Homogenate, Syn = Synaptosomes.

The same process was repeated for proteins, using ratios of absolute intensities in the two compartments. 389 genes significantly correlated with age (p value < 0.05) were identified. I observed a positive correlation with aging of cellular components GO categories cytosolic small ribosomal subunit (q value = 0.0002) and small ribosomal subunit (q value = 0.018). Therefore, I concluded that the gradient from soma to synapse of ribosomal proteins increases with age, while the gradient of transcripts coding for ribosomal proteins decreases with age.

11. Decoupling between synaptic and somatic compartments during aging

A comparison of transcripts regulated between young and adult stage in total cortical homogenate and synaptosomes was performed yielding 3591 genes regulated in either of the two compartments. The Fold Change of these genes in total homogenate and synaptosomes is highly correlated (rho = 0.775 p value < $2.2*10^{-16}$ calculated with Spearman's correlation), suggesting that transcript changes in the synapse are driven by the soma (**Fig.44A**). The same process was repeated for transcripts regulated during aging, yielding 5506 genes commonly regulated in the two compartments. During aging, the correlation between total homogenate and synaptosomes drastically decreases (rho = 0.059, p value = $1.262*10^{-5}$ calculated with Spearman's correlation), suggesting that synaptic compartment becomes decoupled from the soma (**Fig.44B**).

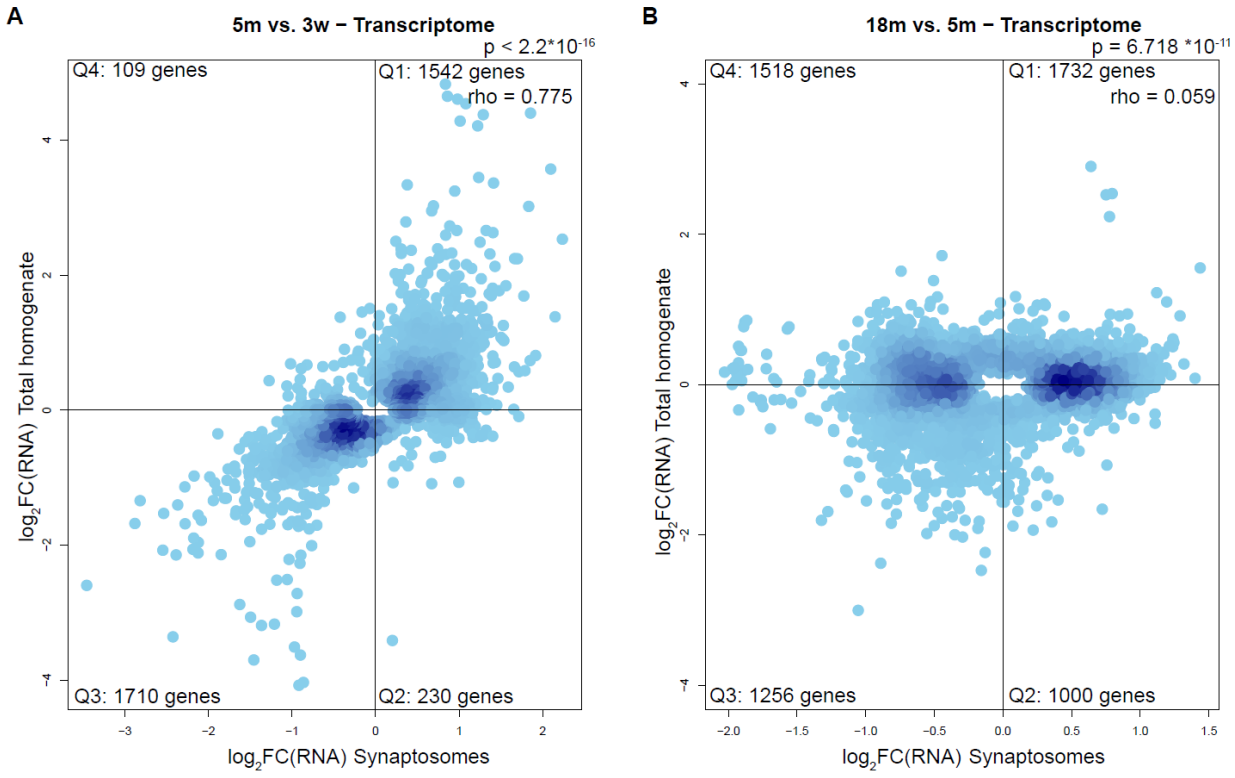

Figure 44. Comparison between transcripts regulated during adulthood and aging in total homogenate and synaptic compartment.**A)** Enrichment is expressed as fold change 5 months vs. 3 weeks in total homogenate and synaptosomes in logarithmic scale. The distribution of genes in each quadrant is not uniform according to Fisher's exact test ($p < 2.2*10^{-16}$). Correlation was computed as using Spearman's correlation coefficient and reported in the upper right corner of the plot (rho = 0.775, $p < 2.2*10^{-16}$). **B)** Enrichment is expressed as fold change 18 months vs. 5 months in total homogenate and synaptosomes in logarithmic scale. The distribution of genes in each quadrant is not uniform according to Fisher's exact test ($p = 6.718*10^{-11}$). Correlation was computed as using Spearman's correlation coefficient and reported in the upper right corner of the plot (rho = 0.059, $p = 1.262* 10^{-5}$).

The same decoupling between total homogenate and synaptosomes during aging was observed at proteome level, with a correlation of the two compartments decreasing from 0.605 during adulthood (**Fig.45A**) to 0.262 during aging (**Fig.45B**).

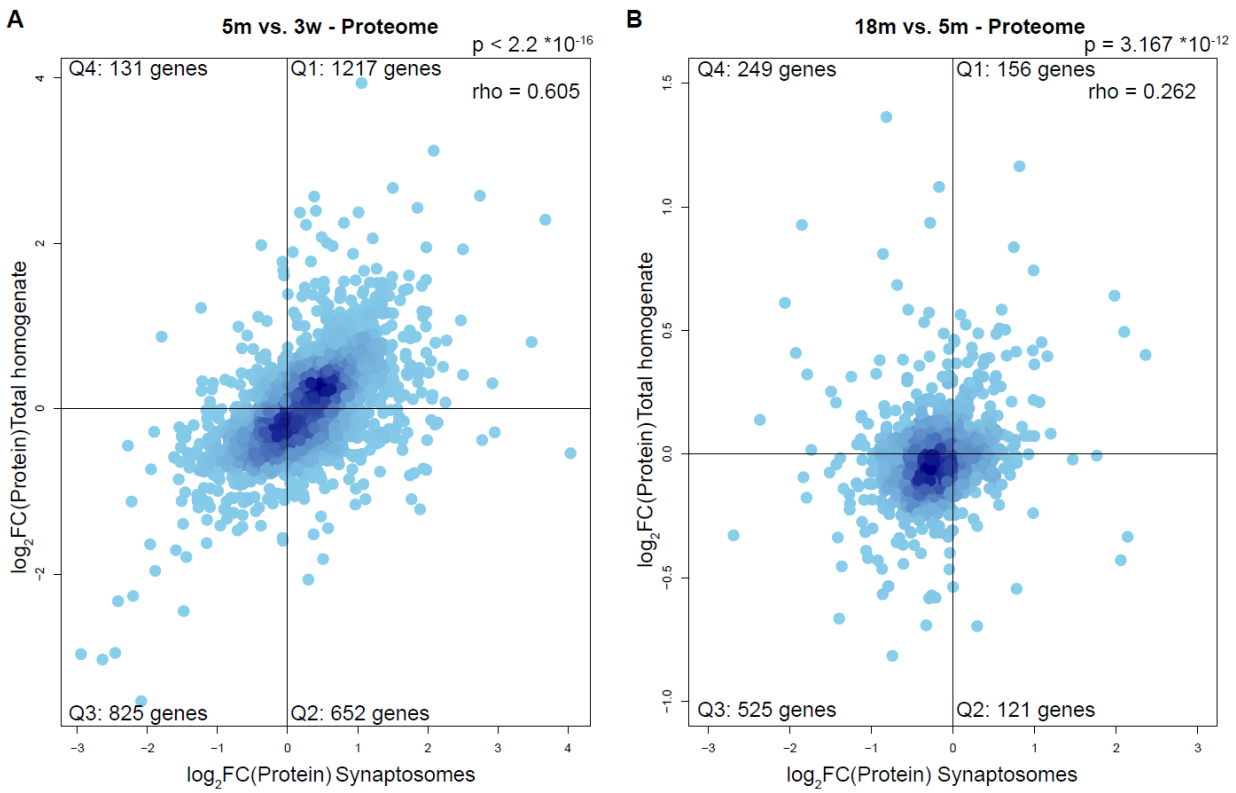

Figure 45. Comparison between proteins regulated during adulthood and aging in total homogenate and synaptic compartment. **A)** Enrichment is expressed as fold change 5 months vs. 3 weeks in total homogenate and synaptosomes in logarithmic scale. The distribution of genes in each quadrant is not uniform according to Fisher's exact test ($p < 2.2*10^{-16}$). Correlation was computed as using Spearman's correlation coefficient and reported in the upper right corner of the plot (rho = 0.605, $p < 2.2*10^{-16}$). **B)** Enrichment is expressed as fold change 18 months vs. 5 months in total homogenate and synaptosomes in logarithmic scale. The distribution of genes in each quadrant is not uniform according to Fisher's exact test ($p = 3.167*10^{-12}$). Correlation was computed as using Spearman's correlation coefficient and reported in the upper right corner of the plot (rho = 0.262, $p < 2.2*10^{-16}$).

The genes of each quadrant of **Fig.44** were analyzed using WebGestalt website (http://www.webgestalt.org/) and ReviGO algorhytm to gain a better insight on the Gene Ontology categories affected (**Fig.46** and **Fig.47**). I observed that ribosomal transcripts are upregulated in both compartments already at 5 months (**Fig.46B**), and this upregulation becomes stronger, especially at synaptic level, during aging (**Fig.47B, D**). At 18 months the upregulation of transcripts related to proteasome and mitochondrial parts is detectable in both total homogenate and synaptosomes (**Fig.47B**). Interestingly, I also noticed an upregulation of transcripts related to the spliceosomal complex only in synaptic compartment during aging (**Fig.47D**).

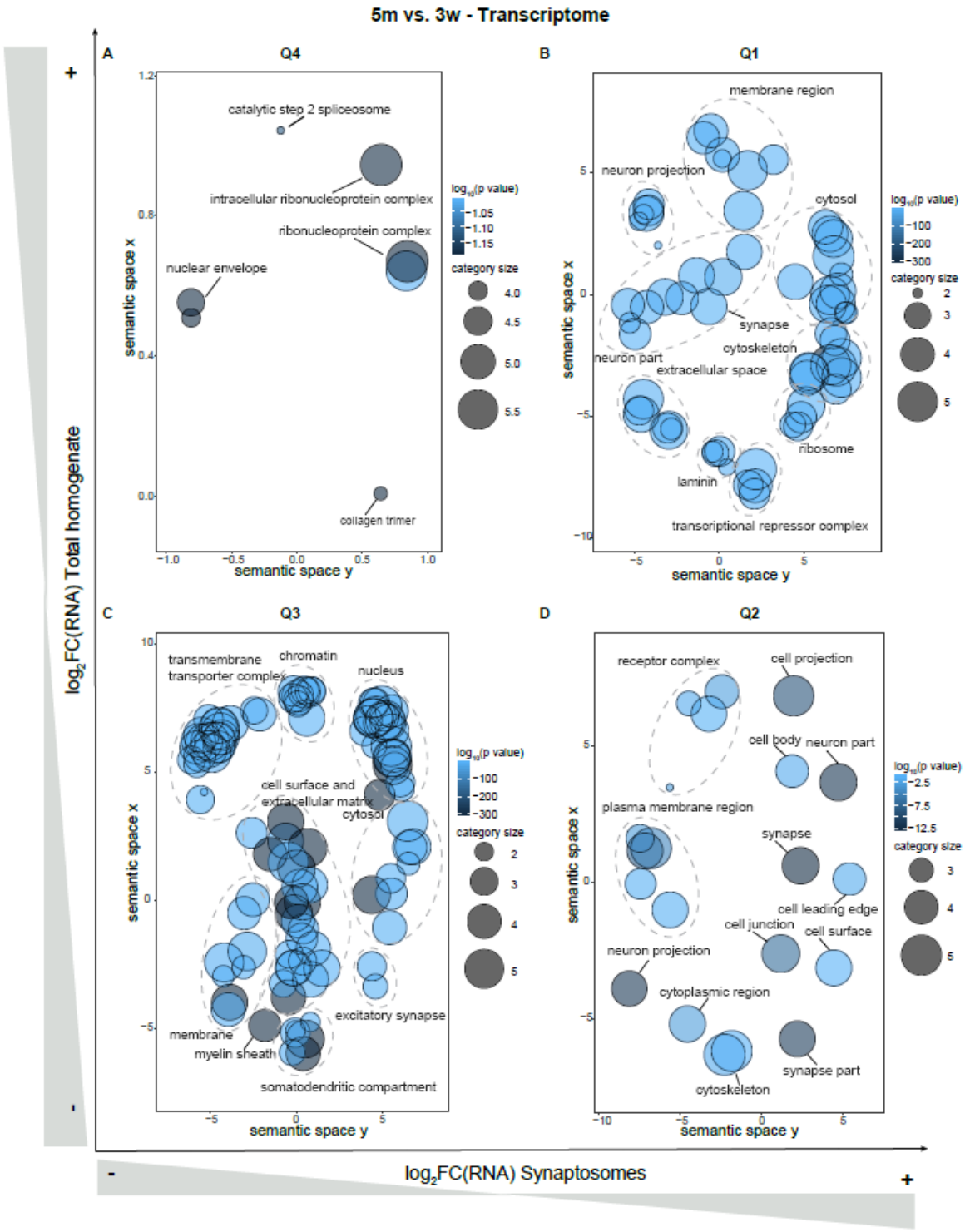

Figure 46. Gene Ontology categories of transcripts regulated during adulthood in total homogenate and synaptic compartment (**Fig.44A**). Similar terms are clustered together based on their semantic similarity using the REVIGO algorithm, and are colored according to $\log_{10}$(p value). **A)**Cellular components of transcripts upregulated at 5 months in total homogenate and synaptosomes. **B)** Cellular components of transcripts upregulated at 5 months in synaptosomes, but not in total homogenate. **C)** Cellular components of transcripts downregulated at 5 months in total homogenate and synaptosomes. **D)** Cellular components of transcripts upregulated at 5 months in total homogenate, but not in synaptosomes.

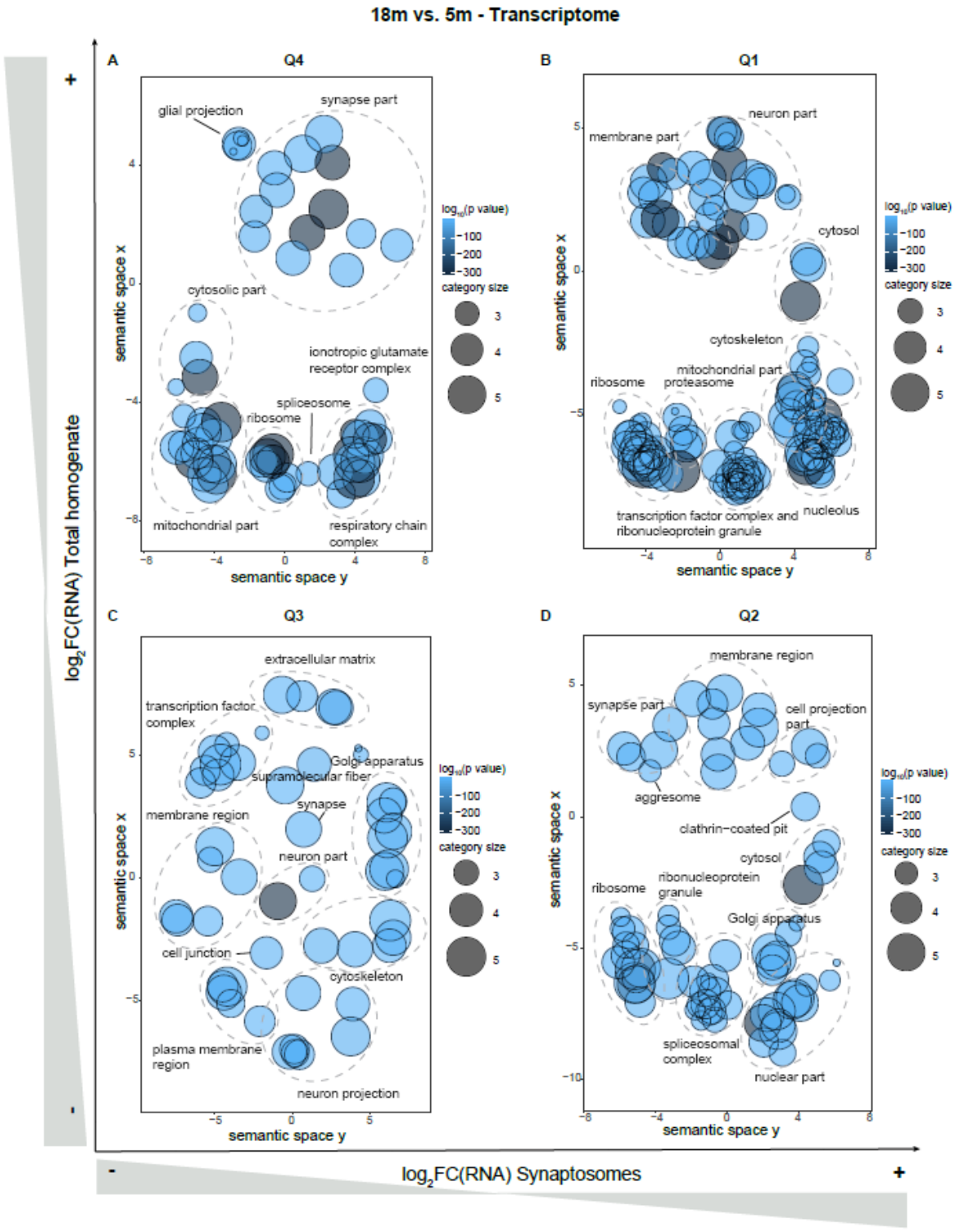

Figure 47. Gene Ontology categories of transcripts regulated during aging in total homogenate and synaptic compartment (**Fig.44B**). Similar terms are clustered together based on their semantic similarity using the REVIGO algorithm, and are colored according to $\log_{10}$(p value). **A)** Cellular components of transcripts upregulated at 18 months in total homogenate and synaptosomes. **B)** Cellular components of transcripts

upregulated at 18 months in synaptosomes, but not in total homogenate. **C)** Cellular components of transcripts downregulated at 18 months in total homogenate and synaptosomes. **D)** Cellular components of transcripts upregulated at 18 months in total homogenate, but not in synaptosomes.

The same Gene Ontology analysis was repeated for each quadrant of **Fig.45** and is reported in **Fig.48** and **Fig.49**. At proteomic level, I observed during adulthood an almost opposite regulation for genes belonging to spliceosome and ribosomes categories. Spliceosomal proteins are indeed upregulated at synaptic level during adulthood (**Fig.48B**), while the upregulation of transcripts related to this category at synaptic level during aging is not mirrored by an upregulation at protein level (**Fig.47D** and **49D**). For what concerns ribosomes, while at transcript level I observed an upregulation of this category in both total homogenate and synaptosomes during adulthood and aging (**Fig.46B** and **47B, D**), at protein level I detected a downregulation in both compartments at 5 months (**Fig.48C**) that is completely reverted at 18 months (**Fig.49B, D**). For what concerns proteins belonging to proteasome category, they are downregulated in both compartments during adulthood (**Fig.48C**) and this regulation is stable during aging, since this category is not detected at 18 months. This differential regulation suggests a decoupling between transcriptome and proteome that I will address in the next section. Finally, there is a downregulation of synaptic proteins both in total homogenate and synapses during aging (**Fig.49C**), and this might justify the decrease of synaptic contacts reported by Morrison & Baxter(2012).

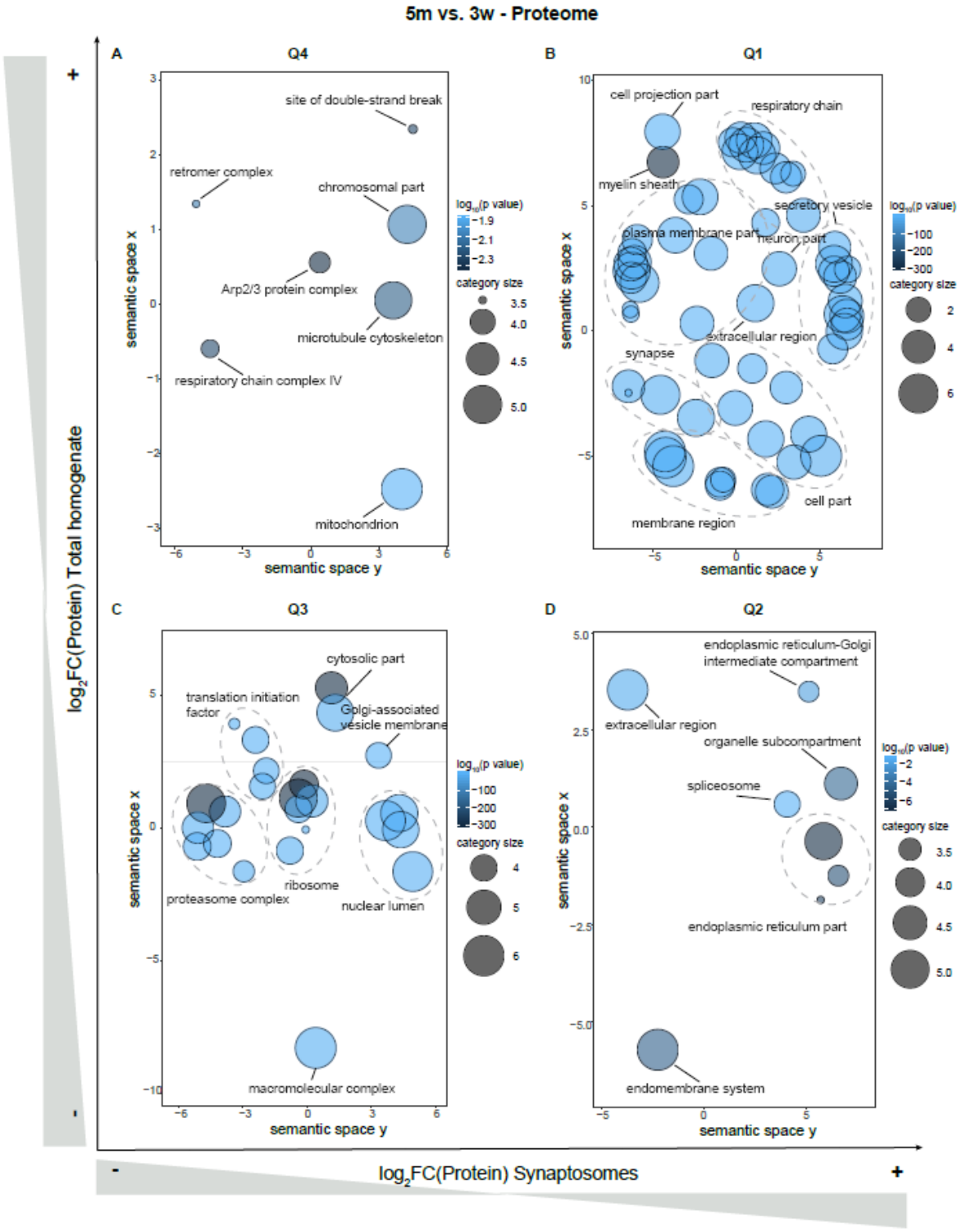

Figure 48. Gene Ontology categories of proteins regulated during adulthood in total homogenate and synaptic compartment (**Fig.45A**). Similar terms are clustered together based on their semantic similarity using the REVIGO algorithm, and are colored according to $\log_{10}$(p value). **A)** Cellular components of proteins upregulated at 5 months in total homogenate and synaptosomes. **B)** Cellular components of proteins upregulated at 5 months in synaptosomes, but not in total homogenate. **C)** Cellular components of proteins

downregulated at 5 months in total homogenate and synaptosomes. **D)** Cellular components of proteins upregulated at 5 months in total homogenate, but not in synaptosomes.

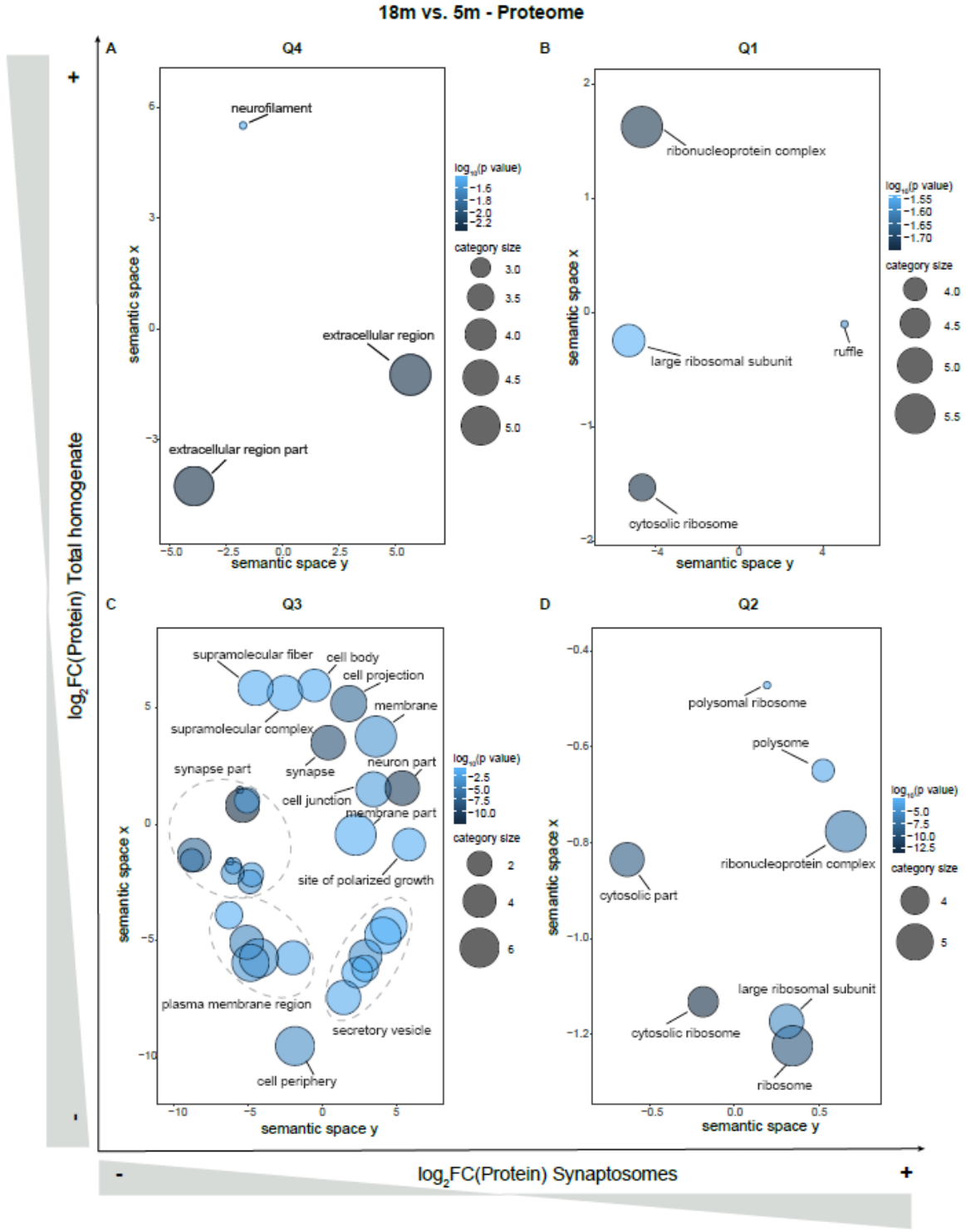

Figure 49. Gene Ontology categories of proteins regulated during aging in total homogenate and synaptic compartment (**Fig.45B**). Similar terms are clustered together based on their semantic similarity using the

REVIGO algorithm, and are colored according to log_{10}(p value). **A)** Cellular components of proteins upregulated at 18 months in total homogenate and synaptosomes. **B)** Cellular components of proteins upregulated at 18 months in synaptosomes, but not in total homogenate. **C)** Cellular components of proteins downregulated at 18 months in total homogenate and synaptosomes. **D)** Cellular components of proteins upregulated at 18 months in total homogenate, but not in synaptosomes.

12. Decoupling between transcriptome and proteome during aging

To better analyze the relationship between transcriptome and proteome in total cortical homogenate during aging, transcripts enriched in total homogenate at 5 months were compared with the respective proteins, yielding 2584 genes significantly regulated at transcript or protein level (**Fig.50A**). I also highlighted in the plot of **Fig.50A** genes belonging to the GO categories translation (GO:0006412), ribosomes (GO:0005840), respiratory chain (GO:0070469) and proteasome (GO:0000502)(**Fig.50B**).

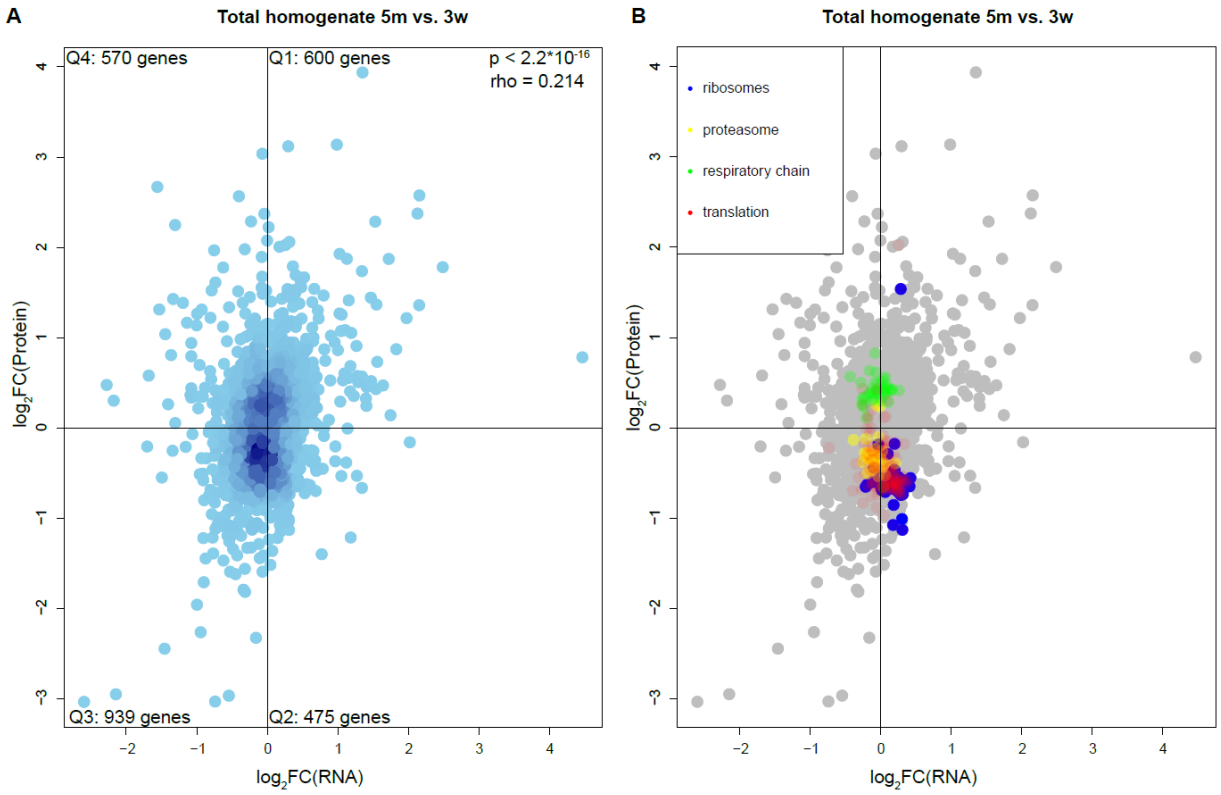

Figure 50. Genes significantly regulated in total cortical homogenate during adulthood at proteome and transcriptome level. **A)** Proteins and RNAs enrichment are plotted as log of the ratio 5 months vs. 3 weeks. Quadrants were named clockwise, starting from the upper right one. The distribution of genes in each quadrant is not uniform according to Fisher's exact test ($p < 2.2*10^{-16}$). Protein and RNA fold changes were correlated using Spearman's correlation (rho = 0.214, $p < 2.2*10^{-16}$). **B)** Genes belonging to specific Gene Ontology (GO) terms were highlighted in different colors, red = translation, yellow = proteasome, blue = ribosome, green = respiratory chain as indicated also in the legend.

The genes of each quadrant of **Fig.50A** were analyzed using WebGestalt website (http://www.webgestalt.org/) and ReviGO algorhytm to have a better insight on the Gene Ontology categories (**Fig.51**).

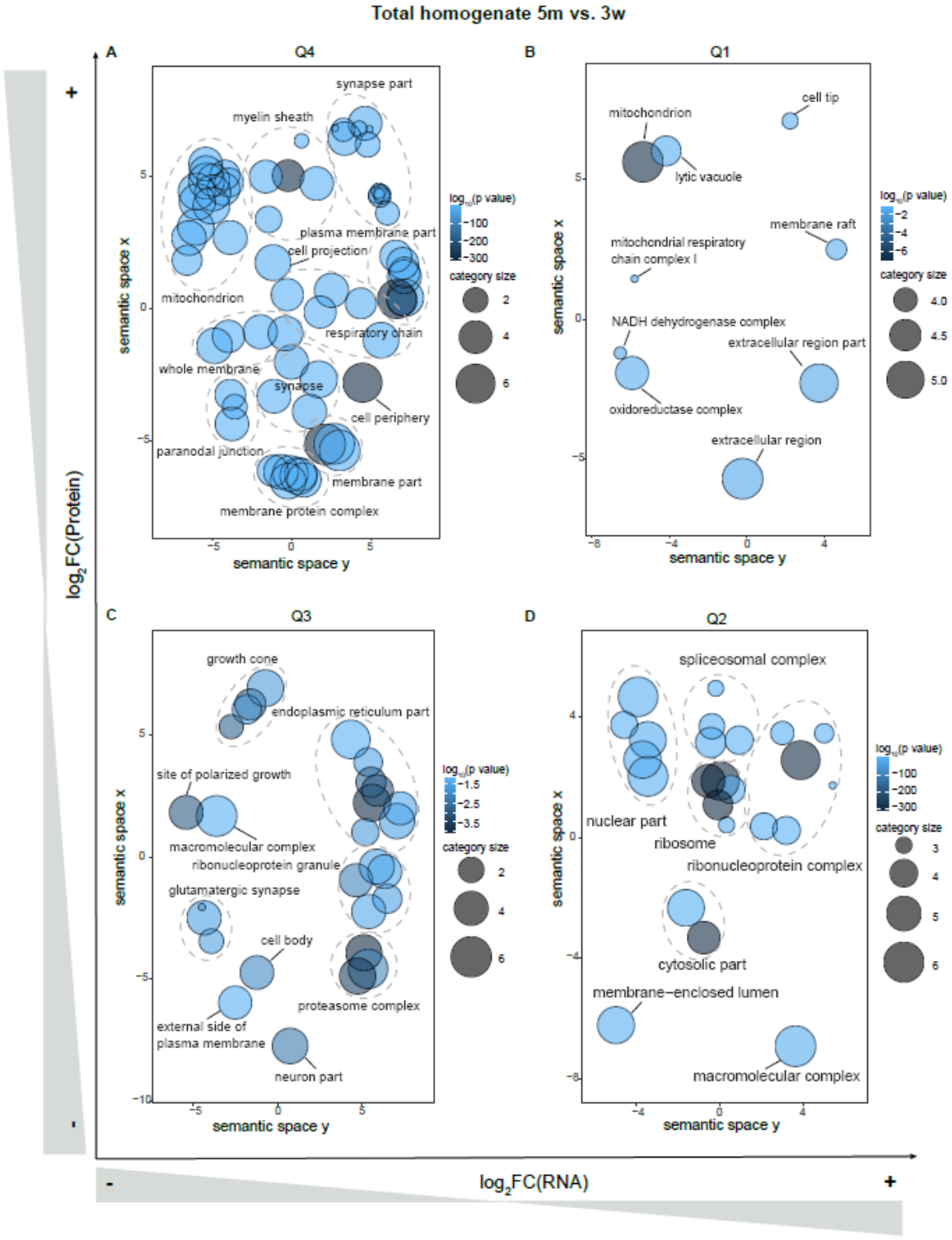

Figure 51. Gene Ontology categories of proteins and RNAs regulated during adulthood in total homogenate (**Fig.34A**). Similar terms are clustered together based on their semantic similarity using the REVIGO algorithm, and are colored according to $\log_{10}$(p value). **A)** Cellular components of genes upregulated at protein and transcript level during adulthood. **B)** Cellular components of genes upregulated at transcript level and downregulated at protein level. **C)** Cellular components of genes downregulated at transcript and protein level

at 5 months of age. **D)** Cellular components of genes upregulated at protein level but downregulated at transcript level.

Similarly, I compared transcripts significantly regulated in total homogenate at 18 months with the respective proteins, obtaining 1136 genes significantly regulated at transcript or protein level (**Fig.52A**). Again, I highlighted genes belonging to the GO categories translation (GO:0006412), ribosomes (GO:0005840), respiratory chain (GO:0070469) and proteasome (GO:0000502)(**Fig.52B**). Remarkably, I observed a complete loss of correlation between transcriptome and proteome during aging and a mild modification in the regulation of ribosomal genes. In fact, while ribosomal genes seem to be translationally repressed during adulthood, they become partially upregulated at protein level during aging.

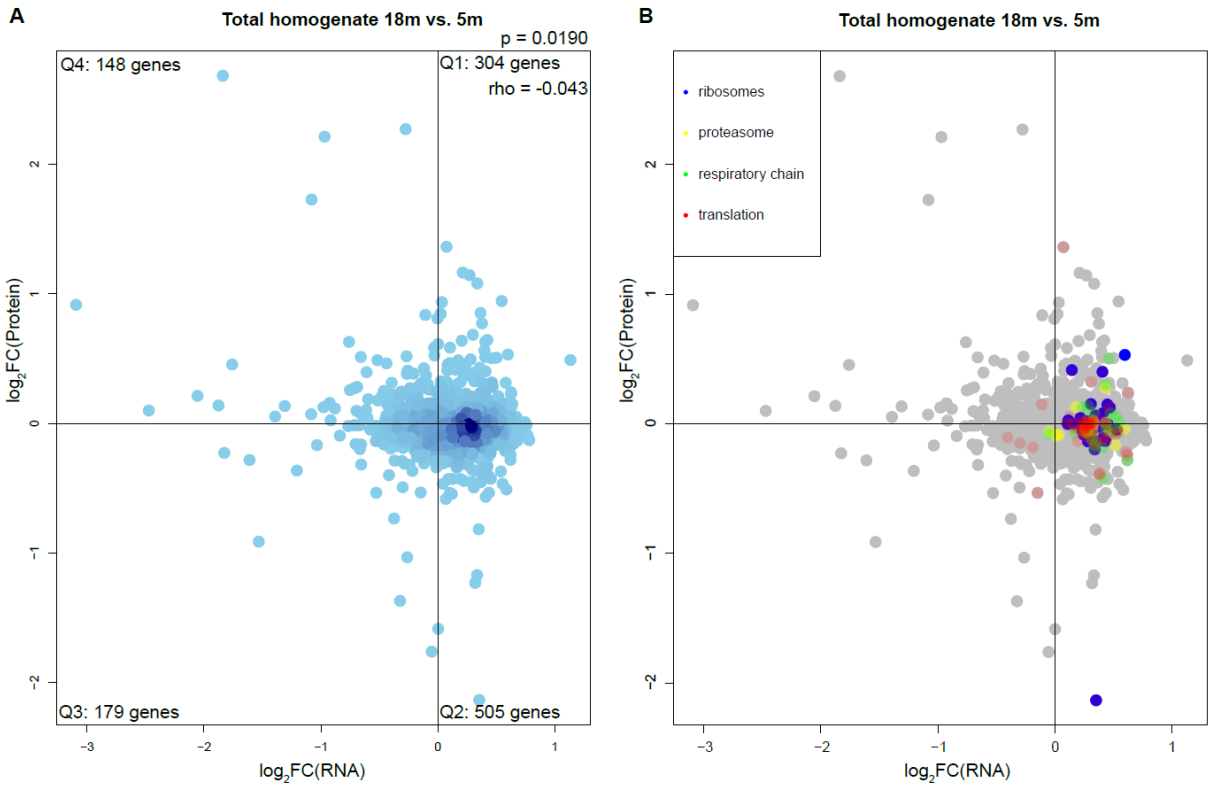

Figure 52. Genes significantly regulated in total cortical homogenate during aging at proteome and transcriptome level. **A)** Proteins and RNAs enrichment are plotted as log of the ratio 18 months vs. 5 months. Quadrants were named clockwise, starting from the upper right one. The distribution of genes in each quadrant is not uniform according to Fisher's exact test (p = 0.0190). Protein and RNA fold changes were correlated using Spearman's correlation (rho = -0.043, p = 0.1394). **B)** Genes belonging to specific Gene Ontology (GO) terms were highlighted in different colors, red = translation, yellow = proteasome, blue = ribosome, green = respiratory chain as indicated also in the legend.

Gene Ontology analysis was performed on the genes of each quadrant of **Fig. 52A** using WebGestalt website (http://www.webgestalt.org/) and ReviGO algorhytm (**Fig.53**).

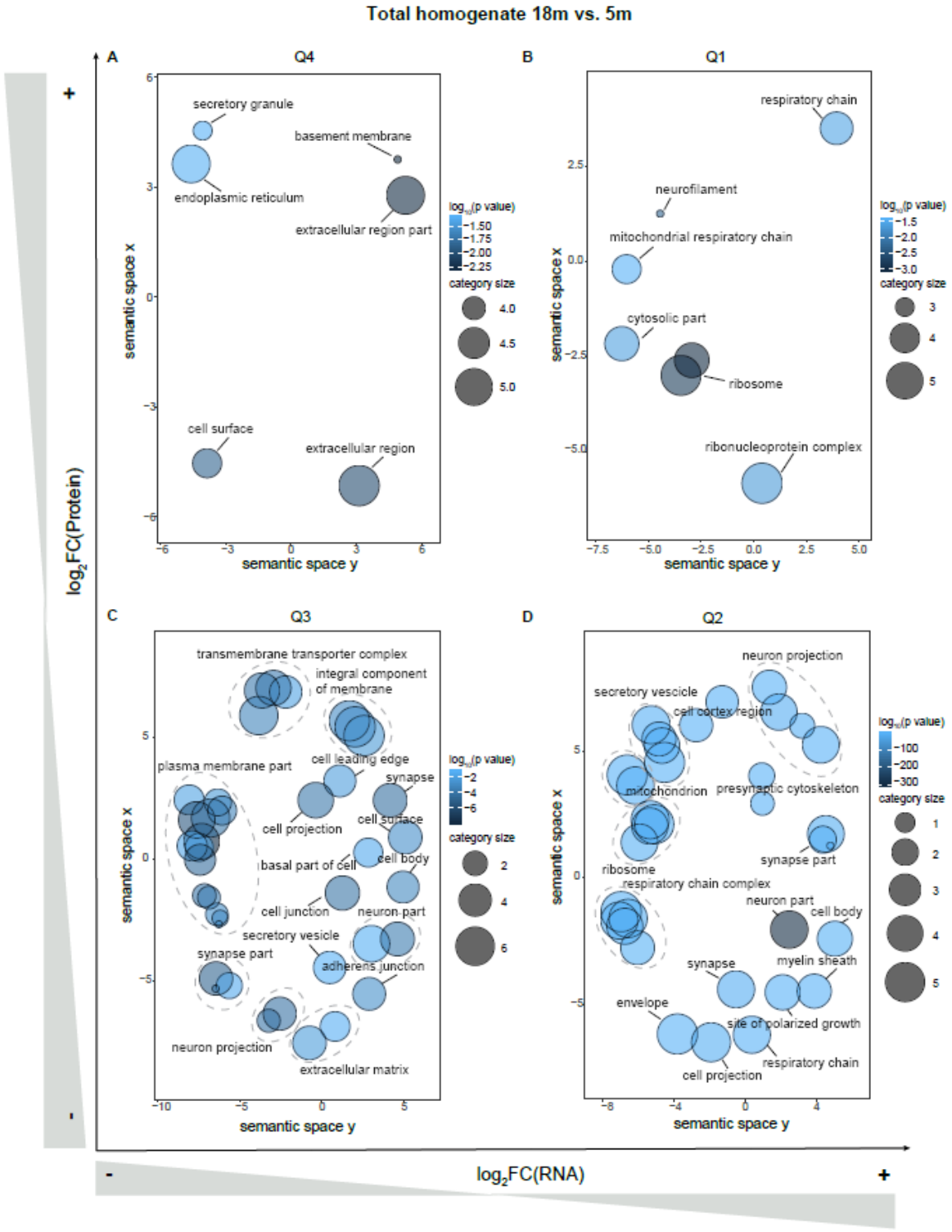

Figure 53. Gene Ontology categories of proteins and RNAs regulated during aging in total homogenate (**Fig.52A**). Similar terms are clustered together based on their semantic similarity using the REVIGO algorithm, and are colored according to $\log_{10}$(p value). **A)** Cellular components of genes upregulated at protein

and transcript level during aging. **B)** Cellular components of genes upregulated at transcript level and downregulated at protein level. **C)** Cellular components of genes downregulated at transcript and protein level at 18 months of age. **D)** Cellular components of genes upregulated at protein level but downregulated at transcript level.

Comparing **Fig.51** and **Fig.53** I observed, as already mentioned, an upregulation at protein level of ribosomal genes during aging (**Fig.51B** and **53B**). Strikingly, ribosomes seem to be translationally repressed at 5 months, and are splitted between quadrant 1 and 2 at old age, indicating a partial translational activation. This result was already observed in a recent work of our group in the short-living fish *Nothobranchius furzeri* (Sacramento et al., 2019).Furthermore, I observed a partial downregulation of mitochondrial genes at protein level upon aging (**Fig.51B** and **Fig.53B, D**). I observed also an upregulation of synaptic proteins at 5 months (**Fig.51A**), which is not maintained at 18 months (**Fig.53A**). As expected, in fact, there is a decrease in synaptic components, both at protein and transcript level (**Fig.53C**).

Transcripts enriched in synaptosomes at 5 months were compared with the respective proteins, similarly to what was done for total homogenate, yielding 2136 genes significantly regulated at transcript or protein level (**Fig.54A**). I also highlighted in the plot of **Fig.54A** genes belonging to the GO categories translation (GO:0006412), ribosomes (GO:0005840), respiratory chain (GO:0070469) and proteasome (GO:0000502) (**Fig.54B**).

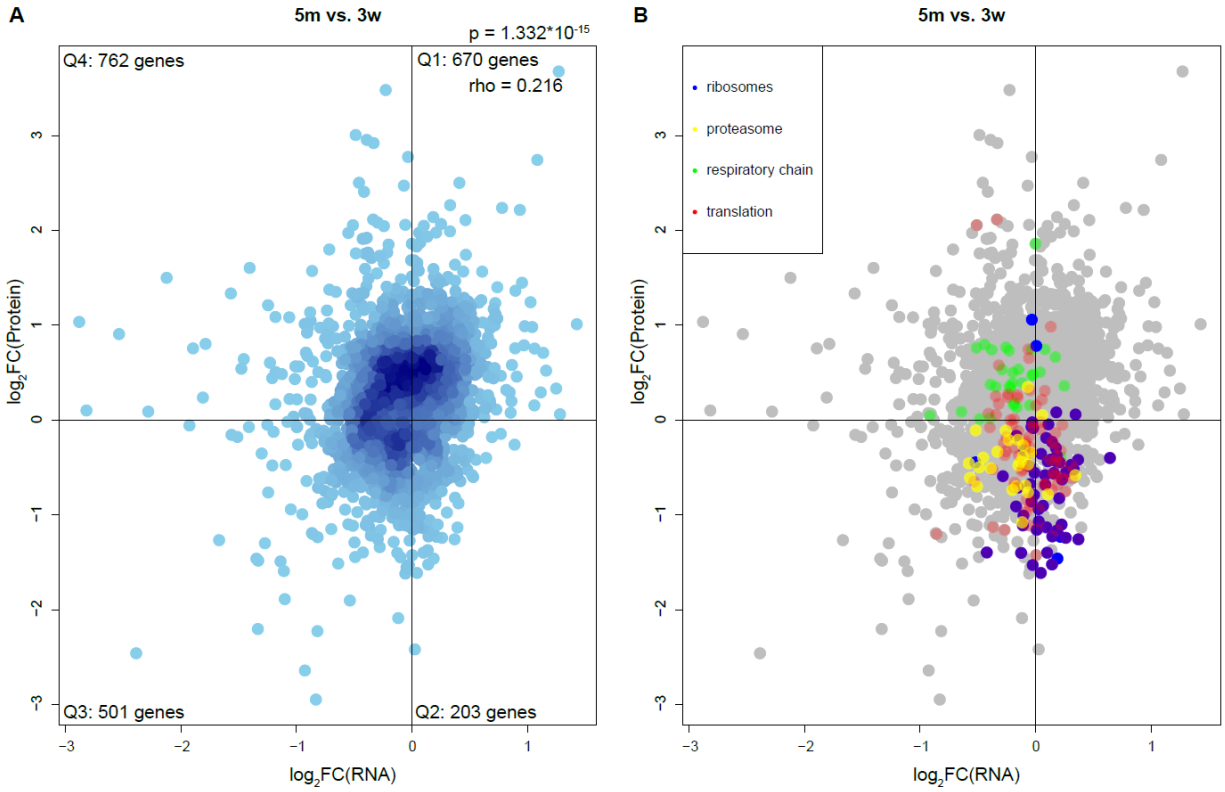

Figure 54. Genes significantly regulated in synaptosomes during adulthood at proteome and transcriptome level. **A)** Proteins and RNAs enrichment are plotted as log of the ratio 5 months vs. 3 weeks. Quadrants were named clockwise, starting from the upper right one. The distribution of genes in each quadrant is not uniform according to Fisher's exact test ($p < 1.332*10^{-15}$). Protein and RNA fold changes were correlated using Spearman's correlation (rho = 0.216, $p < 2.2*10^{-16}$). **B)** Genes belonging to specific Gene Ontology (GO) terms were highlighted in different colors, red = translation, yellow = proteasome, blue = ribosome, green = respiratory chain as indicated also in the legend.

The genes of each quadrant of **Fig. 54A** were analyzed using WebGestalt website (http://www.webgestalt.org/) and ReviGO algorhytm to have a better insight on the Gene Ontology categories (**Fig.55**).

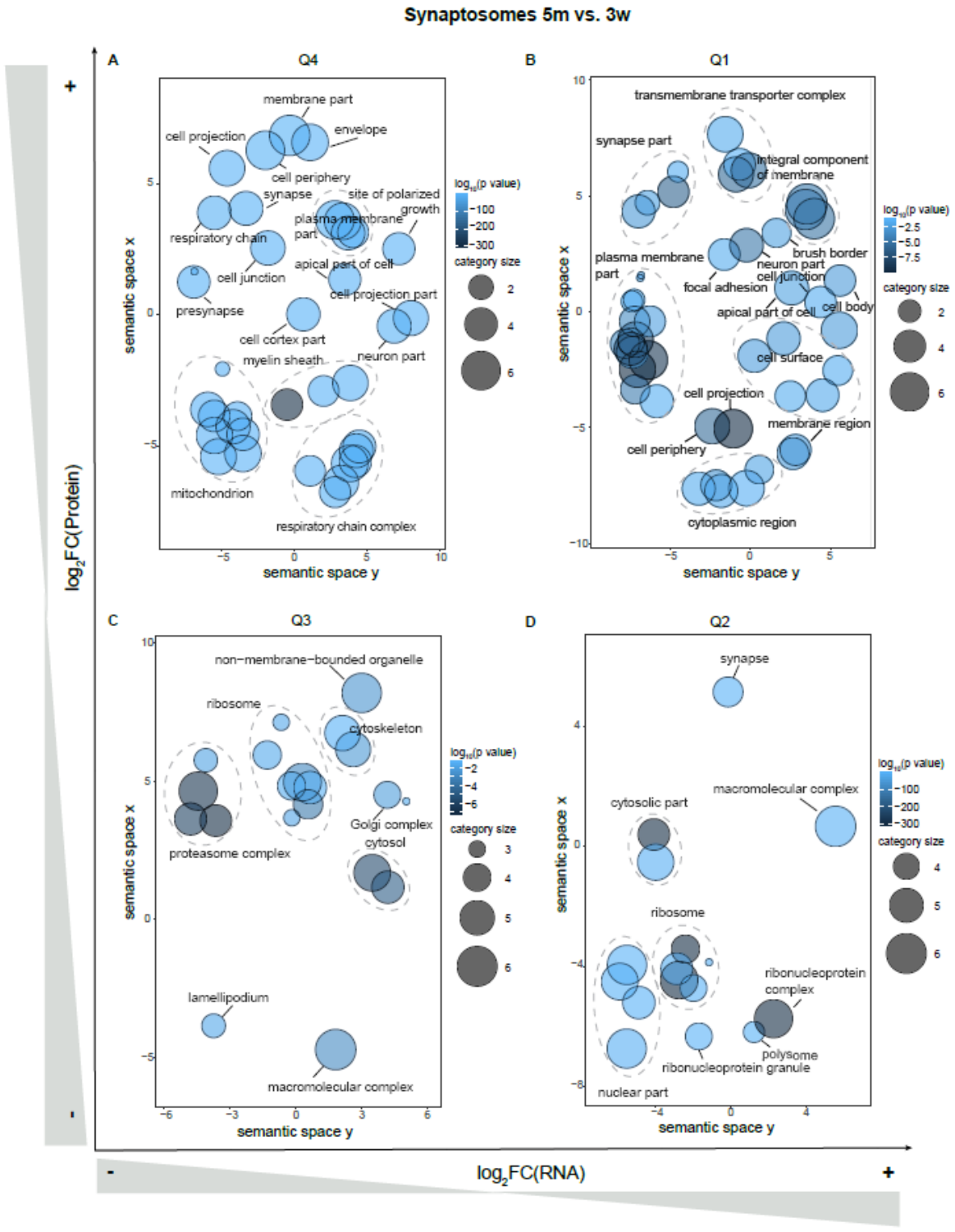

Figure 55. Gene Ontology categories of proteins and RNAs regulated during adulthood in synaptosomes (**Fig.54A**). Similar terms are clustered together based on their semantic similarity using the REVIGO algorithm, and are colored according to $\log_{10}$(p value). **A)** Cellular components of genes upregulated at protein and transcript level during adulthood. **B)** Cellular components of genes upregulated at transcript level and downregulated at protein level. **C)** Cellular components of genes downregulated at transcript and protein level at 5 months of age. **D)** Cellular components of genes upregulated at protein level but downregulated at transcript level.

Similarly to what I observed in total homogenate, at synaptic level ribosomes are mostly translationally repressed during adulthood, but I could observe also a subset of ribosomal genes being downregulated both at transcript and protein level at 5 months.

I then compared transcripts significantly regulated in synaptosomes at 18 months with the respective proteins, obtaining 1917 genes significantly regulated at transcript or protein level (**Fig.56A**). Again, I highlighted genes belonging to the GO categories translation (GO:0006412), ribosomes (GO:0005840), respiratory chain (GO:0070469) and proteasome (GO:0000502)(**Fig.56B**). I observed, as in total homogenate, a complete loss of correlation between transcriptome and proteome during aging. In this case the modification in the regulation of ribosomal genes is even more remarkable than in total homogenate and is strikingly opposed to genes related to translation.

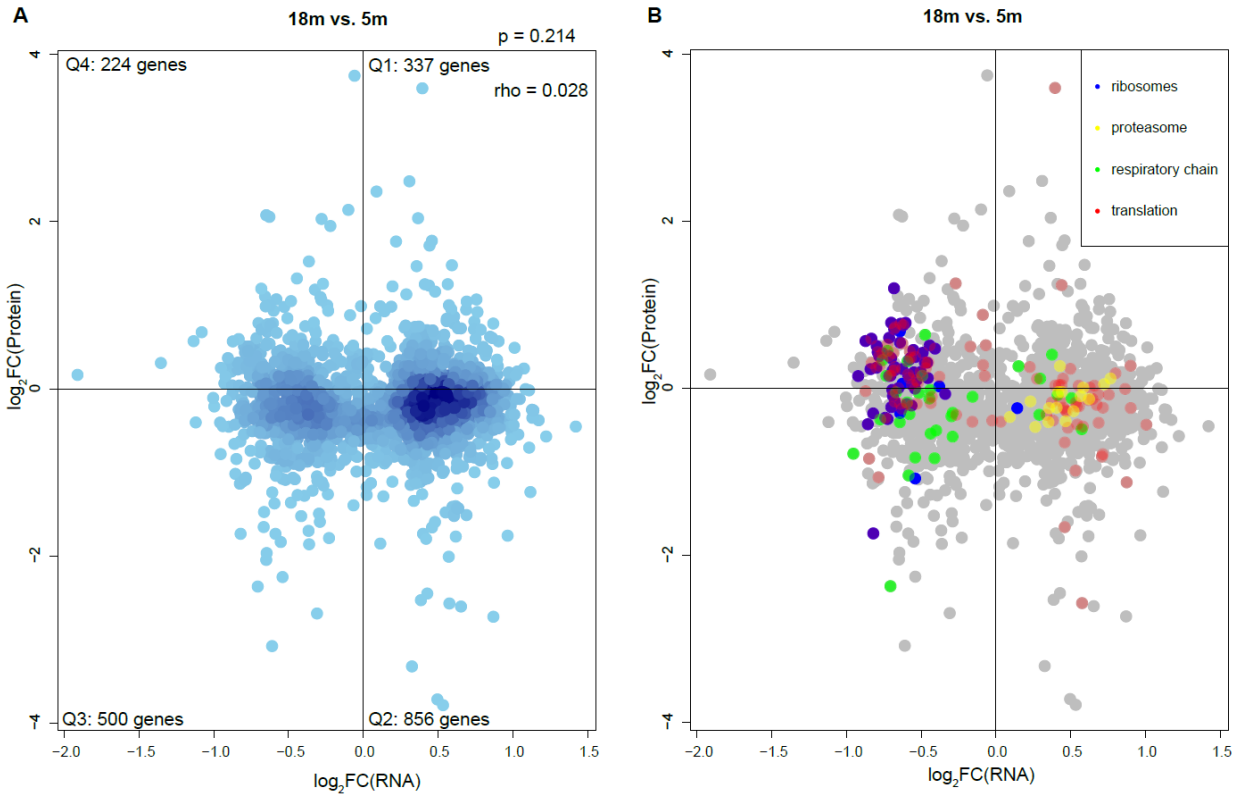

Figure 56. Genes significantly regulated in synaptosomes during aging at proteome and transcriptome level. **A)** Proteins and RNAs enrichment are plotted as log of the ratio 18 months vs. 5 months. Quadrants were named clockwise, starting from the upper right one. Genes are randomly distributed in the quadrants according to Fisher's exact test (p = 0.214). Protein and RNA fold changes were correlated using Spearman's correlation (rho = 0.028, p = 0.2208). **B)** Genes belonging to specific Gene Ontology (GO) terms were highlighted in different colors, red = translation, yellow = proteasome, blue = ribosome, green = respiratory chain as indicated also in the legend.

Gene Ontology analysis was performed on the genes of each quadrant of **Fig. 56A** using WebGestalt website (http://www.webgestalt.org/) and ReviGO algorhytm (**Fig.57**).

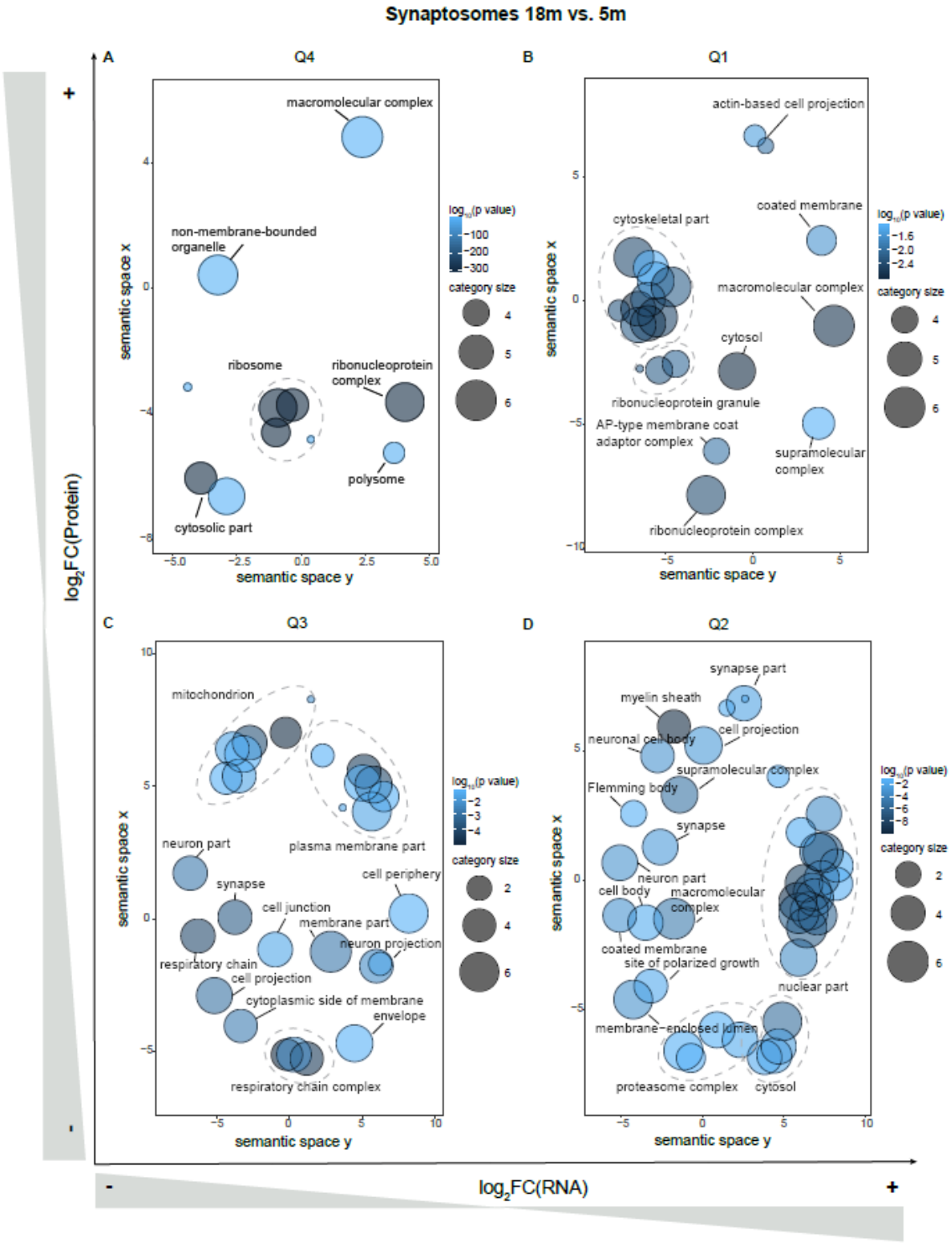

Figure 57. Gene Ontology categories of proteins and RNAs regulated during aging in synaptosomes (**Fig.56A**). Similar terms are clustered together based on their semantic similarity using the REVIGO algorithm, and are colored according to $\log_{10}$(p value). **A)** Cellular components of genes upregulated at protein and transcript level during aging. **B)** Cellular components of genes upregulated at transcript level and downregulated at protein level. **C)** Cellular components of genes downregulated at transcript and protein level at 18 months of age. **D)** Cellular components of genes upregulated at protein level but downregulated at transcript level.

I noticed that, while in total homogenate categories related to ribosomes and respiratory chain were upregulated at transcript and protein level at 18 months (**Fig.53B**), in synaptosomes there is a downregulation at transcript and protein level of respiratory chain genes (**Fig.57C**), whereas ribosomal genes are downregulated at transcript level and upregulated at protein level (**Fig.57A**). Strikingly, in aged synaptosomes there is an upregulation at transcript level of genes related to proteasome (**Fig.57D**) that is not present in total homogenate.

I also observed that during development there is an upregulation at transcript and protein level of synaptic genes (**Fig.55B**), which are then subjected to a downregulation at protein level during aging (**Fig.57D**). For what concerns ribosomal genes, they are upregulated at transcript, but not at protein level during adulthood (**Fig.55D**), and become upregulated at protein, but not at transcript level during aging (**Fig.57A**). The regulation of genes related to respiratory chain also changes during aging: they are upregulated at protein, but not at transcript level during adulthood (**Fig.55A**) and become downregulated both at transcript and protein level at 18 months (**Fig.57C**). Myelin genes, finally, are upregulated only at protein level at 5 months (**Fig.55A**) and become upregulated only at transcript level during aging (**Fig.57D**).

The results illustrated in the last paragraphs are summarized in **Table 3** and **Table 4.**

Table 3. Summary of the results of §8, 9 and 10.

	Correlation RNA/age TH	Correlation protein/age TH	Correlation RNA/age Syn	Correlation protein/age Syn	Soma – Synapse gradient RNA	Soma – Synapse gradient protein
Synapse	↓Correl.	↑Correl.	↑Correl.	–	↑Gradient	–
Nucleus	↑Correl.	↓Correl.	↑Correl.	–	–	–
Respiratory chain	↑Correl.	↑Correl.	↓Correl.	–	↓Gradient	↑Gradient
Ribosome	↑Correl.	↓Correl.	↓Correl.	↓Correl.	↓Gradient	↓Gradient
Spliceosomal complex	↑Correl.	↓Correl.	↑Correl.	–	–	–
Myelin sheath	–	↑Correl.	–	↑Correl.	–	–
Proteasome	–	↓Correl.	–	↓Correl.	–	–

Table 4. Summary of the results of §11 and 12.

	5m vs. 3w RNA	18m vs. 5m RNA	5m vs. 3w Protein	18m vs. 5m Protein	5m vs. 3w TH	18m vs. 5m TH	5m vs. 3w Syn	18m vs. 5m Syn
Synapse	↑Syn	↑Syn ↑TH	↑Syn ↑TH	↓Syn ↓TH	↑Protein ↓RNA	↓Protein ↓RNA	↑RNA	↓Protein ↑RNA
Nucleus	↓Syn ↓TH	↑Syn ↓TH	↓Syn ↓TH	–	↓Protein ↑RNA	–	↓Protein ↑RNA	↓Protein ↑RNA
Respiratory chain	–	↓Syn ↑TH	↑Syn ↓TH	–	↑Protein ↓RNA	↑RNA	↑Protein ↓RNA	↓Protein ↓RNA
Ribosome	↑Syn ↑TH	↑TH	↓Syn ↓TH	↑Syn	↓Protein ↑RNA	↑Protein ↑RNA	↓Protein	↑Protein ↓RNA
Spliceosomal complex	↓Syn ↑TH	↑Syn ↓TH	↑Syn ↓TH	–	–	–	–	–
Myelin sheath	↓Syn ↓TH	–	↑Syn ↑TH	–	↑Protein ↓RNA	↓Protein ↑RNA	↑Protein ↓RNA	↓Protein ↑RNA
Proteasome	–	↑Syn ↑TH	↓Syn ↓TH	–	↓Protein ↓RNA	–	↓Protein ↓RNA	↓Protein ↑RNA

13. Experimental validations

In §10 I analyzed the gradient between soma and synapse and observed that ribosomal proteins are enriched in soma and their gradient to synapses increases with age. On the other hand, transcripts coding for ribosomal proteins are enriched in synaptosomes in young animals and their enrichment decreases with aging, as summarized in **Fig.58**.

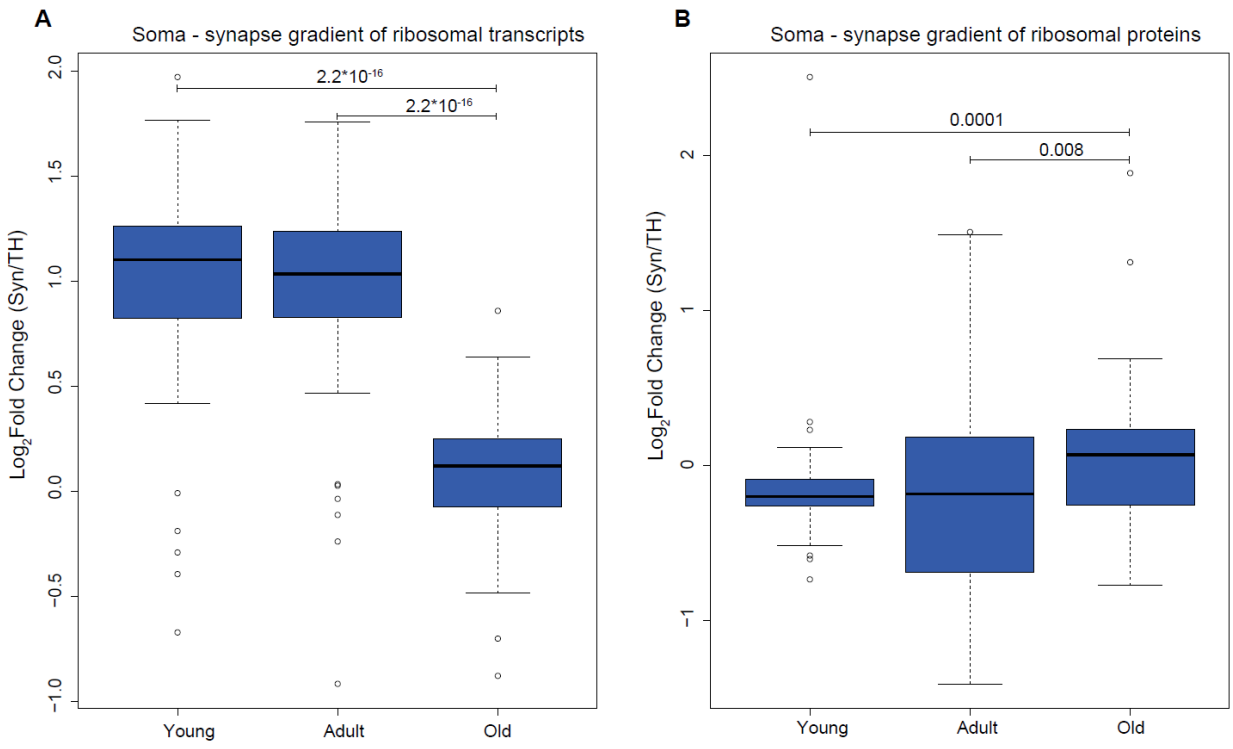

Figure 58. Boxplot of the fold changes between total homogenate and synaptosomes of ribosomal transcripts (**A**) and proteins (**B**). Differences between the means are significant according to t-test.

This means that there is a relative depletion of ribosomal transcripts at synaptic level, which is opposed to an increase of ribosomal proteins in this compartment. These data were validated by means of Western blot (**Fig.59**).

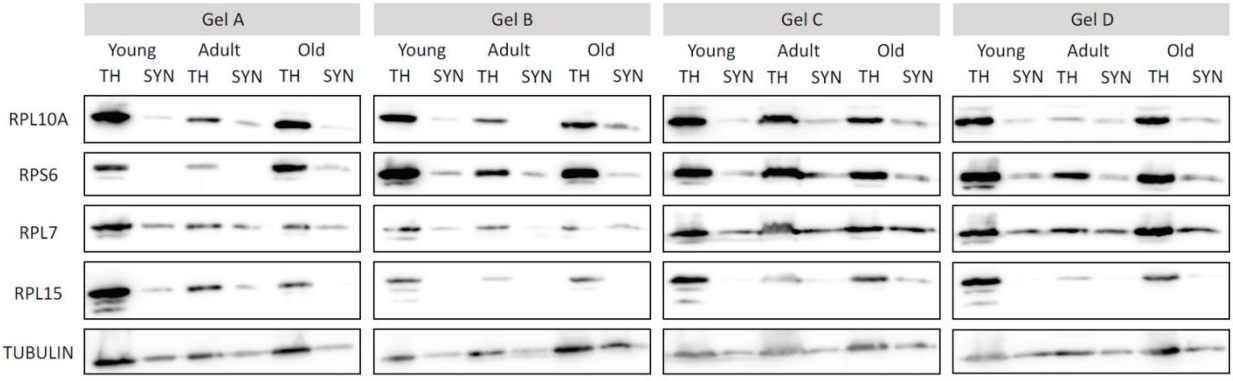

Figure 59. Western blot on ribosomal proteins using total cortical homogenate and synaptosomes of young, adult and old animals. Tubulin was used as loading control in all the experiments.

Although the reduction of ribosomal proteins in synaptosomes is already clear from the pictures, I quantified protein expression relative to tubulin expression level (**Fig.60**). I was able to confirm the reduction of ribosomal proteins in synaptosomes that was observed upon proteomic analysis (p = 0.00717 evaluated by two-way ANOVA).

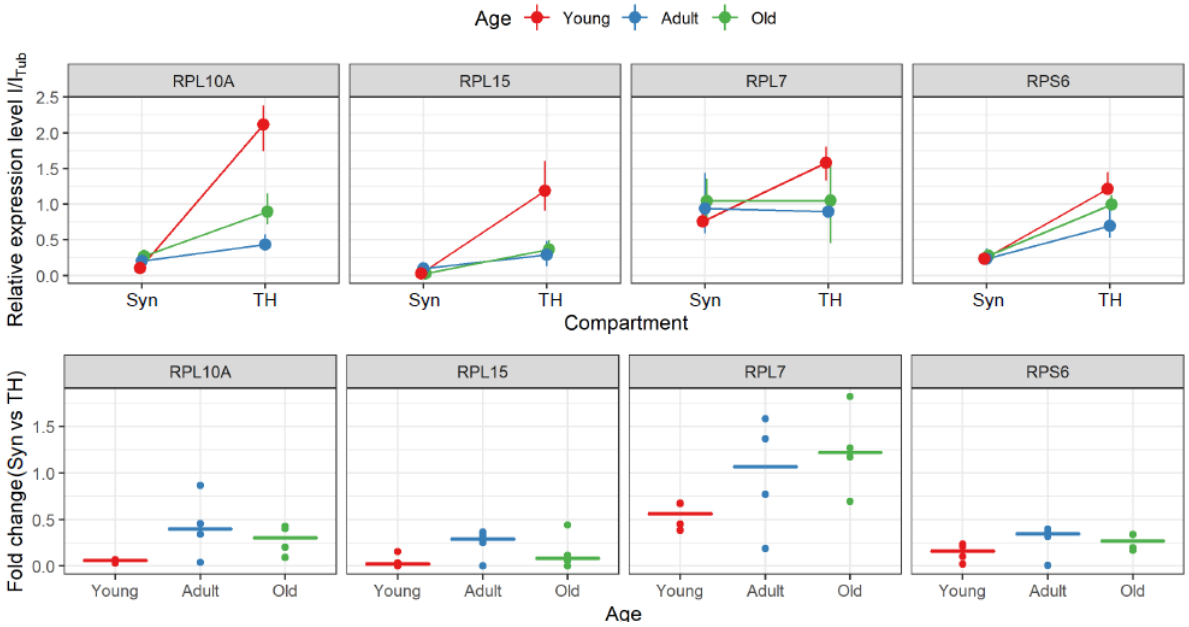

Figure 60. Upper panel: mean of protein intensity quantification in synaptosomes (SYN) and total homogenate (TH) relative to tubulin for each time point of **Fig.59**. Red indicates young animals, blue adult animals and green old animals.Lower panel: Fold change of ribosomal proteins in synaptosomes when compared to total homogenate.

For what concerns qPCR, I chose to normalize data on a gene, Ldhb, whose expression was constant in both total homogenate and synaptosomes across the three time points. Furthermore, to strengthen the statistical power, I used a set of independent animals, 4 for each time point, from which I enriched synaptosomes. Also, in this case I was able to confirm the increase in the expression level of ribosomal genes in synaptosomes that I observed in our transcriptomic analysis (**Fig.61**) (p = 0.00154 evaluated by two-way ANOVA).

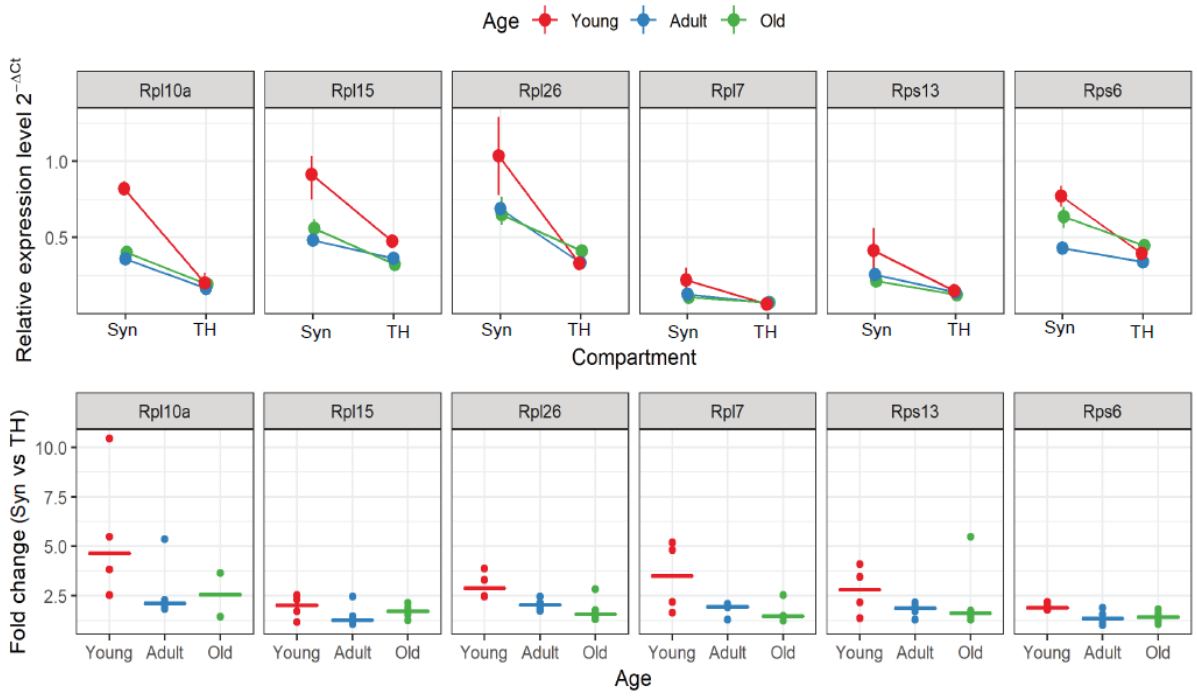

Figure 61. Upper panel: mean of ribosomal transcripts expression in synaptosomes (SYN) and total homogenate (TH) relative to Ldhb for each time point using independent samples**.** Red indicates young animals (N = 4), blue adult animals (N = 4) and green old animals (N = 4). Lower panel: Fold change of ribosomal transcripts in synaptosomes when compared to total homogenate.

I also measured ribosomal RNA (rRNA) content in the same samples by means of a bioanalyzer: in particular, I focused on 18S and 28S areas. I noticed that, similarly to ribosomal proteins, the gradient of rRNAs to synapses increases with age (**Fig.62**) (p-value of 18S = 0.007979 and p-value of 28S = 0.003426 evaluated by Kruskal-Wallis rank sum test).

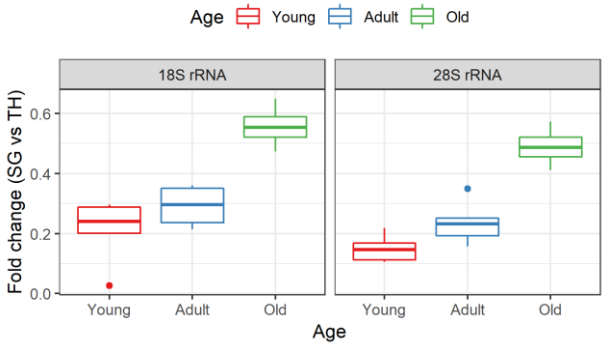

Figure 62. Ribosomal RNA (rRNA) in Total Homogenate (TH) and Synaptosomes (Syn). Box plot of the fold change of 18S and 28S between Synaptosomes and Total homogenate across the ages. Red = young (3 weeks), Blue = adult (5 months), Green = old (18 months).

14. Synaptic aggregates are enriched in ribosomal proteins

Protein aggregation was previously evauated in young and old mouse brain (Sacramento et al., 2019) and it's shown in **Fig.63**. Since the aggregation in younglings is almost absent, SDS-insoluble protein aggregates were only extracted from raw synaptosomes of 23 months-old mice, using a modified version of the protocol reported in Reis-Rodrigues *et al.* (2012). The aggregates were resuspended in formic acid as described in Methods section and analyzed by mass spectrometry.

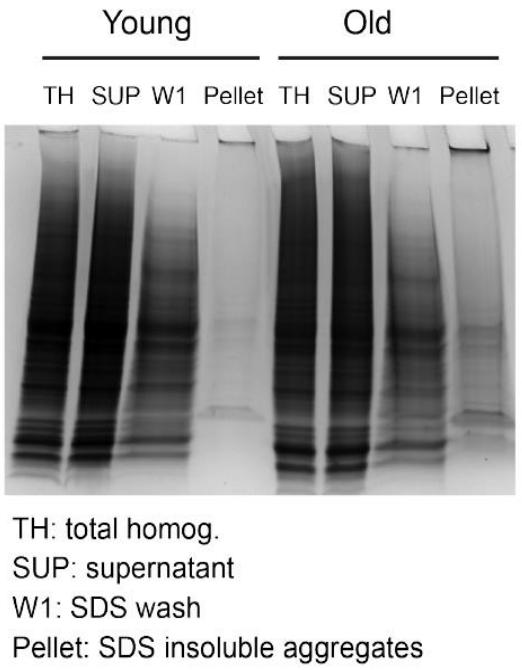

Figura 63. Coomassie-stained SDS-PAGE gel showing the isolation of SDS insoluble aggregates from mouse brain lysates. TH = total homogenate, SUP = supernatant, W1 = SDS-soluble fraction, Pellet = formic-acid soluble fraction. Picture adapted from Sacramento et al., 2019.

Protein abundances were compared with protein abundances in total synaptosomal homogenates to identify proteins specifically enriched in the aggregates. This analysis yielded 259 genes differentially regulated in the two conditions in a significant way (Q value < 0.05) (**Fig.64A**). I observed that synaptic aggregates are highly enriched in ribosomal proteins, whereas only few synaptic proteins tend to aggregate at synaptic level. Notably, in our aggregates data I found a protein belonging to proteasome complex (Psma6) and two lysosomal proteins (Lamp2 and Atp6v0c).

Composition of synaptosomal aggregates was compared with composition of aggregates from total brain homogenates analyzed by the same method and recently published by our group (Kelmer-Sacramento, Kirkpatrick, Mazzetto *et al.*, 2019) (**Fig.64B**): we observed that only 43 proteins are

aggregating both at synaptic level and in total brain, of which only 9 have a p value < 0.05 (**Fig.64C** and **Table 5**), while 78 proteins are specifically aggregating in synaptic compartment (**Table 6**).

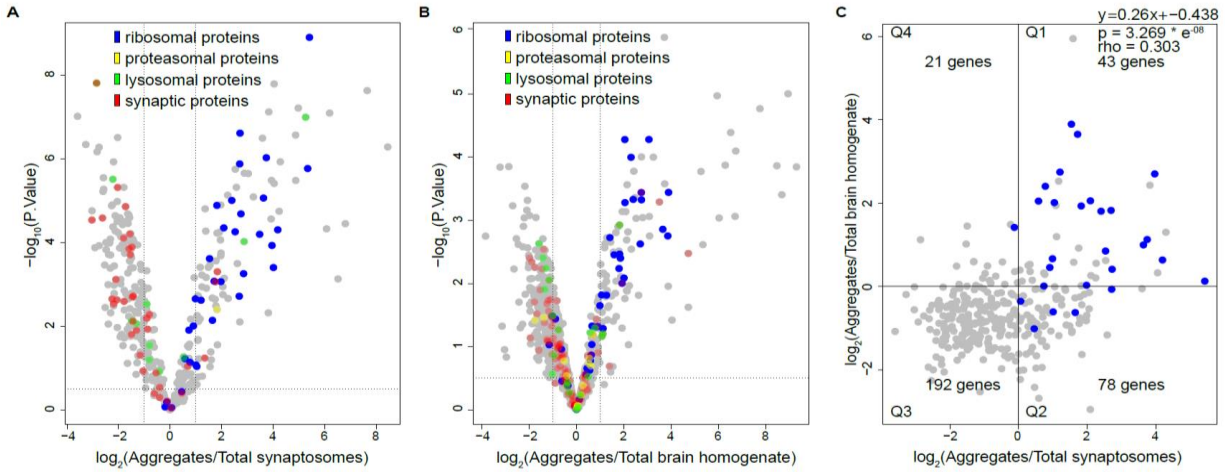

Figure 64. A) Volcano plot of the comparison of synaptic aggregates and total synaptic proteins. Protein enrichment is plotted as log of the ratio synaptosomal aggregates vs. total synaptosomes. **B)** Volcano plot of the comparison of total aggregates and total brain homogenate proteins. Protein enrichment is plotted as log of the ratio total aggregates vs. total brain homogenate. Genes belonging to specific Gene Ontology (GO) terms were highlighted in different colors, red = synapses, yellow = proteasome, blue = ribosome, green = lysosome as indicated also in the legend. **C)** Genes regulated in synaptosomal and total brain aggregates. Proteins enrichments are plotted as log of the ratio aggregates vs. total synaptosomes or total brain homogenate. Quadrants were named clockwise, starting from the upper right one. The distribution of genes in each quadrant is not uniform according to Fisher's exact test ($p = 3.269*e^{-08}$). Fold changes were correlated using Spearman's correlation (rho = 0.303, $p = 1.809*e^{-08}$).

Table 5. Proteins that have the same enrichment in synaptic and total brain aggregates.

logFC synaptic aggregates	P Value	Adjusted P Value	Gene name	ID	logFC total brain aggregates	P Value 1	Adjusted P Value 1
3.957243395	0.0001172	0.000521	Rps26	P62855	2.700505176	0.002371	0.037238492
3.816599199	0.0047703	0.009857	Hist1h1d	P43277	2.428847287	0.000167	0.009047089
2.687492007	0.0019162	0.00482	Rps6	P62754	1.824533825	0.003424	0.043895962
2.086223645	4.45E-05	0.000277	Rpl8	P62918	2.054846718	0.000525	0.016319584
1.715021957	0.0008368	0.002474	Rpl13a	P19253	3.65169339	0.001387	0.028448304
1.534721963	0.0002422	0.0009	Rpl4	Q9D8E6	3.894189457	0.000362	0.014618632
1.202272321	0.0023859	0.005522	Rpl18	P35980	2.743998907	0.000363	0.014618632
1.164030311	0.0066458	0.013003	Cct7	P80313	2.525678075	0.000932	0.020893612
1.081859968	0.0018452	0.00473	Rpl10	Q6ZWV3;P86048	1.941703883	0.000727	0.020138812

-0.87548198	0.0276644	0.044574	Calr	P14211	-1.394122262	0.003461	0.043895962
-1.120790423	0.0204706	0.034401	Stip1	Q60864	-2.530295795	0.001957	0.033877015
-1.494983458	0.0002299	0.000862	Sept6	Q9R1T4	1.448722593	0.002221	0.036917342
-1.567313647	0.0094724	0.017598	Prdx5	P99029	-1.354758852	0.004072	0.046727082
-1.63262739	3.50E-05	0.000232	Map2	P20357	-1.411897365	0.001968	0.033877015
-2.165213172	0.0003599	0.001246	Rtn4	Q99P72	-2.054884422	0.002729	0.039866988
-2.220732612	3.07E-06	4.58E-05	Got1	P05201	-1.410037285	0.003944	0.04627984
-2.538391207	0.0003436	0.001208	Crym	O54983	-2.259274816	0.002633	0.03965545

Table 6. Top 20 synaptically aggregated proteins.

logFC	adj.P.Val	gene name	gene description
8.4535536	1.34E-05	Dsp	Desmoplakin (DP)
7.6551111	2.37E-06	Anxa2	Annexin A2
6.8062292	0.00023155	Jup	Junction plakoglobin
6.5230551	0.00223233	Flna	Filamin-A
6.1958445	4.56E-06	Hnrnpm	Heterogeneous nuclear ribonucleoprotein M
6.0769996	0.00028787	Vim;Des;Prph	Vimentin;Desmin;Peripherin
5.4128485	5.09E-07	Rpl11	60S ribosomal protein L11
5.3445272	3.12E-05	Rpl38	60S ribosomal protein L38
5.2650831	4.56E-06	Lamp2	Lysosome-associated membrane glycoprotein 2
4.9789886	4.56E-06	Rps12	40S ribosomal protein S12
4.8810398	4.58E-05	Lmna;Lmnb1	Prelamin-A/C [Cleaved into: Lamin-A/C];Lamin-B1
4.8753404	9.97E-06	Rrbp1	Ribosome-binding protein 1
4.2814798	2.39E-05	Slc25a1	Tricarboxylate transport protein, mitochondrial
4.2360705	0.00015104	Strn4	Striatin-4 (Zinedin)
4.182811	0.00029955	Rps16	40S ribosomal protein S16
4.0414849	5.22E-05	Hnrnpu	Heterogeneous nuclear ribonucleoprotein U
4.0402179	2.19E-06	Rapgef4	Rap guanine nucleotide exchange factor 4
4.0148237	0.00133345	Rps27	40S ribosomal protein S27
3.9390239	4.58E-05	Hist1h1e;Hist1h1t;Hist1h1a	Histone H1.4;Histone H1t;Histone H1.1
3.925115	0.00019422	Hist2h2bb;Hist1h2bp	Histone H2B type 2-B;Histone H2B type 1-P

I was able to demonstrate the aggregation of desmoplakin in old cortex by means of immunofluorescence (**Fig.65, 66**). In particular, I observed a higher degree of colocalization between desmoplakin and neuronal processes in old animals (**Fig.65D, 66D**).

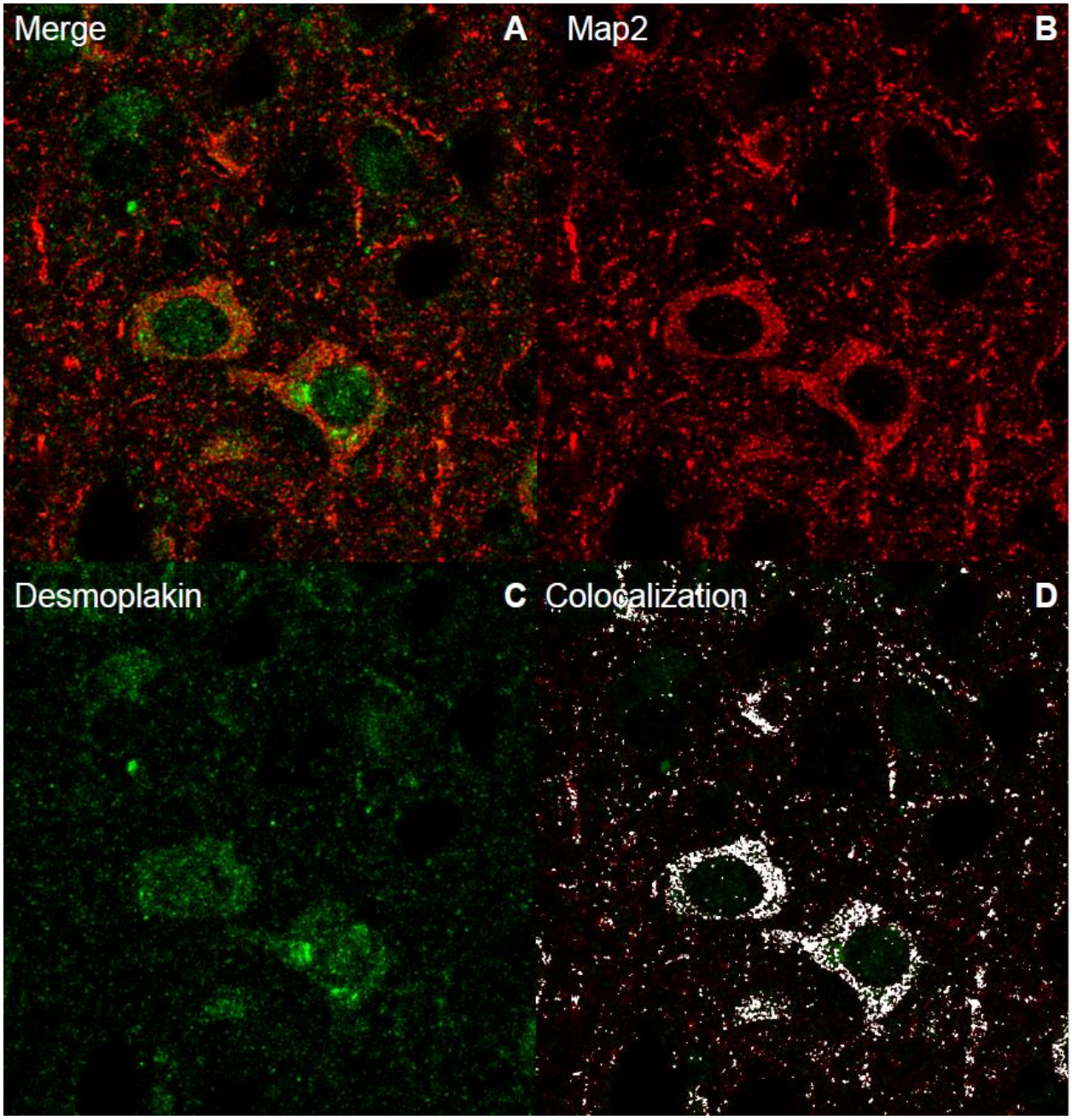

Figure 65. Immunofluorescence of a young (3 weeks-old) cortex (layers II-III). Immunoreactivity for desmoplakin is visualized with green fluorophore, while immunoreactivity for Microtubule associated protein 2 (MAP2) is visualized with a red fluorophore. **A)** Merge; **B)** MAP2; **C)** Desmoplakin; **D)** Colocalization between the two signals is shown as white dots.

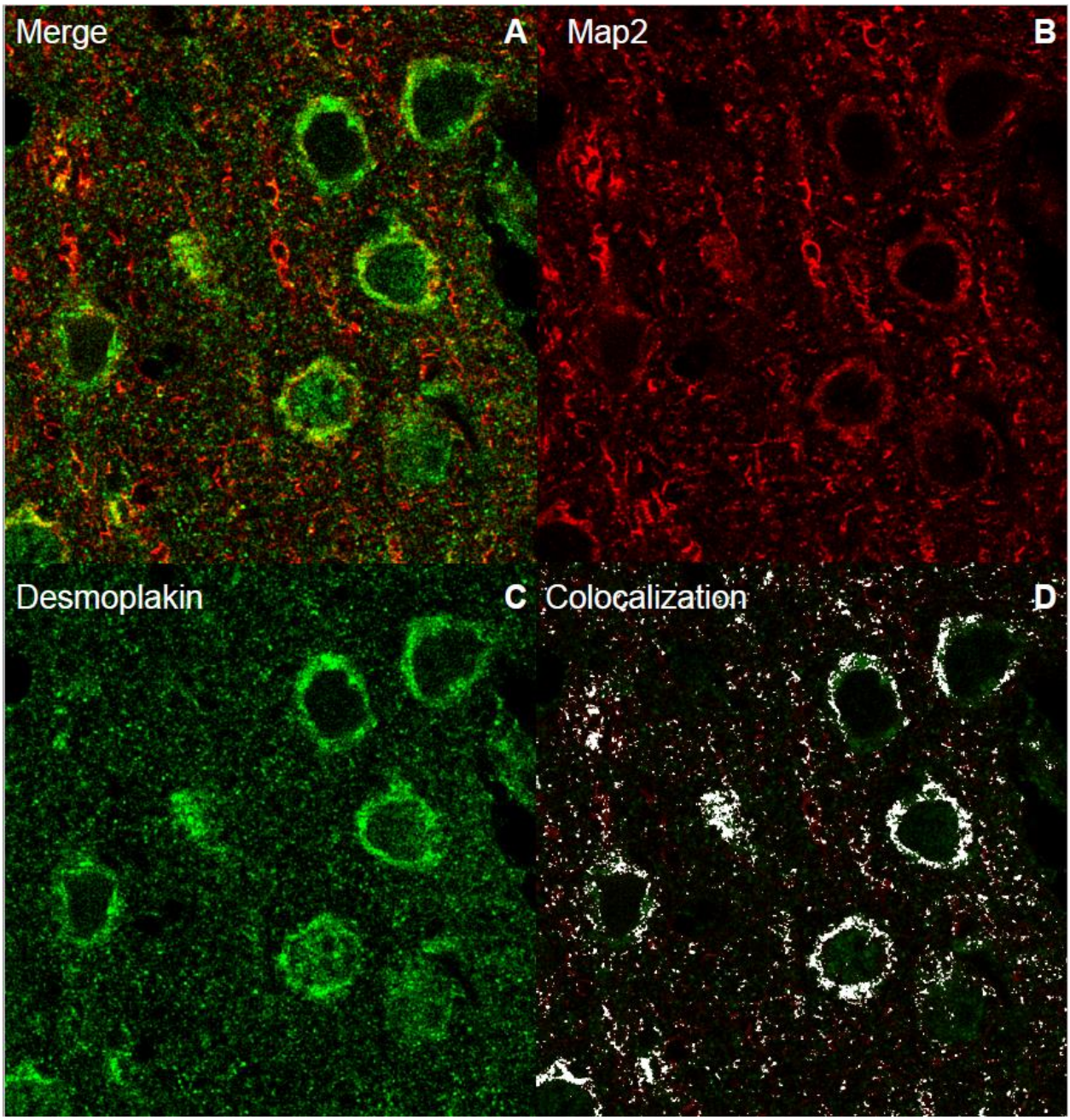

Figure 66. Immunofluorescence of an old (18 months-old) cortex (layers II-III). Immunoreactivity for desmoplakin is visualized with green fluorophore, while immunoreactivity for Microtubule associated protein 2 (MAP2) is visualized with a red fluorophore. **A)** Merge; **B)** MAP2; **C)** Desmoplakin; **D)** Colocalization between the two signals is shown as white dots.

As already mentioned above, in a recently-published paper of my group we observed ribosome aggregation in the brain of old *Nothobranchius furzeri* (Sacramento et al., 2019). Since I found a high number of ribosomal proteins aggregating in synaptosomes, I validated this finding also in mouse cortex by means of immunofluorescence, combining the staining of the ribosomal protein S6 (Fold change synaptic aggregates/total synaptosomes = 2.69, p value = 0.005) with a dye specific for

aggregated proteins called aggresome (**Fig. 67, 68**). In the adult cortex I didn't observe any aggregation of ribosomal protein S6 (**Fig.67D**), while in the old cortex I observed colocalization of the signals also outside the somata (**Fig.68D**).

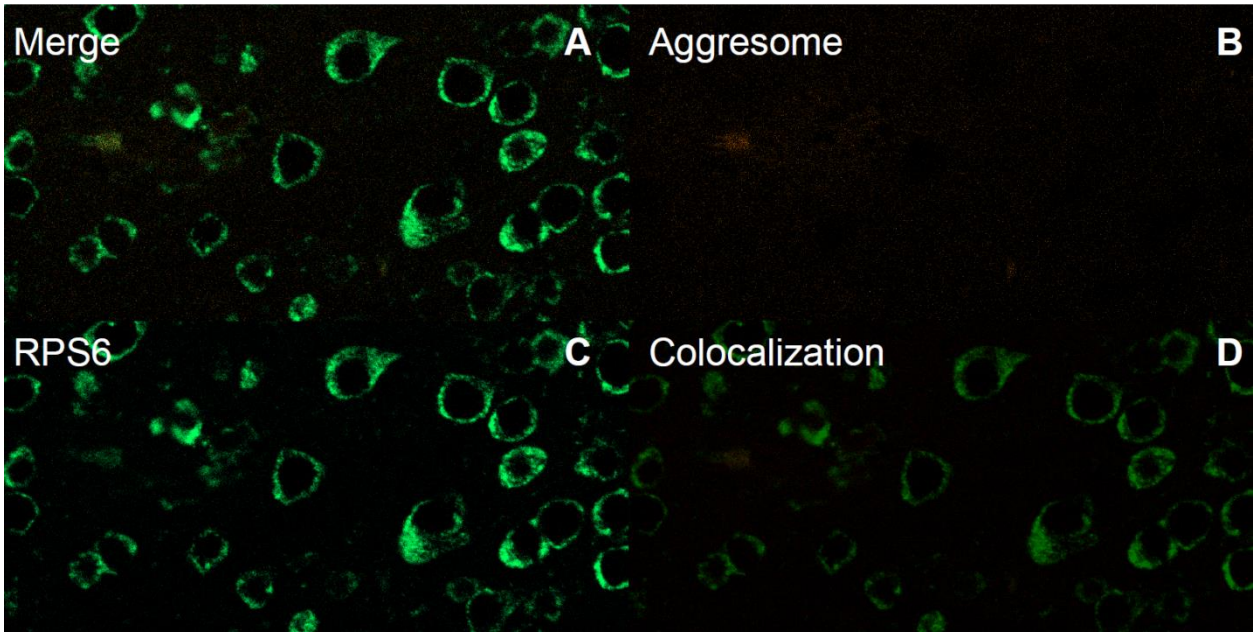

Figure 67. Immunofluorescence of an adult (6 months-old) cortex (layers II-III). Immunoreactivity for RPS6 is visualized with green fluorophore, while aggresome dye emits in the red spectrum. **A)** Merge; **B)** Aggresome; **C)** RPS6; **D)** Colocalization between the two signals is shown as white dots.

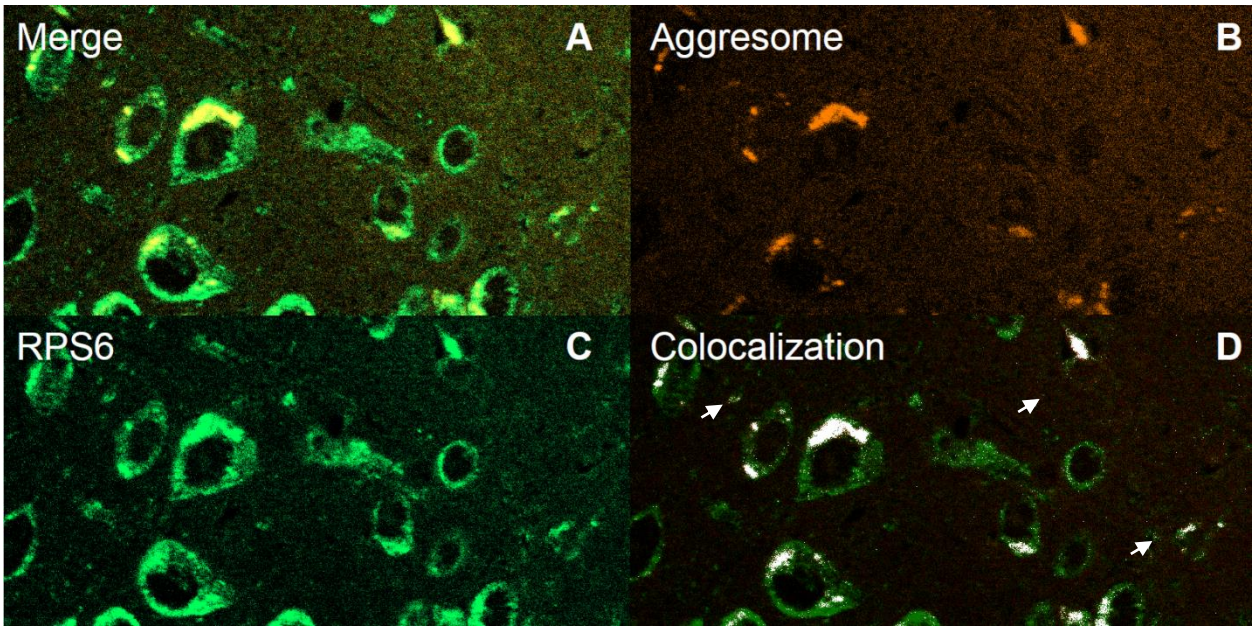

Figure 68. Immunofluorescence of an old (26 months-old) cortex (layers II-III). Immunoreactivity for RPS6 is visualized with green fluorophore, while aggresome dye emits in the red spectrum. **A)** Merge; **B)** Aggresome; **C)** RPS6; **D)** Colocalization between the two signals is shown as white dots. Extracellular signals are indicated with arrows.

As a control we chose a ribosomal protein (RPL15) absent in our data, but highy enriched in total brain aggregates according to Sacramento et al.(2019) (Fold change brain aggregates/total brain homogenate = 3.86, p vaue = 0.002). I performed immunofluorescence of adult and old cortex, combining the staining for RPL15 and aggresome dye (**Fig.69, 70**). I observed that RPL15 aggregation in the old cortex is restricted almost only to the somata (**Fig.70D**).

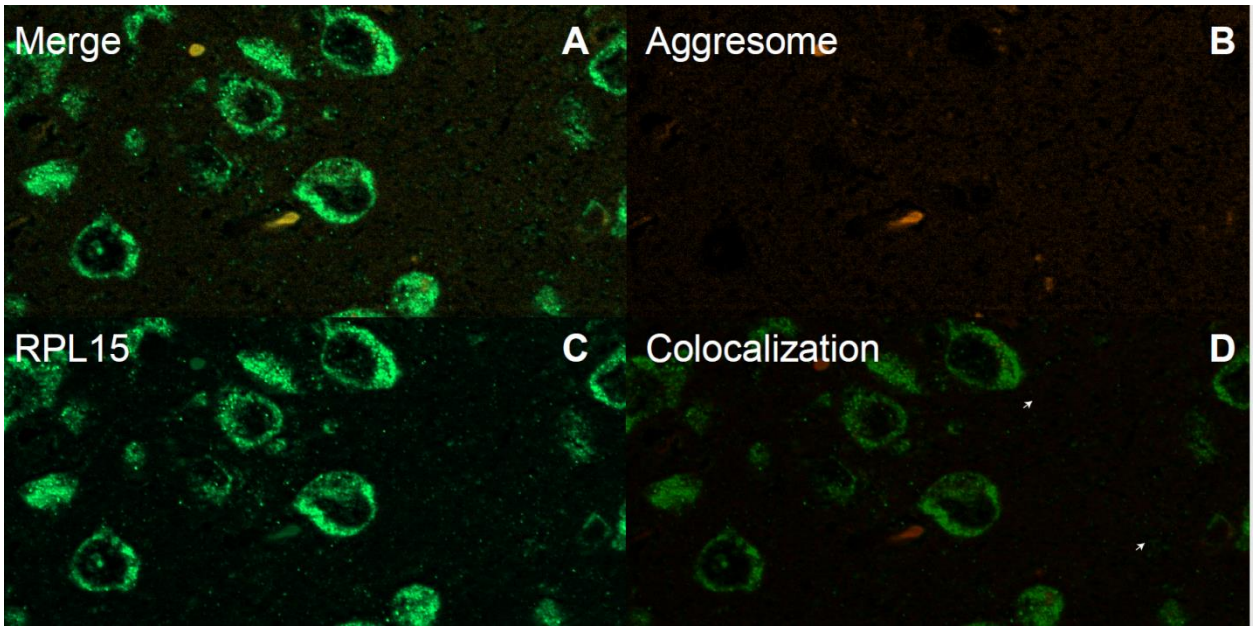

Figure 69. Immunofluorescence of an adult (6 months-old) cortex (layers II-III). Immunoreactivity for RPL15 is visualized with green fluorophore, while aggresome dye emits in the red spectrum. **A)** Merge; **B)** Aggresome; **C)** RPL15; **D)** Colocalization between the two signals is shown as white dots.

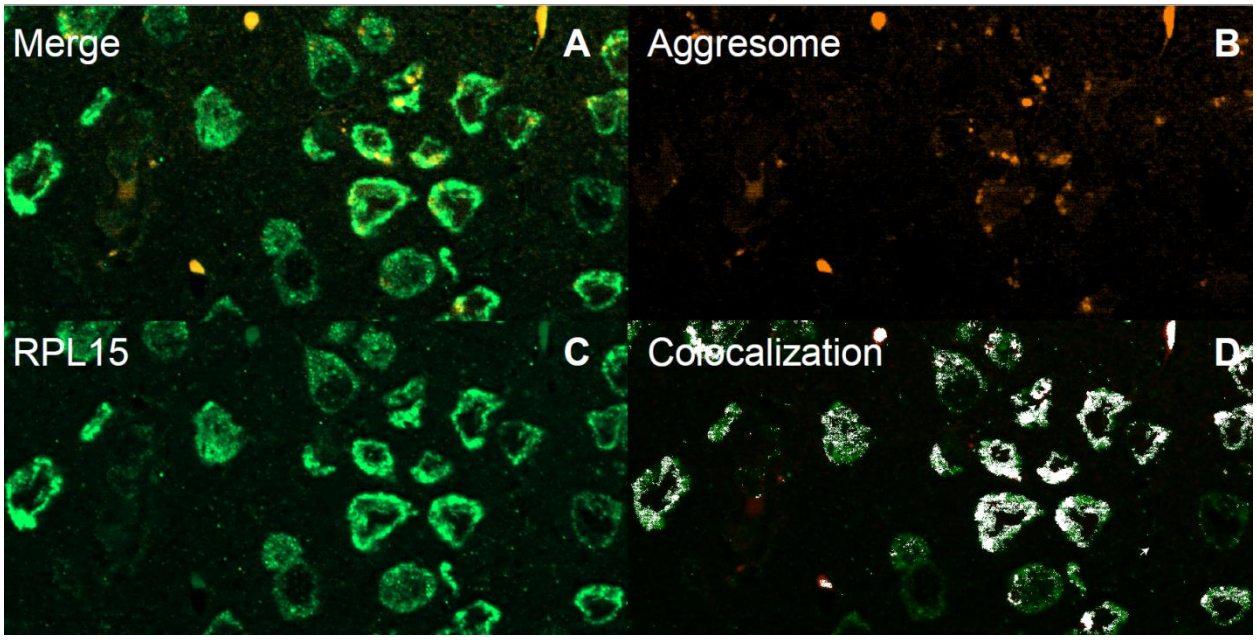

Figure 70. Immunofluorescence of an old (26 months-old) cortex (layers II-III). Immunoreactivity for RPS6 is visualized with green fluorophore, while aggresome dye emits in the red spectrum. **A)** Merge; **B)** Aggresome; **C)** RPS6; **D)** Colocalization between the two signals is shown as white dots.

Discussion

1. Synaptosomes are enriched in known synaptic components

I isolated synaptosomes from the cerebral cortex of young, adult and old animals (3 weeks-, 5 months- and 18 months-old, respectively) using an optimized version of a published protocol (Moczulska et al., 2014). When compared with total cortical homogenate, my synaptosomes resulted significantly enriched in known synaptic transcripts (Cajigas et al., 2012) and proteins (**Fig.17**). Ribozero RNA-seq and Data Independent Acquisition (DIA) proteomics of synaptosomes and total homogenates were then performed. When reads were aligned to the reference genome, I observed that the percentage of reads mapping to intronic regions was greatly reduced in synaptosomal fraction, further confirming the quality of my preparation (**Fig.18**). I was able to detect a total of 32978 (19097 coding) and 27905 (17911 coding) transcripts with at least one read in the total homogenate and synaptosomal fraction, respectively and 4083 and 3221 proteins with non-null peptide absolute intensity in the total homogenates and synaptosomal fraction, respectively. Compared to previous works on synaptosomes, such as Moczulska et al. (Moczulska et al., 2014) and Chen et al. (Chen et al., 2017), my approach was able to identify a comparable number of synaptosomal proteins (3500 protein groups were identified in the work by Moczulska et al.) and transcripts (a mean of 20000 transcripts was identified in the work by Chen et al.). To further confirm the good quality of synaptosomal enrichment, I visualized the distribution of fold changes of genes related to synapse (GO:0045202) and nucleus (GO:0005634) in synaptosomes with respect to total homogenate (**Fig.19**). As expected, the first gene set resulted to be enriched in synaptosomes, while the latter was depleted from synaptosomes, at both protein and transcript level. Finally, I compared my transcriptomic and proteomic data with published datasets of dendritic RNAs (Middleton et al., 2019; Ouwenga et al., 2017; Zappulo et al., 2017), in order to obtain an independent confirmation of the quality of my preparation. I found my data to be particularly correlated to Ouwenga dataset: they performed TRAP-seq (Translating Ribosome Affinity Purification) on synaptosomes isolated from 3 weeks-old mouse cortex to identify actively translated synaptic transcripts, thereby suggesting that the transcripts I detected might also be actively translated (**Fig.20A**). I found a lower correlation with Zappulo dataset: in this work, they performed proteomic and transcriptomic analysis of mechanically isolated neurites of *in vitro* differentiated neurons (iNeurons). The regional identity of the iNeurons used in this study is not known and that their development stage corresponds to embryonic neurons (DIV6),these two facts likely account for the lower correlation (**Fig.20B-C**). Finally, I compared our data with highly conserved dendritic transcripts from Middleton *et al.* (**Fig.20D**). Taken together, these comparisons demonstrate the good quality of the preparation I analyzed here.

2. Comparison of synaptosomal enrichment in transcriptome and proteome.

I specifically analyzed genes that were differentially expressed between synaptosomes and total homogenate both at protein and transcript level (N = 3149) in young animals using Fisher's method

(Lury & Fisher, 1972) (**Fig.21**). I found that genes coding for synaptic proteins were enriched in synaptosomes both at protein and transcript level (Quadrant 1 of **Fig.21** and **Fig.22B**), while genes coding for nuclear proteins were depleted from synaptosomes both at protein and transcript level (Quadrant 3 of **Fig.21** and **Fig.22C**). Proteins enriched in synaptosome whose corresponding transcript is depleted were related to synaptic vescicles and membrane and SNARE complex (Quadrant 4 of **Fig.21** and **Fig.22A**): these proteins might be enriched at synapses due to active transport. In fact, it has recently been reported that synaptic vescicles- and active zone-proteins are transported to the presynapse in presynaptic lysosome-related vesicles (PLVs) by means of Arl8, a GTPase involved in the active transport of lysosome-related organelles (Vukoja et al., 2018). Interestingly, I found that transcripts related to ribosomes, translation and respiratory chain were also enriched in synaptosome, as previously reported (Middleton et al., 2019; Quadrant 2 of **Fig.21** and **Fig.22D**). However, the proteins coded by these genes were depleted from synaptosome. The more likely explanation for this observation is that these transcripts are translationally repressed. To obtain support for this hypothesis, I compared genes of quadrant 1 and 2 of **Fig.21** with data from Zappulo (2017). In this paper, local translation and protein synthesis rates were quantified by ribo-Seq and SILAC (**Fig.23**). Interestingly, genes of quadrant 1 showed significantly higher association to ribosome and protein synthesis rates than genes of quadrant 2. Furthermore, I used the same ribo-seq dataset (Zappulo et al., 2017) to confirm that genes related to specific Gene Ontology (GO) categories were translationally repressed: in particular, I observed that transcripts related to translation, ribosomes and respiratory chain had lower translation rates in synapse as compared to synaptic genes (**Fig.24**). This analysis provides only indirect support for the hypothesis that transcripts belonging to these GO categories are translationally repressed. It would have been necessary, in fact, to perform ribo-seq on our samples to have a direct estimate of translation rates, since Zappulo's dataset relates to embryonic neurons and synaptic enrichment in this dataset is lower than in datasets obtained from adult animals, as discussed above. This has not been possible due to time constrains.

I compared genes that were differentially expressed between synaptosomes and total homogenate both at protein and transcript level also in adult (N = 2726, **Fig.25**) and old animals (N = 3055, **Fig.26**). During aging, there is no substantial change in the GO categories corresponding to genes enriched at synaptic level. The most relevant changes in GO categories affect genes that are enriched at transcript, but not protein level in synaptosomes (located in the second quadrant). An intriguing finding was that, in young animals there was an overrepresentation of categories related to spliceosome, both in quadrants 2 and 3 (**Fig.22C-D**); in adult and old animals these categories are overrepresented only in the 3rd quadrant (**Fig.27C, 28C**). These data might suggest a role of spliceosomal transcripts during development and is probably related to local protein synthesis: in fact, these transcripts might be part of the ribonucleoprotein complexes which transport mRNAs and they might be locally translated to catalyze the local processing of miRNAs. GO categories related to ribosomes and respiratory chain are on the other hand overrepresented in the 2nd quadrant in young and adult animals (**Fig.22D, 27D**), but not in old animals (**Fig.28D**). At 18 months, in fact, respiratory chain GO category is overrepresented in Q3 (**Fig.28C**). This finding could be related to the high energy demand of the synapse: the stimulated transient local production of proteins that enhance the capacity to make ATP might, in fact, facilitate translation of other synaptic proteins.

To evaluate whether there are changes in the stoichiometry of protein complexes between somatic and synaptic compartment, I applied a previously published method (Ori et al., 2015). This method identifies proteins that are up- or downregulated when normalized to the other members of the complex. Among the proteins most affected with respect to the complex, I observed an overrepresentation at synaptic level of complexes involved in spliceosome and mRNA binding (**Table 2**). This was already reported by Zappulo et al.(2017), who identified specific RNA binding proteins (RBPs) located in the neurites. I found two of these RBPs to be enriched at synaptic level in young animals (Ybx1, RRbp1). Interestingly, Rrbp1 is enriched at transcript but not protein level in young animals (it is in fact located in quadrant 2 of **Fig.21**), and it becomes enriched at transcript and protein level at 5 months and 18 months (located in quadrant 1 of **Fig.25** and **Fig.26**). I hypothesize that spliceosome proteins might be responsible for local splicing or for the translational repression of genes related to ribosomes and respiratory chain at synaptic level.

Finally, I was able to confirm in the cerebral cortex the finding that ribosomes are located in synapses originally reported for the hippocampus (Hafner et al., 2019), combining the staining of a ribosomal protein with MAP2, a marker of neuronal processes (**Fig.29**) and the staining of ribosomal RNA with the presynaptic marker VGLUT1 (**Fig.30**). Furthermore, I observed that ribosomes are fully assembled, both in somata and processes, combining the staining of ribosomal protein and RNA (**Fig.31**).

3. Long non-coding RNA (lncRNA) in synaptosomes.

LncRNAs, which are involved in a wide range of structural, regulatory, and catalytic processes(Ward, McEwan, Mills, & Janitz, 2015), were recently reported to be present at synapses (Chen et al., 2017; Rybak-Wolf et al., 2014). In my data, I found that 35% of genes differentially expressed between soma and synapse to be non-coding RNAs. I correlated synaptic enrichment of these lncRNA with those found by other authors (Ouwenga et al., 2017; You et al., 2015; Zappulo et al., 2017). Again, the highest correlation was found with Ouwenga dataset, although in this case, since they purified specifically ribosome-bound transcripts, I found a lower number of common synaptic ncRNAs (**Fig.32B**). When comparing our data with Zappulo dataset, I found the highest number of common synaptic ncRNAs (N = 289), therefore I used the ribo-seq dataset described in §2 to confirm that the putative synaptic ncRNAs are translationally inactive, using as comparison all protein-coding RNAs that were significantly enriched in synaptosomes (**Fig.32D**). Finally, I confirmed synaptic enrichment for three ncRNAs of our dataset by means of qPCR (**Fig.33**). Nevertheless, it would be interesting to validate their enrichment also by Fluorescent In Situ Hybridization (FISH), an experiment I could not perform due to time constraints.

4. Global effects of age on protein and RNA.

In order to gain a first insight on the effect of age on total homogenate and synaptosomes, I performed Principal Component Analysis (**Fig.34**) and hierarchical clustering (**Fig.35**) of the samples based on either transcript or protein abundance. In general, I could observe a clear segregation of young samples from those of older ages. This is consistent with the notion that at 3 weeks of age, the mouse cortex is highly plastic, and the genes expressed to support this synaptic plasticity are likely responsible for the observed separation. I also observed a clear separation between the ages at RNA level. This separation becomes less evident at protein level, suggesting a more homogeneous protein composition across the ages possibly due to buffering events (Y. Liu, Beyer, & Aebersold, 2016), although I have to remark that RNA data have much higher depth that protein data.

I then examined the correlation between RNA and protein in total homogenate and synaptosomes at each time point (**Fig.36**). I detected a significant higher correlation in total homogenate as opposed to synaptosomes ($p=0.0002$ evaluated by two-way ANOVA), likely due to transport of some proteins from the soma. I also observed a decrease in correlation as a function of age ($p < 0.0001$ evaluated by two-way ANOVA) indicating age-dependent decoupling between protein and transcript concentrations. This phenomenon was extensively reported in the brain of other vertebrates, such as primate (Wei et al., 2015) and very recently by our group in the short-lived fish *Nothobranchius furzeri* (Sacramento et al., 2019).

I analyzed protein and RNA correlation with age in total homogenate. I observed that, transcripts whose abundance correlates positively with age are related to spliceosome, ribosomes and respiratory chain, while those negatively correlated with age are mostly related to synapse, membrane and extracellular matrix (**Fig.38** and **Table 3**). For what concerns proteins whose abundance positively correlates with age, I found that they were related to respiratory chain, synapse and membrane, while those negatively correlated with age were related to ribosomes and spliceosome (**Fig.40** and **Table 3**).

The fact that respiratory chain genes have the same positive correlation with age at protein and transcript level in total homogenate, might indicate a compensatory effect to age-induced oxidative stress. It was reported that, the most important functional deficits in aged brain mitochondria include a loss of mitochondrial membrane potential and phosphorylation capacity, decreased respiration and ATP synthesis and activation of mitochondrial permeability transition pore(Chakrabarti et al., 2011). Although most studies have reported a moderate decrease in the activities of respiratory complexes in aged brain mitochondria, the pattern and the extent of such decrease are quite variable and some studies have even indicated an increase in complex IV activity in aged rodent brain (Takai, Inoue, Shisa, Kagawa, & Hayashi, 1995). The positive correlation with age of transcripts coding for ribosomal proteins, as opposed to the negative correlation with age of ribosomal proteins in total homogenate is consistent with previously published data of our group (Sacramento et al., 2019) and might be due to aggregation of ribosomal proteins as described below. I observed the same opposite behavior also for transcripts and proteins related to spliceosome and synaptic components.

Finally, I analyzed protein and RNA correlation with age in synaptosomes. I observed that, transcripts whose abundance is positively correlated with age in synaptosomes are related to membrane and synaptic components, while those negatively correlated with age are mostly related to respiratory chain and ribosomes (**Fig.41** and **Table 3**). For what concerns proteins positively correlated with age in synaptosomes, I found that they were related to myelin sheath and membrane, while those negatively correlated with age were related to ribosomes and proteasome (**Fig.42** and **Table 3**). Respiratory chain transcripts at synaptic level are negatively correlated with age, which is in opposition to what happens at total homogenate level. This could be explained by the fact that synaptic mitochondria express a different set of transcripts (Winden et al., 2009) and they might be differentially regulated with respect to somatic mitochondria. Interestingly, in synaptosomes I found a negative correlation with age of ribosomal genes both at transcript and protein level, which is opposed to what I observed in total homogenate. Therefore, I hypothesized that the transport of transcripts coding for ribosomal proteins might be affected by aging. I will address this question in the next section.

5. Synaptic gradient of proteins and transcripts is affected by age.

To test whether synaptic enrichment of specific transcripts or proteins changes during aging, for each gene I correlated the ratio of the expression level in the two compartments with age using Spearman's method. I then analyzed the rho values of all the expressed genes using GAGE algorithm to detect Gene Ontology categories enriched in members whose enrichment is positively- or negatively-correlated with age. I observed that transcripts related to mitochondria and respiratory chain have a positive correlation with age and therefore their gradient from soma to synapse increases with age (**Fig.43A**). Ribosomal proteins are enriched in soma and their gradient to synapses increases with age. On the other hand, transcripts coding for ribosomal proteins are enriched in synaptosomes in young animals and their enrichment decreases with aging, therefore they are negatively correlated with age (**Fig.43B**). I successfully validated these data by means of western blot and qPCR (**Fig.59-61**). Interestingly, aging blunts the soma-to-synapse gradient of ribosomal proteins and their corresponding transcripts even if these are with age opposed to a decrease of soma-to-synapse gradient of ribosomal transcripts. I hypothesized that, this might indicate a compensatory mechanism to the impairment of protein synthesis and the aggregation of ribosomal proteins that happen during aging: to sustain synaptic translation, in fact, ribosomal proteins might be provided by the soma, thereby causing a compensatory decrease of ribosomal transcripts.

6. Decoupling between somatic and synaptic compartment during aging.

I compared transcripts regulated during adulthood (between 3 weeks and 5 months) and aging (between 5 months and 18 months) in total homogenate and synaptosomes (**Fig.44A** and **B**). I observed that, during adulthood, there is a high correlation in the age-dependent fold-changes between the two compartments at transcriptome level, which is completely lost during aging. The

same phenomenon is observed also at proteome level (**Fig.45A** and **B**), with a correlation coefficient decreasing from 0.605 during adulthood to 0.262 during aging. This suggests that in the last phase of synaptogenesis and until the stage of young adult, there is a strong dependency between synaptosomes and somata and that changes observed in the first compartment are driven by changes in the latter. I then performed Gene Ontology (GO) analysis for each of the comparisons described above (**Fig.46-49**) and noticed that genes related to synapse are upregulated during adulthood at transcript and protein level both in total homogenate and synaptosomes (quadrant 1 of **Fig.46** and **48**) and are downregulated from both compartments during aging (quadrant 3 of **Fig.47** and **49**). The fact that at 3 weeks synaptogenesis is still ongoing could explain this upregulation in young age of synaptic genes. Furthermore, the downregulation of synaptic proteins during aging might justify the decrease of synaptic contacts reported by Morrison & Baxter (2012). Notably, I observed that transcripts coding for ribosomal proteins are upregulated in both compartments during adulthood and aging, while ribosomal proteins are downregulated from both compartments at 5 months and become upregulated at 18 months. This differential regulation of ribosomes suggests a decoupling between transcriptome and proteome that I will address in the next section. Finally, I detected a downregulation of genes related to proteasome in both total homogenate and synaptosomes that starts at 5 months and is stable during aging, since this category is not detected at 18 months. The downregulation of proteasome components during aging is correlated to the loss of proteostasis and is an established marker of aging (López-Otín, Blasco, Partridge, Serrano, & Kroemer, 2013) and might explain the formation of protein aggregates in old animals, an issue that I will address in §8.

7. Decoupling between transcriptome and proteome during aging.

Next, I analyzed the correlation between transcriptome and proteome in total homogenate, comparing genes significantly regulated either at protein or transcript level in this compartment during adulthood and aging (**Fig.50** and **52**). I observed a decrease in the correlation between RNA- and protein regulation, that I already discussed in §4. Then, I made a Gene Ontology analysis on genes of **Fig.50** and **52** (**Fig.51** and **53** and **Table 4**). I observed that genes related to synapse and myelin sheath are upregulated at protein, but not transcript level in total homogenate during adulthood and this regulation is completely reverted during aging, meaning that they are upregulated at transcript, but not protein level. This regulation might be due to the particularly long halflife of some myelinic and synaptic proteins (Heo et al., 2018). In my data, in fact, I found representative myelin proteins, such as Myelin basic protein (Mbp), that were reported to have extremely long turnover times (Toyama et al., 2013). Further, I observed that ribosomal genes are upregulated at transcript, but not protein level during adulthood; interestingly, during aging they are partially upregulated at protein level. They are, in fact, present in both quadrant 1 and 2 of **Fig.53**. This result was already observed in a recent work of our group in the short-living fish *Nothobranchius furzeri* (Sacramento et al., 2019). These findings might indicate an imbalance in the relative levels of ribosomal proteins during aging, which is likely to impair ribosome assembly and to create a pool of disassembled proteins at risk of aggregation. Finally, as already discussed in §6, I detected a decrease

in proteasome genes both at transcript and protein level already at 5 months of age, which is stable during aging.

When I analyzed the relationship between transcriptome and proteome during adulthood and aging at synaptic level (**Fig.54** and **56**), I again detected a loss of correlation between RNA- and protein-regulation comparable to what I observed in total homogenate. I then performed GO analysis (**Fig.55** and **57** and **Table 4**) and noticed that, while myelin and synaptic genes have the same regulation in synaptosomes and in total homogenate, respiratory chain genes are regulated differently, since they increase at protein but not transcript level during adulthood and are downregulated during aging. For what concerns ribosomal genes, as it is evident also from **Fig.54** and **56**, they are downregulated at protein level during adulthood and become upregulated at protein but not transcript level during aging. Transcripts coding for ribosomal proteins are translationally repressed at synaptic level. The upregulation of ribosomal proteins with age could be connected to loss of translational repression. In general terms, it has been shown, in fact, that inhibition of TOR pathway, thereby a mild inhibition of protein synthesis, extends lifespan in yeast, nematodes, fruit flies and mice (Johnson, Rabinovitch, & Kaeberlein, 2013). Furthermore, deletion of ribosomal proteins was shown to extend replicative lifespan in yeast (Chiocchetti et al., 2007). Furthermore, I hypothesized that, ribosomes might physiologically aggregate during aging and the upregulation of ribosomal proteins in old animals might be a compensatory effect for this mechanism. I will address this question in the next section.

8. Synaptic aggregates are enriched in ribosomal proteins.

Protein aggregation is a phenomenon in which misfolded protein, that are not in the conformation required for their functionality, form large multimeric complexes or interact inappropriately with other cellular components impairing cell viability (Stefani & Dobson, 2003). It was reported that protein aggregates play an important role in the onset of many neurodegenerative diseases such as Alzheimer's or Parkinson's disease (Dobson et al., 2001). SDS-insoluble protein aggregates were extracted from raw synaptosomes of 23 months-old mice, using a modified version of the protocol reported in Reis-Rodrigues *et al.* (2012) and subjected to Mass spectrometry analysis. For this analysis I used only old mice, because from recently published data of my group appears that young and adult brains do not contain protein aggregates (Sacramento et al., 2019). I compared these data with protein composition of total synaptosomes to identify proteins that are enriched in the aggregates when normalized to their abundance in the total homogenate and found that synaptic aggregates are highly enriched in ribosomal proteins, whereas only few synaptic proteins tend to aggregate at synaptic level. Ribosomal proteins were reported to aggregate *in vitro* in presence of lysozyme and reducing conditions (Pathak, Mondal, Banerjee, Ghosh, & Barat, 2017). More recently, a study of my group showed the aggregation of ribosomal proteins in *N.furzeri* and mouse brain (Sacramento et al., 2019). I compared these data with synaptosomal data and observed that only 43 proteins are aggregating both at synaptic level and in total brain, of which only 9 have a p value < 0.05 (**Fig.64B-C** and **Table 5**), while 78 proteins are specifically aggregating in synaptic compartment (**Table 6**). I

validated ribosome aggregation in mouse cortex by means of immunofluorescence, combining the staining of the ribosomal protein S6 with aggresome dye (Shen et al., 2011)(**Fig. 67, 68**). In the adult cortex I did not observe any aggregation of ribosomal protein S6 (**Fig.67D**), while in the old cortex I observed colocalization of the signals also outside the somata (**Fig.68D**). As a control, I chose a ribosomal protein (RPL15) absent in the synaptosomal dataset, but highy enriched in aggregates from total homogenates according to Sacramento et al. (2019). I performed immunofluorescence of adult and old cortex, combining the staining for RPL15 and aggresome dye (**Fig.69, 70**). I observed that RPL15 aggregation in the old cortex is restricted almost only to the somata (**Fig.70D**).

Notably, in my aggregates data I found a protein belonging to proteasome complex (Psma6) and two lysosomal proteins (Lamp2 and Atp6v0c) (**Fig.64A** and **Table 6**). Strikingly, desmoplakin resulted to be the most enriched protein in synaptic aggregates. Desmoplakin is an insoluble protein of desmosomes plaque structure, which regulates cell adhesion. Desmosomal structure was recently resolved by super-resolution microscopy in human keratinocytes (Stahley, Bartle, Atkinson, Kowalczyk, & Mattheyses, 2016). Interestingly, desmoplakin has never been reported in synapses, therefore I decided to validate this finding by means of immunofluorescence (**Fig.65** and **66**). I combined the staining for desmoplakin with Map2, a marker of neuronal processes; I observed that, in young animals, desmoplakin puncta are mainly located in somata, while in old animals the distribution outside the cell body becomes predominant, with aggregate-like structures colocalized with Map2. Taken together, these data indicate synaptic aggregation of ribosomal proteins, which is probably caused by an altered stoichiometry of the ribosome during aging. The aggregation of a cell adhesion protein like Desmoplakin might be due to its particular structure and underlie the loss of synaptic contacts during aging.

9. Conclusion and outlooks.

Aging is defined as the time-dependent functional decline that, in the brain, is associated to synaptic loss and impairment of specific cognitive functions such as working memory (Morrison & Baxter, 2012). At a cellular level, oxidative stress, mitochondrial dysfunction, DNA damage and failure of proteostasis with accumulation of protein aggregates have been proposed as possible causes for neuronal dysfunction. (López-Otín et al., 2013). In this study, I combined, for the first time, proteomic and transcriptomic analysis in aging synapses. It emerged that, during aging, there is a reduction of correlation between transcript and protein both in soma and synapse. In the soma there is complete loss of correlation between somata and synapse and this affects both transcriptome and proteome and is caused mainly by genes related to synaptic function. I also observed a decoupling between the regulation of transcriptome and proteome at synaptic and soma level. Furthermore, I showed that soma-synapse gradient of ribosomal genes is affected by age: in particular I observed an increase in soma-to-synapse gradient of ribosomal proteins with age and a decrease of soma-to-synapse gradient of ribosomal transcripts. Finally, I analyzed aggregates in old cortical synaptosomes and showed the aggregation of ribosomal, lysosomal and adhesion proteins. This study suggests that aging affects both the local translational machinery and the trafficking of transcripts and proteins.

This study leaves some open questions that might be addressed in follow-up studies. First of all, the notion that transcripts coding for ribosomal proteins are translationally repressed in young animals and become de-repressed in old animals should be properly supported by an experiment of Ribo-seq. I managed to successfully isolate ribosomes using sucrose cushion, but for time reasons I could not apply this protocol to enriched synaptosomes and perform RNA-seq. Another important weakness of this thesis is the lack of validations by in situ hybridization (ISH) that has been used in other studies to confirm the synaptic localization of transcripts. Due to the low abundance of synaptic transcripts, this study would however require high-sensitivity RNAscope, a complex protocol that I did not have the time to establish. Finally, it could be more convenient to image synapses using super-resolution microscopy, since this could also allow the measurement of particle size.

Methods

1. Animals

Wild-type C57BL/6J were housed in standard cages and fed standard lab chow and water ad libitum. Euthanasia was carried out by cervical dislocation in accordance with the European Council Directive of 22 September 2010 (2010/63/EU). The scientific purposes of the experiments were approved by the local authorities and supervised by the local veterinary (Anzeige N. O_AC_04, O_AC_08, O_AC_10).

For the synaptosome protocol, cerebral cortices of young (3 weeks), adult (5 months) and old (23 months) mice were dissected and immediately processed (**Table 7** shows an overview of the animals). For immunohistochemistry the brain was carefully removed, divided into two halves along the median plane, fixed overnight in 4% paraformaldehyde (PFA) and dehydrated by ethanol gradient.

Table 7. Overview of animals used for all the experiments. For each animal age, strain, sex, RNA and protein concentrations are reported and the experiments for which it was used is specified. TH = Total Homogenate, Syn = Synaptosomes

ID	Age	Strain (sex)	Sample	RNA concentration [ng/uL]	Protein concentration [µg/µL]	Single-end RNA Seq	Paired-end RNA Seq	WB validation	RT-qPCR validation
57	3w	C57BL/6 (♂)	TH	336	1.68			✔	✔
			Syn	20	1.17			✔	✔
58	3w	C57BL/6 (♂)	TH	208	2.77			✔	✔
			Syn	32	1.2			✔	✔
59	3w	C57BL/6 (♂)	TH	273	1.94	✔	✔		✔

			Syn	28	0.9	✔	✔			✔
60	3w	C57BL/6 (♂)	TH	311	1.01	✔	✔	✔	✔
			Syn	26	0.79	✔	✔	✔	✔
61	3w	C57BL/6 (♂)	TH	311	1.07	✔	✔	✔	
			Syn	26	0.56	✔	✔	✔	
62	3w	C57BL/6 (♂)	TH	280	1.06	✔	✔		
			Syn	22	0.75	✔	✔		
130	3w	C57BL/6 (♀)	TH	281	38.15			✔	✔
			Syn	27	2.68			✔	✔
131	3w	C57BL/6 (♀)	TH	289	24.2			✔	✔
			Syn	62	6.05			✔	✔
132	3w	C57BL/6 (♂)	TH	328	14.03			✔	✔
			Syn	52	3.36			✔	✔
133	3w	C57BL/6 (♂)	TH	318	14			✔	✔
			Syn	49	4.49			✔	✔
71	5m	C57BL/6 (♂)	TH	246	7.77			✔	✔
			Syn	20	0.95			✔	✔
72	5m	C57BL/6 (♂)	TH	305	8.45	✔	✔	✔	✔
			Syn	21	1.4	✔	✔	✔	✔
73	5m	C57BL/6 (♂)	TH	260	13.59			✔	✔
			Syn	16	0.46			✔	✔
74	5m	C57BL/6 (♂)	TH	276	18.1	✔	✔		
			Syn	16	0.51	✔	✔		
75	5m	C57BL/6 (♂)	TH	253	16.67	✔	✔	✔	✔
			Syn	18	0.38	✔	✔	✔	✔
76	5m	C57BL/6 (♂)	TH	286	28.55	✔	✔		
			Syn	18	0.45	✔	✔		
122	6m	C57BL/6 (♂)	TH	65	14.87			✔	✔
			Syn	26	3.89			✔	✔
123	6m	C57BL/6 (♂)	TH	195	14.73			✔	✔
			Syn	37	3.88			✔	✔
124	6m	C57BL/6 (♂)	TH	208	8.03			✔	✔
			Syn	32	3.65			✔	✔
125	6m	C57BL/6 (♂)	TH	145	29.4			✔	✔

			Syn	30	2.52			✔	✔
46	18m	C57BL/6 (♂)	TH	94	1.08	✔		✔	
			Syn	16	0.29	✔		✔	
47	18m	C57BL/6 (♂)	TH	265	1.6	✔		✔	
			Syn	18	0.15	✔		✔	
48	18m	C57BL/6 (♂)	TH	231	1.7	✔		✔	
			Syn	15	0.2	✔		✔	
49	18m	C57BL/6 (♂)	TH	223	1.4	✔		✔	
			Syn	17	0.23	✔		✔	
67	19m	C57BL/6 (♂)	TH	305	14.25	✔	✔		✔
			Syn	56	0.81	✔	✔		✔
68	19m	C57BL/6 (♂)	TH	286	21.97	✔	✔		✔
			Syn	26	0.92	✔	✔		✔
69	19m	C57BL/6 (♂)	TH	275	16.51	✔	✔		✔
			Syn	22	0.15	✔	✔		✔
70	19m	C57BL/6 (♂)	TH	277	16.69	✔	✔		✔
			Syn	21	0.1	✔	✔		✔
126	18m	C57BL/6 (♂)	TH	194	16.37			✔	✔
			Syn	43	2.94			✔	✔
127	18m	C57BL/6 (♂)	TH	212	4.34			✔	✔
			Syn	56	4.49			✔	✔
128	18m	C57BL/6 (♂)	TH	237	15.5			✔	✔
			Syn	61	5.16			✔	✔
129	18m	C57BL/6 (♂)	TH	120	40.05			✔	✔
			Syn	31	1.5			✔	✔

2. Synaptosome preparation

Synaptosome enrichment was performed according to the protocol of (Gray &Whittaker, 1962) with small modifications. Cerebral cortices were homogenized in ice cold homogenizing buffer (10 mM HEPES, 1 mM EDTA, 2 mM EGTA, 0.5 mM DTT, 0.32 M sucrose, pH 7) containing protease inhibitors (1 tablet/10 mL, Roche, Cat. N. 11836170001) with 12 strokes using a Teflon-glass tissue grinder (Sigma Aldrich, Cat. N. D9063) with pestle A (clearance of 0.0028-0.0047 inches)on ice. The homogenate was centrifuged at 1000 g for 10 minutes at 4 °C using a tabletop centrifuge (Eppendorf 5417R). The supernatant was centrifuged again at 10000 g for 40 minutes at 4 °C. The obtained pellet (p2), containing raw synaptosomes, was resuspended in cold homogenizing buffer, layered

over a discontinuous sucrose gradient (0.85 M/1 M/1.18 M sucrose), and centrifuged at 20000 rpm (50512g), 4 °C, for 2 h using SW-40Ti rotor and Optima XP-N80 ultracentrifuge (Beckman Coulter). The interface between 1 M and 1.18 M, containing synaptosomes, was collected with a needle and stored at −80 °C. Small aliquots were withdrawn from the total homogenate, after the first centrifugation (cytosolic fraction) and from the pellet loaded on the sucrose gradient (raw synaptosomes).

3. RNA isolation from synaptosomes

RNA extraction from synaptosomes was performed as previously described (Smalheiser & Lugli 2014). The synaptosomes were diluted in synaptosomal RNA buffer (50 mM Hepes, pH 7.5, 125 mM NaCl, 100 mM sucrose, 2 mM K acetate, 10 mM EDTA) containing protease inhibitors (1 tablet/10 mL, Roche, Cat. N. 11836170001), 160 U/mL Superase-In (Invitrogen, Cat.N. AM2694), 160 U/mL Rnase-OUT (Invitrogen, Cat. N. 10777019), quickly pelleted at 20000 g for 20 minand rinsed twice in 4 × volume of synaptosomal RNA buffer and spundown again 20000 g for 20 minutes. They were then resuspended in 100 μL of synaptosomal RNA buffer and RNA was extracted with standard Trizol protocol (Chomczynski & Sacchi, 1987), using Qiazol lysis reagent (Qiagen Cat. N. 79306).

In brief 0.2 mL of chloroform were added per mL of Trizol reagent, samples were mixed and centrifuged at 20000 g for 20 minutes at 4 °C in a tabletop centrifuge. After the centrifugation, the upper aqueous phase was withdrawn and mixed with 0.5 volumes of isopropyl alcohol, 0.16 volumes of sodium acetate and 1μL of GlycoBlue Coprecipitant (Thermo Scientific, Cat. N. AM9515) to precipitate RNA. Samples were then centrifuged at 20000 g for 30 minutes at 4 °C, washed twice with 80% ethanol and centrifuged at 7500 g for 5 minutes at 4 °C. The resulting pellet was dried for 5 minutes and resuspended in nuclease-free water (Qiagen, Cat N. 129114). RNA concentration was measured using the Nanodrop ND-1000 (PeqLab). Concentrations of RNA samples are reported in **Table 7**.

4. Protein quantification and Western blotting

Proteins were quantified using an EZQ kit (ThermoScientific, Cat. N. R33200), according to manufacturer's instructions. The protein concentrations of the Total Homogenate and Synaptosomes samples are reported in **Table 7**. For Western blotting, equal amounts of protein (usually 10μg) were mixed with Lysis buffer (50mM Tris-HCl (pH 7.4), 150mM NaCl, 1% v/v Triton X-100, 0.5% w/v sodium deoxycholate, 1mM EDTA, 1% v/v Protease Inhibitor Cocktail (Sigma-Aldrich, Cat. N. P8340), 1mM NaF, 1mM Na 3 VO 4 , 1% v/v Phosphatase Inhibitor Cocktail 3 (Sigma-Aldrich, Cat . N. P0044)) and Loading Dye (5% v/v β-Mercaptoethanol, 0.05% w/v bromophenol blue, 30% v/v glycerol, 10% w/v SDS, 250mM Tris-HCl, pH 6.8) and loaded onto a

12% sodium dodecyl sulfate (SDS) polyacrylamide gel and separated by electrophoresis (BioRad miniProtean system chamber, BioRad). Proteins were blotted onto a Nitrocellulose Blotting Membrane Amersham Protran Premium 0.45µm NC (GE Healthcare Life Science, Cat. N. 10600003), blocked for 1 hour with 5% powder milk (Carl Roth, Cat. N. T145) in TBST (15mM Tris-HCl, 5mM Tris base, 150mM NaCl, 0.1% v/v Tween 20) and incubated with primary antibodies (**Table 8**) overnight at 4 °C. The nitrocellulose membrane was washed 3 times with TBST and incubated with the secondary antibody (**Table 9**) for 1 hour at room temperature (RT). Membranes were washed 3 times with TBST and incubated with Immobilon Forte Western HRP Substrate (Merck, Cat. N. WBLUF0100) for 2 minutes. Blots were imaged using an Amersham Imager 600 (GE Healthcare Life Sciences) scanner. For normalization of protein levels on Western blots, alpha-tubulin levels were determined and used as reference for each individual sample. To this end, blots were incubated for 15 minutes at 37 °C with Restore Western Blot Stripping Buffer (Thermo FisherCat. N. 21059), then washed 2 times with TBST, blocked again for 1 hour and incubated with anti-alpha-tubulin antibody (**Table 8**) for 1 hour at RT. After washing, the membrane was incubated with the secondary antibody (**Table 9**), washed with TBST, incubated with Immobilon Forte Western HRP Substrate (Merck, Cat. N. WBLUF0100) for 2 minutes, and imaged as described above.

The quantification of the relative expression level is done using ImageJ2 (Rueden *et al.,* 2017). Briefly, the bands are highlighted using a Region Of Interest (ROI) and the intensity is measured by the Analyze function of the software. The same ROI is then used to measure the background, then the background is subtracted to the protein expression level. Finally the expression level is normalized on the expression level of the housekeeping, in this case α-Tubulin.

Table 8. List of primary antibodies used for Western Blot.

Target	Host species	Clonality	Isotype	Predicted band	Dilution used	Cat. N.
RPL10A	Rabbit	Polyclonal	IgG	25kDa	1:1000	ab226381 (Abcam)
RPS6	Rabbit	Monoclonal	IgG	32kDa	1:1000	2217 (Cell Signaling)
RPL7	Rabbit	Polyclonal	IgG	29kDa	1:1000	A300-741A (Bethyl)
RPL15	Rabbit	Polyclonal	IgG	24kDa	1:1000	LS-C162700 (LSBio)
α-TUBULIN	Mouse	Monoclonal	IgG	55kDa	1:1500	T9026 (Sigma-Aldrich)
Histone H3	Rabbit	Polyclonal	IgG	17kDa	1:1000	ab1791 (Abcam)

NMDAR2B	Rabbit	Polyclonal	IgG	166kDa	1:1000	ab65783 (Abcam)

Table 9. List of secondary antibodies used for Western Blot.

Target	Host species	Clonality	Isotype	Conjucation	Dilution used	Cat. N.
Mouse	Horse	Not reported	IgG	HRP	1:2000	7076 (Cell Signaling)
Rabbit	Goat	Not reported	IgG	HRP	1:2000	7074 (Cell Signaling)
Biotin	Goat	Not reported	IgG	HRP	1:1000	7075 (Cell Signaling)

5. Sample preparation for Mass spectrometry (MS)

Samples were brought to the same sample volume (125 µL) with MilliQ water, then a 2x lysis buffer was added in equal volume, to yield the samples in 250 µL volume containing 1% SDS, 100 mM HEPES pH 8.5 and 50 mM DTT. For samples 69SG, 70SG, and 75SG (A detailed list of samples submitted for proteomic analysis can be found in **Table 10**) where the volume was greater than 125 uL (therefore the addition of water to final vol of 125 uL was insufficient to dilute the sucrose to a low enough molarity, whereby on addition of 4x acetone there would be a phase separation), samples were diluted to a final concentration of sucrose ¼ of the supplied concentration. These samples then had to be processed in falcon tubes rather than Eppendorf tubes to accommodate the 4x acetone volume added for precipitation. Thereby under the centrifugation conditions post-precipitation a maximum g of 3220 could be used during all steps to obtain protein pellets.

Samples were sonicated with 10 cycles (60 seconds ON, 30 seconds OFF)using the high energy mode in a Bioruptor (Diagenode) at 20 °C. The samples were then boiled (95 °C, 10 minutes) before being subjected to another 10 cycles in the Bioruptor. Iodoacetamide (IAA) was added to a final concentration of 15mM and the samples incubated in the dark for 30 minutes at room temperature. Proteins were precipitated with 4 (8 for protein aggregates) volumes equivalent of ice-cold acetone overnight at -20 °C. The following day, samples were centrifuged at 4 °C, 14000 rpm for 30 minutes (Eppendorf 5804R benchtop centrifuge), then the acetone supernatant carefully removed. Protein pellets were washed twice with ice cold 80% acetone/20% water (500 µl each time), and centrifuged 4 °C, 14000 rpm 10 minutes each wash. After the last wash, the acetone/water was removed and the pellets allowed to air dry at room temperature.

Protein pellets were then resuspended in digestion buffer (3 M Urea in 100mM HEPES, pH 8) at a concentration of 1 µg/µL and sonicated using a Bioruptor for 3 cycles (60 seconds ON/30 seconds

OFF). Proteins were digested with Lys-C protease (Wako, Cat. N. 125-05061) 1:100 enzyme : protein ratio (4 hours, 37 °C, with shaking 1000 rpm) then diluted with milliQ water (for a final concentration of 1.5 M Urea) and further digested with Trypsin (Promega, Cat. N. V5280) 1:100 enzyme : protein ratio (overnight, 37 °C, 650 rpm). Samples were acidified the following day by addition of 10% Trifluoracetic Acid (TFA) and then desalted with Waters Oasis® HLB μElution Plate 30μm(Cat. N. 186001828BA) in the presence of a slow vacuum. In this process, the columns were conditioned with 3x100 μL solvent B (80% acetonitrile; 0.05% formic acid) and equilibrated with 3x 100 μL solvent A (0.05% formic acid in milliQ water). The samples were loaded, washed 3 times with 100 μL solvent A, and then eluted into PCR tubes with 50 μL solvent B. The eluates were dried down with the speed vacuum centrifuge and dissolved at a concentration of 1 μg/μL in5% acetonitrile, 95% milliQ water, with 0.1% formic acid prior to analysis by LC-MS/MS.

Table 10. Samples used for proteomic analysis.

Sample Name	Composition	Age	Buffer composition	μg protein for DIA experiment	Volume for DIA experiment (μL)	Notes
46TH	Total Homogenate	18 months	Homogenizing buffer (cfr. Section 2)	50	9.255978	Problems with data analysis cfr. Section 7
46SG	Synaptosomes	18 months	Homogenizing buffer 1M sucrose	15	51.140	Problems with data analysis cfr. Section 7
48TH	Total Homogenate	18 months	Homogenizing buffer (cfr. Section 2)	50	5.882	
48SG	Synaptosomes	18 months	Homogenizing buffer 1M sucrose	15	72.483	
49TH	Total Homogenate	18 months	Homogenizing buffer (cfr. Section 2)	50	7.140	
49SG	Synaptosomes	18 months	Homogenizing buffer 1M sucrose	15	66.244	
59TH	Total Homogenate	3 weeks	Homogenizing buffer (cfr. Section 2)	50	1.713	
59SG	Synaptosomes	3 weeks	Homogenizing buffer 1M sucrose	50	27.745	
60TH	Total Homogenate	3 weeks	Homogenizing buffer (cfr. Section 2)	50	2.468	
60SG	Synaptosomes	3 weeks	Homogenizing buffer 1M sucrose	50	31.507	

61TH	Total Homogenate	3 weeks	Homogenizing buffer (cfr. Section 2)	50	2.324	
61SG	Synaptosomes	3 weeks	Homogenizing buffer 1M sucrose	50	44.890	
62TH	Total Homogenate	3 weeks	Homogenizing buffer (cfr. Section 2)	50	2.357	
62SG	Synaptosomes	3 weeks	Homogenizing buffer 1M sucrose	50	33.384	
67TH	Total Homogenate	18 months	Homogenizing buffer (cfr. Section 2)	50	3.507	
67SG	Synaptosomes	18 months	Homogenizing buffer 1M sucrose	50	61.310	
68TH	Total Homogenate	18 months	Homogenizing buffer (cfr. Section 2)	50	2.276	
68SG	Synaptosomes	18 months	Homogenizing buffer 1M sucrose	10.134	110	
69TH	Total Homogenate	18 months	Homogenizing buffer (cfr. Section 2)	50	3.028	
69SG	Synaptosomes	18 months	Homogenizing buffer 1M sucrose	39.271	260	Problems with protein precipitation, cfr. Section 5
70TH	Total Homogenate	18 months	Homogenizing buffer (cfr. Section 2)	50	2.995	
70SG	Synaptosomes	18 months	Homogenizing buffer 1M sucrose	27.854	270	Problems with protein precipitation, cfr. Section 5
72TH	Total Homogenate	5 months	Homogenizing buffer (cfr. Section 2)	50	5.913	
72SG	Synaptosomes	5 months	Homogenizing buffer 1M sucrose	50	35.408	
74TH	Total Homogenate	5 months	Homogenizing buffer (cfr. Section 2)	50	2.761	
74SG	Synaptosomes	5 months	Homogenizing buffer 1M sucrose	50	98.434	
75TH	Total Homogenate	5 months	Homogenizing buffer (cfr.	50	2.999	

			Section 2)			
75SG	Synaptosomes	5 months	Homogenizing buffer 1M sucrose	50	130.572	Problems with protein precipitation, cfr. Section 5
76TH	Total Homogenate	5 months	Homogenizing buffer (cfr. Section 2)	50	1.751	
76SG	Synaptosomes	5 months	Homogenizing buffer 1M sucrose	50	109.823	

6. LC-MS/MS for Data Independent Analysis (DIA)

Peptides were separated using the nanoAcquity UPLC MClass system (Waters) fitted with a trapping (nanoAcquity Symmetry C_{18}, 5µm, 180 µm x 20 mm) and an analytical column (nanoAcquity BEH C_{18}, 1.7µm, 75µm x 250mm). The outlet of the analytical column was coupled directly to Q-Exactive HFX (Thermo Fisher Scientific) using the Proxeon nanospray source. Solvent A was water, 0.1 % formic acid and solvent B was acetonitrile, 0.1 % formic acid. The samples (approx. 1 µg) were loaded with a constant flow of solvent A at 5 µL/min onto the trapping column. Trapping time was 6 minutes. Peptides were eluted via the analytical column with a constant flow of 0.3 µL/min. During the elution step, the percentage of solvent B increased in a non-linear fashion from 0 % to 40 % in 60 minutes. Total runtime was 75 minutes, including clean-up and column re-equilibration. The peptides were introduced into the mass spectrometer via a Pico-Tip Emitter 360 µm OD x 20 µm ID; 10 µm tip (New Objective) and a spray voltage of 2.2 kV was applied. The capillary temperature was set at 300 °C. The RF ion funnel was set to 40%. Data from the total homogenate samples were first acquired in DDA mode to contribute to a sample specific spectral library. The conditions were as follows: full scan MS spectra with mass range 350-1650 m/z were acquired in profile mode in the Orbitrap with resolution of 60000. The filling time was set at maximum of 20 ms with limitation of 1 x 10^6 ions. The "Top N" method was employed to take the 15 most intense precursor ions (with an intensity threshold of 4 x 10^4) from the full scan MS for fragmentation (using HCD normalized collision energy, 31%) and quadrupole isolation (1.6 Da window) and measurement in the Orbitrap (resolution 15000, fixed first mass 120 m/z).The peptide match 'preferred' option was selected and the fragmentation was performed after accumulation of 2 x 10^5 ions or after filling time of 25 ms for each precursor ion (whichever occurred first). MS/MS data were acquired in profile mode. Only multiply charged (2^+ - 5^+) precursor ions were selected for MS/MS. Dynamic exclusion was employed with maximum retention period of 30 s and relative mass window of 10 ppm. Isotopes were excluded. In order to improve the mass accuracy, internal lock mass correction using a background ion (m/z 445.12003) was applied. For data acquisition and processing of the raw data Xcalibur 4.0 (Thermo Scientific) and Tune version 2.9 were employed.

For the DIA data acquisition the same gradient conditions were applied to the LC as for the DDA and the MS conditions were varied as described: Full scan MS spectra with mass range 350-1650 m/z were acquired in profile mode in the Orbitrap with resolution of 120000. The default charge state was set to 3+. The filling time was set at maximum of 60 ms with limitation of 3 x 10^6 ions. DIA scans were acquired with 34 mass window segments of differing widths across the MS1 mass range. HCD fragmentation (stepped normalized collision energy; 25.5, 27, 30%) was applied and MS/MS spectra were acquired with a resolution of 30000 with a fixed first mass of 200 m/z after accumulation of 3 x 10^6 ions or after filling time of 47 ms (whichever occurred first). Data were acquired in profile mode. All samples (both total homogenate and synaptosomes) had data acquired in DIA mode.

7. Data analysis for DIA data

For library creation, the DDA data was searched using Pulsar (v. 1.0.15764.0.27599) (Biognosys AG, Switzerland). The data were searched against a species specific (*Mus musculus*) Swissprot database with a list of common contaminants appended, as well as the HRM peptide sequences. The data were searched with the following modifications: Carbamidomethyl (C) (Fixed) and Oxidation (M)/ Acetyl (Protein N-term) (Variable). A maximum of 1 missed cleavage was allowed and the identifications were filtered to satisfy FDR of 1 % on peptide and protein level.

Also for library creation, the DIA data was searched using Pulsar (v.1.0.15764.0.27599The data were searched against a species specific (*Mus musculus*) Uniprot database with a list of common contaminants appended, as well as the HRM peptide sequences. The data were searched with the following modifications: Carbamidomethyl (C) (Fixed) and Oxidation (M)/ Acetyl (Protein N-term) (Variable). DpD (DDA plus DIA) libraries were then created by combining the spectral library created from the output of the DDA runs with the searched libraries using Spectronaut (v. 11, Biognosys AG, Switzerland)(Bruderer et al., 2015). This library contained 78629 precursors, corresponding to 4216 protein groups using Spectronaut protein inference. DIA data were then uploaded and searched against this spectral library. Relative quantification was performed in Spectronaut for each pairwise comparison using the replicate samples from each condition. The data (candidate table) and data reports were then exported to excel and further data analyses and visualization were performed with R-studio (version 0.99.902) using in-house pipelines and scripts. Due to issues with the sample, both the synaptosomal data and total homogenate data for sample 46 (**Table 10**) were removed before the further analysis.

8. Synaptosomal insoluble aggregates purification

The synaptosomal pellet (p2) obtained in section 2 was resuspended in Lysis buffer (4% SDS, 100mM HEPES, 1mM EDTA, 100mM DTT) and sonicated using a Bioruptor (Diagenode) set to high mode for 10 cycles of 60 seconds with 30 seconds breaks between each cycle at 20°C. After a

quick spin down at 20000 g for 5 minutes at RT to remove debris, samples were transferred in 200 µL polycarbonate tubes and ultracentrifuged at 100000g for 30 minutes at 20°C in an Optima TLX ultracentrifuge using the TLA100 rotor. Pellets (the SDS insoluble proteins) were washed twice with lysis buffer and then dissolved in 50 µL of 100 % Formic acid (FA) under agitation at 400 rpm for 1 hour at 37 °C. Formic acid was then removed by means of a SpeedVac (Eppendorf) and pellets were dissolved in 20 µL of Lysis buffer 4 % SDS, boiled for 4 minutes and homogenized with a Bioruptor mode for 5 cycles of 60 seconds with 30 seconds breaks between each cycle at 20 °C. Samples were then prepared for MS as described in section 5.

9. Data acquisition for aggregates vs. raw synaptosomes

9.1 LC-MS/MS

Peptides were separated using the nanoAcquity UPLC system (Waters) fitted with a trapping (nanoAcquity Symmetry C_{18}, 5µm, 180 µm x 20 mm) and an analytical column (nanoAcquity BEH C_{18}, 1.7µm, 75µm x 250mm). The outlet of the analytical column was coupled directly to an Orbitrap Fusion Lumos (Thermo Fisher Scientific) using the Proxeon nanospray source. Solvent A was water, 0.1 % formic acid and solvent B was acetonitrile, 0.1 % formic acid. The samples (20 µL) were loaded with a constant flow of solvent A at 5 µL/min onto the trapping column. Trapping time was 6 minutes. Peptides were eluted via the analytical column with a constant flow of 0.3 µL/min. During the elution step, the percentage of solvent B increased in a linear fashion from 3 % to 25 % in 30 minutes, then increased to 32 % in 5 more minutes and finally to 50 % in a further 0.1 minutes. Total runtime was 60 minutes. The peptides were introduced into the mass spectrometer via a Pico-Tip Emitter 360 µm OD x 20 µm ID; 10 µm tip (New Objective) and a spray voltage of 2.2 kV was applied. The capillary temperature was set at 300 °C. The RF lens was set to 30%. Full scan MS spectra with mass range 375-1500 m/z were acquired in profile mode in the Orbitrap with resolution of 120000. The filling time was set at maximum of 50 ms with limitation of 2×10^5 ions. The "Top Speed" method was employed to take the maximum number of precursor ions (with an intensity threshold of 5×10^3) from the full scan MS for fragmentation (using HCD collision energy, 30%) and quadrupole isolation (1.4 Da window) and measurement in the ion trap, with a cycle time of 3 seconds. The MIPS (monoisotopic precursor selection) peptide algorithm was employed but with relaxed restrictions when too few precursors meeting the criteria were found. The fragmentation was performed after accumulation of 2×10^3ions or after filling time of 300 ms for each precursor ion (whichever occurred first). MS/MS data were acquired in centroid mode, with the Rapid scan rate and a fixed first mass of 120 m/z. Only multiply charged (2^+ - 7^+) precursor ions were selected for MS/MS. Dynamic exclusion was employed with maximum retention period of 60 seconds and relative mass window of 10 ppm. Isotopes were excluded. Additionally only 1 data dependent scan was performed per precursor (only the most intense charge state selected). Ions were injected for all available parallelizable time. In order to improve the mass accuracy, a lock mass correction using a background ion (m/z 445.12003) was applied. Data acquisition was performed using Xcalibur 4.0/Tune 2.1 (Thermo Fisher Scientific)

9.2 Data analysis

For the quantitative label-free analysis, raw files from the Orbitrap Fusion Lumos were analyzed using MaxQuant (version 1.5.3.28)(Cox & Mann, 2008). MS/MS spectra were searched against the *Mus musculus* Swiss-Prot entries of the Uniprot KB (database release 2016_01) using the Andromeda search engine (Cox et al., 2011). A list of common contaminants was appended to the database search. The search criteria were set as follows: full tryptic specificity was required (cleavage after lysine or arginine residues, unless followed by proline); 2 missed cleavages were allowed; oxidation (M), and acetylation (protein N-term) were applied as variable modifications, with mass tolerances of 20 ppm set for precursor and 0.5 Da for fragments. The reversed sequences of the target database were used as decoy database. Peptide and protein hits were filtered at a false discovery rate of 1% using a target-decoy strategy (Elias & Gygi, 2007). Additionally, only proteins identified by at least 1 unique peptide were retained. The LFQ intensity values per protein (from the proteinGroups.txt output of MaxQuant) were used for further analysis. All comparative analyses were performed using R version 3.2.3. (R Core Team, 2012), in particular the R packages MSnbase (Gatto & Lilley, 2012) for processing proteomics data. The data was quantile normalized to reduce technical variations. Protein differential expression between aggregates and synaptosomal samples was evaluated using the Limma package(Smyth, 2005). Differences in protein abundances were statistically determined using the Student's t-test with variances moderated by *limma*'s empirical Bayes method. False discovery rate was estimated using *fdrtool*(Strimmer, 2008).

10. Immunohistochemical staining

Mice were killed by cervical dislocation, the brain was carefully removed, divided into two halves along the median plane, fixed overnight in 4 % paraformaldehyde (PFA) and dehydrated by ethanol gradient. The tissue was cleared in xylene and embedded in paraffin. Paraffin blocks were cut into 5 µm serial sections along the sliding microtome (HM-340E; Microm) in the coronal position. Tissue slices were collected and placed on polylysine-coated slides. Following deparaffinization and hydration, the sections were subjected to antigen retrieval using citrate buffer pH 6.0 (10mM citric acid, 0.05% v/v Tween 20, pH 6.0) in a decloaking chamber (Bio Care Medical). The sections were incubated with Blocking buffer (20 % Normal Goat Serum Blocking Solution (BioLegend, Cat. N. 927503), 5% BSA, 0.3% Triton X-100), to block non-specific binding, followed by overnight incubation with primary antibody (**Table 11**) diluted in blocking buffer at 4 °C. After washing with PBS, the sections were incubated with Alexa-Fluor-conjugated secondary antibodies (**Table 12**) for 2 hours at RT. Slides were washed with PBS, then stained with a 0.2 % w/v Sudan Black solution in ethanol for 10 min at RT, washed again with PBS and closed with some drops of ProLong Gold Antifade Mountant with DAPI (ThermoScientific, Cat. N. P36931) and imaged with ApoTome II microscope (Zeiss). When ProteoStat® dye was used, slides were incubated with the 1:2000 diluted dye for 3 min, rinsed in water and destained in 1% acetic acid for 20 min, then the staining with primary and secondary antibodies was performed as described above.

Table 11. Primary antibodies used for immunofluorescent stainings.

Target	Host species	Clonality	Isotype	Dilution used	Cat. N.
RPL10A	Rabbit	Polyclonal	IgG	1:100	ab226381 (Abcam)
Y10b	Mouse	Monoclonal	IgG	1:500	NB100-662SS (NovusBio)
VGLUT1	Rabbit	Polyclonal	IgG	1:500	135 303 (Synaptic System)
MAP2	Rabbit	Polyclonal	IgG	1:500	Ab11267 (Abcam)
DESMOPLAKIN	Goat	Polyclonal	IgG	1:130	Ab136662 (Abcam)

Table 12. Fluorophore-conjugated secondary antibodies used for immunofluorescent stainings.

Target	Host species	Conjugation	Dilution used	Cat. N.
Mouse	Goat	Alexa Fluor 568	1:500	A-11004 (Thermo Scientific)
Mouse	Goat	Alexa Fluor 488	1:500	A-11029 (Thermo Scientific)
Rabbit	Goat	Alexa Fluor 568	1:500	A-11011 (Thermo Scientific)
Rabbit	Goat	Alexa Fluor 488	1:500	A-11008 (Thermo Scientific)
Goat	Donkey	Alexa Fluor 647	1:500	A-32849 (Thermo Scientific)

11. Reverse transcription and qPCR

In order to study the presence and abundance of a certain RNA molecule in a sample, remaining genomic DNA that could still be present in the RNA sample was degraded through the endonuclease DNase I, RNase-free (ThermoScientific, Cat. N. EN0521). Then, in order to obtain complementary DNA (cDNA) to use as a substrate for PCR and qPCR experiments a

retrotranscription reaction was performed using the SuperScript IV Reverse Transcriptase (ThermoScientific, Cat. N. 18090010), following manufacturer's instructions.cDNA was obtained from 100 ng of total brain extract RNA and total synaptosomal RNA, it was diluted with 20 µL of nuclease-free water and 1 µL (~2.5 ng) was used for qPCR using SYBR Green PCR Master Mix(Qiagen, Cat. N. 208052) according to manufacturer's instructions and primers listed in **Table 13**. A two-step program was run on a Biorad C1000 Touch cycler (Biorad) with the following temperatures:

PCR activation	**40 Cycles**		**Melting curve analysis**
95°C 2min	95°C 5s	60°C 10s	65°C → 95°C 5min (0.5°C/5s)

Table 13. qPCR primers

Target transcript	**Forward primer**	**Reverse primer**	**Amplicon size**
Ldhb-201 (ENSMUSG00000030246)	ccgaacaacaagatcactgta (exon 2)	gagcttgtcttccaacacat (exon 3)	120bp
Rpl10a-201 (ENSMUSG00000037805)	gcactgtgatgaagccaagg (exon 4)	tcagagactcagaggccaaa (exon 5)	134bp
Rpl15-202 (ENSMUSG00000012405)	cggcctgataaagctcga (exon 2)	gccgtaagttgcacccttag (exon 3)	117bp
Rpl26-201 (ENSMUSG00000060938)	tgacgaagttcaggttgttcg (exon junction 2-3)	cttctctcgctggactcgtt (exon 3)	112bp
Rpl7-201 (ENSMUSG00000043716)	tccttgattgctcggtctct (exon 5)	tgaagggccacaggaagtta (exon 6)	118bp
Rps13-201 (ENSMUSG00000090862)	tgacgacgtgaaggaacaga (exon 3)	gtcacaaaacggacctggg (exon 4)	111bp
Rps6-201 (ENSMUST00000102814)	agaagatgatgtccgccagt (exon 4)	cgaggagtaacaagtcgctg (exon 5)	102bp
Rps29-201 (ENSMUSG00000034892)	ccgactcgttccttttctcct (exon 1)	gcacatgttcagcccgtatt (exon 2)	158bp
Camk2a (ENSMUSG00000024617)	acctgcacccgattcacag (exon 1)	tggcagcatactcctgacca (exon 2)	112bp
Dlg4 (ENSMUSG00000020886)	accagaagagtatagccgattcg (exon 10-11)	ggtcttgtcgtagtcaaacagg (exon 12)	148bp
Gria1 (ENSMUSG00000020524)	gctttgtcacaactcacgga (exon 2)	cctttggagaactgggaaca (exon 3)	110bp

Arc (ENSMUSG00000022602)	ggtgagctgaagccacaaat (exon 1)	gctgagctctgctcttcttca (exon 2)	101bp
H3f3b (ENSMUSG00000016559)	aagcagaccgctaggaagtc (exon 4)	ggtaacgacggatctctctcag (exon 5)	154bp
Gm34838 (ENSMUSG00000110028)	ggctcctctatgttggaatatg (exon 2)	tgcttccaaagtccttcagt (exon 3)	119bp
Gm10925 (ENSMUSG00000100862)	aatcctattcccatcctcaa(exon1)	agggaaacaattattagggttc (exon 1)	141bp
Gm13340 (ENSMUSG00000083563)	aataccaataataatcggaggc (exon1)	agactgttcatcctgttcctg (exon1)	176bp

12. RNA sequencing

RNA Sequencing was performed on the Total Homogenate and Sucrose Gradient Samples reported in **Table 7**. Prior to that RNA integrity (RIN Score) and RNA concentration were estimated using the Bioanalyzer 2100 (Agilent) and the RNA 6000 Pico Kit and RNA 6000 Nano Kit for the Sucrose Gradient and Total Homogenate Samples, respectively. The results are reported in **Table 14**. For RNA sequencing 10ng of RNA were used for library preparation, which was done using the SMARTer Stranded Total RNA-Seq Kit – Pico Input Mammalian (TaKaRa, Cat. N. 635006) according to the manufacturer's instructions (see**Fig.70**for a schematic summary). This method allows to prepare a library that is compatible with Illumina sequencing (Bentley et al., 2008), starting from small quantities (0.25-10ng) of mammalian RNA.

In brief, samples with RIN Score > 3 are fragmented by incubation at 94°C for a time (2-4min) that depends on the RIN Score (the higher the RIN Score, the longer the incubation time). cDNA is then obtained by using the SMARTScribe Reverse Transcriptase, which is an engineered polymerase based on the Moloney murine leukemia virus (MMLV) Reverse Transcriptase, and Random Hexamers Primers with an adapter sequence at the 5' end (N_6 Primers). Once the reverse transcriptase reaches the 5' end of the template it keeps adding nucleotides to the cDNA filament due to its terminal transferase activity, forming a so called non-templated nucleotide stretch that is represented in the schematic summary as a string of five X. At this point Template Switching Oligonucleotides (TSO), which are chimeric DNA/RNA oligonucleotides, bind to the non-templated nucleotide stretch added by the reverse transcriptase to the 5' end of the template through their RNA 5' end, that is specifically designed in order to bind to non-templated nucleotide stretches. At this point the reverse transcriptase starts using the DNA 3' end of the TSO, which functions as an adapter, as a template. This method to synthesize the cDNA is called Switching Mechanism At the 5' end of RNA Template (SMART), and allows to incorporate adapter sequences at the 5' and 3' ends of the cDNA filaments and to preserve the strand orientation of the RNA template. The adapter sequences incorporated at this step correspond to the binding sites of the sequencing primers Read Primer 1 and Read Primer 2. A PCR is then performed by using primers that bind to the adapter sequences that have been incorporated in the previous step and that lead to the incorporation of the Illumina P5 and P7 Adapters at both ends of the PCR products (Forward and

Reverse PCR Primers). Adapters with different Illumina TruSeq HT i5 and i7 indexes can be used when multiple libraries will be pooled together on one flow cell lane. PCR products are purified through the paramagnetic beads of the Agencourt AMPure XP PCR Purification Kit Beads (Beckman Coulter, Cat. N. A63880), which bind them through Solid Phase Reversible Immobilization (SPRI). Amplicons that derive from 18S and 28S rRNA are then cleaved by ZapR in the presence of mammalian-specific R-Probes, and the remaining, uncleaved amplicons are enriched through a second PCR in which a universal primer pair is used that binds to all amplicons, independently of the used indexes. PCR products are again purified through AMPure beads. The DNA concentration of the libraries is then measured with the Qubit dsDNA HS Assay Kit (Life Technologies) and diluted to 1.5ng/uL. The distribution of amplicon sizes, which should be in a range of 200-1.000bp with a peak at around 300-400bp, is finally measured using the Bioanalyzer 2100 (Agilent) and the DNA 7500 Kit.

Sequencing was done using the Illumina HiSeq 2500 System and the HiSeq Rapid SBS Kit v2, which is a second generation sequencing system in which fragment clusters are formed through bridge PCR and the sequencing is performed through sequencing by synthesis (SBS) with reversible terminators. In particular the following settings were used: 50 cycles, single-end rapid mode. 8 samples were pooled in two lanes, yielding an average of 34mio reads per sample.

Finally, reads are mapped to the Genome Reference Consortium Mouse Build 38 (GRCm38.85) using STAR 2.7 (Dobin et al., 2013), obtaining SAM files. Using SAMtools 1.7(H. Li et al., 2009) sorted BAMfiles and BAI files are generated.

Table 14. RNA integrity and concentration as estimated using the Bioanalyzer 2100 (Agilent)

ID	Age	Sample	RIN Score	RNA concentration [ng/uL]
59	3w	TH	9.4	202
		SG	4.9	5.458
60	3w	TH	9.0	241
		SG	3.6	25.218
61	3w	TH	9.1	191
		SG	3.7	8.499
62	3w	TH	9.1	201
		SG	2.5	12.656
72	5m	TH	9.0	255
		SG	5.3	5.528
74	5m	TH	9.0	227
		SG	4.0	3.436
75	5m	TH	9.1	189
		SG	4.6	3.586
76	5m	TH	9.0	305
		SG	6.0	4.664
46	18m	TH	5.1	73
		SG	5.5	4.736

47	18m	TH	5.2	165
		SG	6.4	0.737
48	18m	TH	5.1	186
		SG	5.6	3.737
49	18m	TH	5.1	145
		SG	5.8	2.622
67	19m	TH	9.0	267
		SG	3.5	23.883
68	19m	TH	9.2	212
		SG	5.0	3.467
69	19m	TH	9.1	214
		SG	4.7	4.783
70	19m	TH	9.2	244
		SG	4.5	4.520

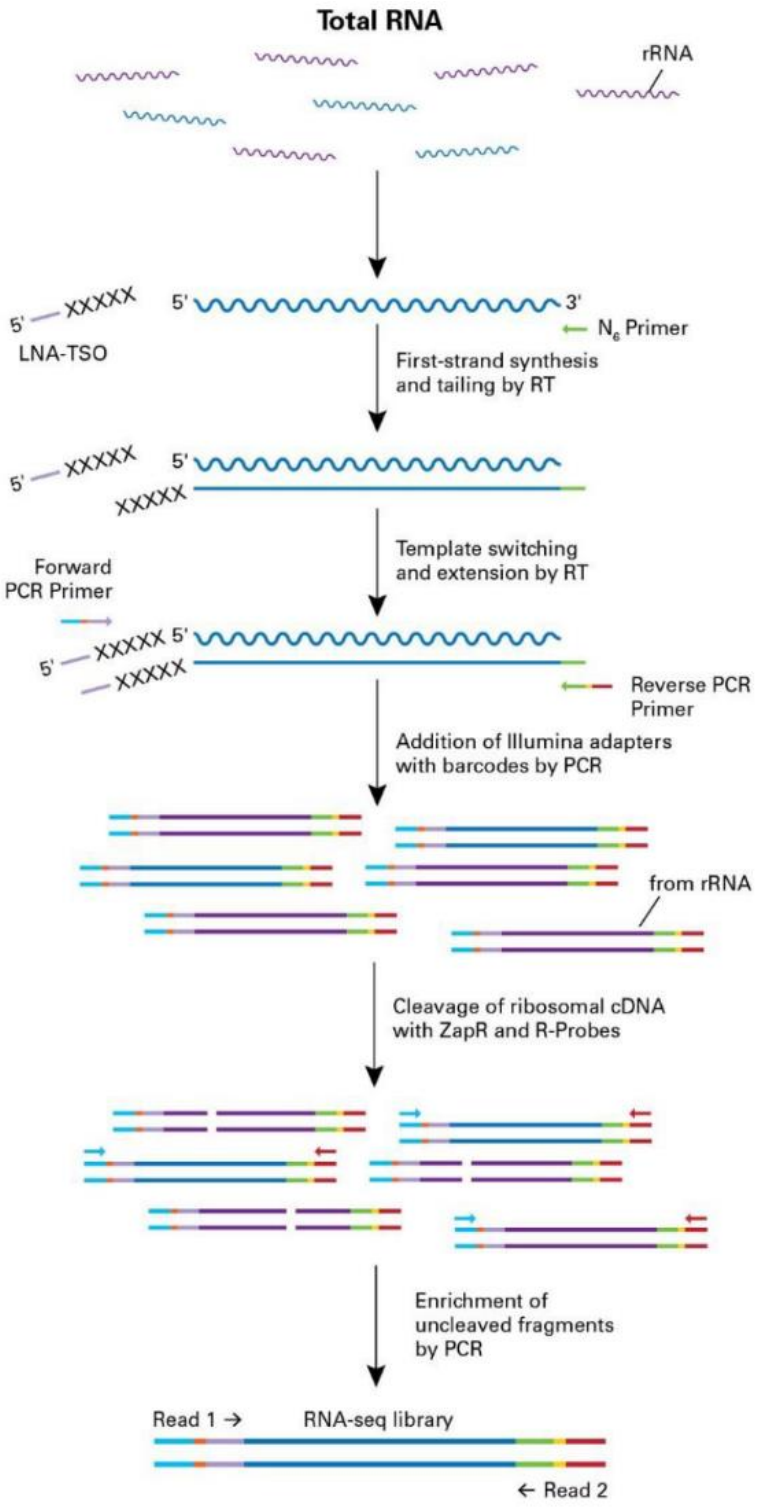

Figure 71. Schematic summary of the library preparation.rRNA (purple), other RNA (blue), N6 Primers (green), non-templated nucleotide stretch (XXXXX), LNA-TSO (light purple), Illumina P5 and P7 Adapters (light blue and red, respectively), Illumina TruSeq HT i5 and i7 indexes (orange and yellow, respectively). Figure derived from the Manufacturer's manual.

13. Data analysis

All the analyses were performed using R-Studio 1.1.456 (Leemans et al., 2009). Starting from the raw counts, normalized counts and $\log_2$ fold changes were estimated using DESeq2 1.22.2 (Love, Huber, & Anders, 2014). DESeq2 allows to estimate variance-mean dependence in count data from high-throughput sequencing assays and test for differential expression based on a model using the negative binomial distribution.

To combine transcriptomic and proteomic data, p-values for differential expression at the protein and transcript level are combined in a meta-analysis (Fisher's method) (Lury & Fisher, 1972). Fisher's method combines extreme value probabilities from each test, commonly known as "p-values", into one test statistic (X^2) using the formula:

$$X_{2k}^2 \sim -2\sum_{i=1}^{k} \ln(p_i),$$

where pi is the p-value for the ith hypothesis test.

The visualization of sample's similarity through Gene Enrichment has been evaluated by performing over representation analysis (ORA) using WebGestalt website (http://webgestalt.org/) (Liao, Wang, Jaehnig, Shi, & Zhang, 2019). This website uses affinity propagation to cluster similar gene sets; it identifies the most enriched GO categories in a given dataset and provides the FDR-corrected p-value of the enrichment. The categories of the GO database (Ashburner et al., 2000; Carbon et al., 2017) that contain at least five genes were considered, and the p-values have been corrected for multiple comparisons through the FDR method described in (Benjamini & Hochberg, 1995). Visualization of Gene Enrichment was achieved using ReviGO software (http://revigo.irb.hr/). ReviGO allows to obtain a flexible reduction in size for large user-supplied lists of overlapping GO categories, and visualize the remaining GO terms in a two-dimensional space which reflects the terms' semantic interrelations.

Classification of genes as coding or non-coding was done using Ensembl BioMart (https://www.ensembl.org/biomart/) annotation version GRCm38.p6.

Protein complex stoichiometry analysis was performed using limma 3.40.2 (Ritchie et al., 2015) and gplots 3.0.1.1. The main feature of limma package is the use of linear models to assess differential expression in the context of multifactor designed experiments. Limma provides the ability to analyze comparisons between many targets simultaneously.

Principal Component Analysis and Heatmap representation of their hierarchical clustering has been performed using DESeq2's internal functions and the packages ComplexHeatmap 2.0.0, pcaMethods 1.76.0 and ggpubr 0.2. Volcano plots and density plots have been drawn using the packages ggplot2 3.1.1 and ggpubr 0.2.

Generally Applicable Gene-set Enrichment for Pathway Analysis (GAGE) was performed using gage 2.34.0 and GO.db 3.8 packages (Luo et al., 2009). GAGE is a published method for gene set (enrichment or GSEA) or pathway analysis. GAGE is generally applicable independent of microarray or RNA-Seq data attributes including sample sizes, experimental designs, assay platforms, and other types of heterogeneity. GAGE uses curated gene sets collected from individual studies or pathway

databases for regulatory mechanisms inference. In contrast to other gene set analysis approaches, GAGE requires that each curated gene set be identified as either a pathway set (canonical pathways) or an experimentally derived differential expression set (experiment sets). Genes in an experimental set are assumed to be regulated in the same direction, either all up or all down. In contrast, genes associated with a pathway gene set may be heterogeneously regulated in either direction. To test whether a gene set is significantly correlated with a phenotype or an experiment condition, the fold changes of gene expression level in the experiment condition (or phenotype) are compared to a control condition. Then, a two-sample t-test is applied to verify whether the mean fold changes of a target gene set is significantly different from that of the background set (the whole gene set of the microarray).

Bibliography

Adams, M. D., Kelley, J. M., Gocayne, J. D., Dubnick, M. A. K., Polymeropoulos, M. H., Xiao, H., … Venter, J. C. (1991). Complementary DNA sequencing: Expressed sequence tags and human genome project. *Science*, *252*(5013), 1651–1656. https://doi.org/10.1126/science.2047873

Ainsley, J. A., Drane, L., Jacobs, J., Kittelberger, K. A., & Reijmers, L. G. (2014). Functionally diverse dendritic mRNAs rapidly associate with ribosomes following a novel experience. *Nature Communications*, *5*. https://doi.org/10.1038/ncomms5510

An, J. J., Gharami, K., Liao, G. Y., Woo, N. H., Lau, A. G., Vanevski, F., … Xu, B. (2008). Distinct Role of Long 3' UTR BDNF mRNA in Spine Morphology and Synaptic Plasticity in Hippocampal Neurons. *Cell*, *134*(1), 175–187. https://doi.org/10.1016/j.cell.2008.05.045

Ashburner, M., Ball, C. A., Blake, J. A., Botstein, D., Butler, H., Cherry, J. M., … Sherlock, G. (2000). Gene ontology: Tool for the unification of biology. *Nature Genetics*, *25*(1), 25–29. https://doi.org/10.1038/75556

Bai, F., & Witzmann, F. A. (2007). Synaptosome proteomics. *Sub-Cellular Biochemistry*, *43*, 77–98.

Barrow, S. L., Constable, J. R., Clark, E., El-Sabeawy, F., McAllister, A. K., & Washbourne, P. (2009). Neuroligin1: A cell adhesion molecule that recruits PSD-95 and NMDA receptors by distinct mechanisms during synaptogenesis. *Neural Development*, *4*(1). https://doi.org/10.1186/1749-8104-4-17

Bateman, N. W., Goulding, S. P., Shulman, N. J., Gadok, A. K., Szumlinski, K. K., MacCoss, M. J., & Wu, C. (2014). Maximizing peptide identification events in proteomic workflows using data-dependent acquisition (DDA). *Molecular and Cellular Proteomics*, *13*(1), 329–338. https://doi.org/10.1074/mcp.M112.026500

Belmonte, M. K., Allen, G., Beckel-Mitchener, A., Boulanger, L. M., Carper, R. A., & Webb, S. J. (2004). Autism and abnormal development of brain connectivity. *Journal of Neuroscience*, *24*(42), 9228–9231. https://doi.org/10.1523/JNEUROSCI.3340-04.2004

Benjamini, Y., & Hochberg, Y. (1995). Controlling the False Discovery Rate - a Practical and Powerful Approach to Multiple Testing. Journal of the Royal Statistical Society Series B-

Methodological 1995.pdf. *Journal of the Royal Statistical Society Series B (Methological)*, Vol. 57, pp. 289–300. https://doi.org/10.2307/2346101

Bentley, D. R., Balasubramanian, S., Swerdlow, H. P., Smith, G. P., Milton, J., Brown, C. G., … Smith, A. J. (2008). Accurate whole human genome sequencing using reversible terminator chemistry. *Nature*, *456*(7218), 53–59. https://doi.org/10.1038/nature07517

Biesemann, C., Grønborg, M., Luquet, E., Wichert, S. P., Bernard, V., Bungers, S. R., … Herzog, E. (2014). Proteomic screening of glutamatergic mouse brain synaptosomes isolated by fluorescence activated sorting. *EMBO Journal*, *33*(2), 157–170. https://doi.org/10.1002/embj.201386120

Biever, A., Glock, C., Tushev, G., Ciirdaeva, E., Langer, J. D., & Schuman, E. M. (2019). Monosomes actively translate synaptic mRNAs in neuronal processes. *BioRxiv*. https://doi.org/10.1101/687475

Bilbao, A., Varesio, E., Luban, J., Strambio-De-Castillia, C., Hopfgartner, G., Müller, M., & Lisacek, F. (2015). Processing strategies and software solutions for data-independent acquisition in mass spectrometry. *Proteomics*, Vol. 15, pp. 964–980. https://doi.org/10.1002/pmic.201400323

Booth, R. F., & Clark, J. B. (1978). A rapid method for the preparation of relatively pure metabolically competent synaptosomes from rat brain. *The Biochemical Journal*, *176*(2), 365–370.

Bruderer, R., Bernhardt, O. M., Gandhi, T., Miladinović, S. M., Cheng, L. Y., Messner, S., … Reiter, L. (2015). Extending the limits of quantitative proteome profiling with data-independent acquisition and application to acetaminophen-treated three-dimensional liver microtissues. *Molecular and Cellular Proteomics*, *14*(5), 1400–1410. https://doi.org/10.1074/mcp.M114.044305

Cajigas, I. J., Tushev, G., Will, T. J., Tom Dieck, S., Fuerst, N., & Schuman, E. M. (2012). The Local Transcriptome in the Synaptic Neuropil Revealed by Deep Sequencing and High-Resolution Imaging. *Neuron*, *74*(3), 453–466. https://doi.org/10.1016/j.neuron.2012.02.036

Carbon, S., Dietze, H., Lewis, S., Mungall, C. J., Munoz-Torres, M. C., Basu, S., … Westerfield, M. (2017). Expansion of the gene ontology knowledgebase and resources: The gene ontology consortium. *Nucleic Acids Research*, *45*(1), 331–338. https://doi.org/10.1093/nar/gkw1108

Chakrabarti, S., Munshi, S., Banerjee, K., Thakurta, I. G., Sinha, M., & Bagh, M. B. (2011). Mitochondrial Dysfunction during Brain Aging: Role of Oxidative Stress and Modulation by Antioxidant Supplementation. *Aging and Disease*, *2*(3), 242–256.

Chen, B. J., Ueberham, U., Mills, J. D., Kirazov, L., Kirazov, E., Knobloch, M., … Janitz, M. (2017). RNA sequencing reveals pronounced changes in the noncoding transcriptome of aging synaptosomes. *Neurobiology of Aging*, *56*, 67–77. https://doi.org/10.1016/j.neurobiolaging.2017.04.005

Chiocchetti, A., Zhou, J., Zhu, H., Karl, T., Haubenreisser, O., Rinnerthaler, M., … Breitenbach-Koller, L. (2007). Ribosomal proteins Rpl10 and Rps6 are potent regulators of yeast replicative life span. *Experimental Gerontology*, *42*(4), 275–286. https://doi.org/10.1016/j.exger.2006.11.002

Chiu, S. L., & Cline, H. T. (2010). Insulin receptor signaling in the development of neuronal structure and function. *Neural Development*, Vol. 5. https://doi.org/10.1186/1749-8104-5-7

Chomczynski, P., & Sacchi, N. (1987). Single-step method of RNA isolation by acid guanidinium thiocyanate-phenol-chloroform extraction. *Analytical Biochemistry*, *162*(1), 156–159. https://doi.org/10.1016/0003-2697(87)90021-2

Cox, J., & Mann, M. (2008). MaxQuant enables high peptide identification rates, individualized p.p.b.-range mass accuracies and proteome-wide protein quantification. *Nature Biotechnology*, *26*(12), 1367–1372. https://doi.org/10.1038/nbt.1511

Cox, J., Neuhauser, N., Michalski, A., Scheltema, R. A., Olsen, J. V., & Mann, M. (2011). Andromeda: A peptide search engine integrated into the MaxQuant environment. *Journal of Proteome Research*, *10*(4), 1794–1805. https://doi.org/10.1021/pr101065j

Cracco, J. B., Serrano, P., Moskowitz, S. I., Bergold, P. J., & Sacktor, T. C. (2005). Protein synthesis-dependent LTP in isolated dendrites of CA1 pyramidal cells. *Hippocampus*, *15*(5), 551–556. https://doi.org/10.1002/hipo.20078

Daniel, J. A., Malladi, C. S., Kettle, E., McCluskey, A., & Robinson, P. J. (2012). Analysis of synaptic vesicle endocytosis in synaptosomes by high-content screening. *Nature Protocols*, *7*(8), 1649–1655. https://doi.org/10.1038/nprot.2012.070

Dobin, A., Davis, C. A., Schlesinger, F., Drenkow, J., Zaleski, C., Jha, S., … Gingeras, T. R. (2013). STAR: Ultrafast universal RNA-seq aligner. *Bioinformatics*. https://doi.org/10.1093/bioinformatics/bts635

Dobson, C. M., Swoboda, B. E. P., Joniau, M., & Weissman, C. (2001). The structural basis of protein folding and its links with human disease. *Philosophical Transactions of the Royal Society B: Biological Sciences*, *356*(1406), 133–145. https://doi.org/10.1098/rstb.2000.0758

Doyle, M., & Kiebler, M. A. (2011). Mechanisms of dendritic mRNA transport and its role in synaptic tagging. *EMBO Journal*, Vol. 30, pp. 3540–3552. https://doi.org/10.1038/emboj.2011.278

Duan, H., Wearne, S. L., Rocher, A. B., Macedo, A., Morrison, J. H., & Hof, P. R. (2003). Age-related dendritic and spine changes in corticocortically projecting neurons in macaque monkeys. *Cerebral Cortex*, *13*(9), 950–961. https://doi.org/10.1093/cercor/13.9.950

Dumitriu, D., Hao, J., Hara, Y., Kaufmann, J., Janssen, W. G. M., Lou, W., … Morrison, J. H. (2010). Selective changes in thin spine density and morphology in monkey prefrontal cortex correlate with aging-related cognitive impairment. *Journal of Neuroscience*, *30*(22), 7507–7515. https://doi.org/10.1523/JNEUROSCI.6410-09.2010

Elias, J. E., & Gygi, S. P. (2007). Target-decoy search strategy for increased confidence in large-scale protein identifications by mass spectrometry. *Nature Methods*, *4*(3), 207–214. https://doi.org/10.1038/nmeth1019

Filiou, M. D., Bisle, B., Reckow, S., Teplytska, L., Maccarrone, G., & Turck, C. W. (2010). Profiling of mouse synaptosome proteome and phosphoproteome by IEF. *Electrophoresis*, *31*(8), 1294–1301. https://doi.org/10.1002/elps.200900647

Frey, U., Krug, M., Brödemann, R., Reymann, K., & Matthies, H. (1989). Long-term potentiation induced in dendrites separated from rat's CA1 pyramidal somata does not establish a late phase. *Neuroscience*, *97*(1–2), 135–139. https://doi.org/10.1016/0304-3940(89)90152-3

Fukushima, H., Maeda, R., Suzuki, R., Suzuki, A., Nomoto, M., Toyoda, H., … Kida, S. (2008). Upregulation of calcium/calmodulin-dependent protein kinase IV improves memory formation and rescues memory loss with aging. *Journal of Neuroscience*, *28*(40), 9910–9919. https://doi.org/10.1523/JNEUROSCI.2625-08.2008

Gatto, L., & Lilley, K. S. (2012). Msnbase-an R/Bioconductor package for isobaric tagged mass spectrometry data visualization, processing and quantitation. *Bioinformatics*, *28*(2), 288–289. https://doi.org/10.1093/bioinformatics/btr645

Grant, S. G. N. (2012). Synaptopathies: Diseases of the synaptome. *Current Opinion in Neurobiology*, Vol. 22, pp. 522–529. https://doi.org/10.1016/j.conb.2012.02.002

Graus-Porta, D., Blaess, S., Senften, M., Littlewood-Evans, A., Damsky, C., Huang, Z., … Müller, U. (2001). β1-Class integrins regulate the development of laminae and folia in the cerebral and cerebellar cortex. *Neuron*, *31*(3), 367–379. https://doi.org/10.1016/S0896-6273(01)00374-9

Gray, E. G. (1959). Axo-somatic and axo-dendritic synapses of the cerebral cortex: an electron microscope study. *Journal of Anatomy*, *93*, 420–433. Retrieved from http://www.ncbi.nlm.nih.gov/pubmed/13829103%0Ahttp://www.pubmedcentral.nih.gov/articlerender.fcgi?artid=PMC1244535

Gray, E. G., & Whittaker, V. P. (1962). The isolation of nerve endings from brain: an electron-microscopic study of cell fragments derived by homogenization and centrifugation. *Journal of Anatomy*, *96*, 79–88. Retrieved from http://www.ncbi.nlm.nih.gov/pubmed/13901297%0Ahttp://www.pubmedcentral.nih.gov/articlerender.fcgi?artid=PMC1244174

Grillo, F. W., Song, S., Teles-Grilo Ruivo, L. M., Huang, L., Gao, G., Knott, G. W., … De Paola, V. (2013). Increased axonal bouton dynamics in the aging mouse cortex. *Proceedings of the National Academy of Sciences of the United States of America*, *110*(16), 1514–1523. https://doi.org/10.1073/pnas.1218731110

Hafner, A. S., Donlin-Asp, P. G., Leitch, B., Herzog, E., & Schuman, E. M. (2019). Local protein synthesis is a ubiquitous feature of neuronal pre- And postsynaptic compartments. *Science*, *364*(6441). https://doi.org/10.1126/science.aau3644

Hall, B. J., & Ghosh, A. (2008). Regulation of AMPA receptor recruitment at developing synapses. *Trends in Neurosciences*, Vol. 31, pp. 82–89. https://doi.org/10.1016/j.tins.2007.11.010

Hanus, C., & Schuman, E. M. (2013). Proteostasis in complex dendrites. *Nature Reviews Neuroscience*, Vol. 14, pp. 638–648. https://doi.org/10.1038/nrn3546

Harney, S. C., Rowan, M., & Anwyl, R. (2006). Long-term depression of NMDA receptor-mediated synaptic transmission is dependent on activation of metabotropic glutamate receptors and is altered to long-term potentiation by low intracellular calcium buffering. *Journal of Neuroscience*, *26*(4), 1128–1132. https://doi.org/10.1523/JNEUROSCI.2753-05.2006

Heo, S., Diering, G. H., Na, C. H., Nirujogi, R. S., Bachman, J. L., Pandey, A., & Huganir, R. L. (2018). Identification of long-lived synaptic proteins by proteomic analysis of synaptosome protein turnover. *Proceedings of the National Academy of Sciences of the United States of America*, *115*(16), 3827–3836. https://doi.org/10.1073/pnas.1720956115

Hu, A., Noble, W. S., & Wolf-Yadlin, A. (2016). Technical advances in proteomics: New developments in data-independent acquisition. *F1000Research*, *5*. https://doi.org/10.12688/f1000research.7042.1

Huang, Y. Y., Nguyen, P. V., Abel, T., & Kandel, E. R. (1996). Long-lasting forms of synaptic potentiation in the mammalian hippocampus. *Learning Memory*, Vol. 3, pp. 74–85. https://doi.org/10.1101/lm.3.2-3.74

Huber, K. M., Gallagher, S. M., Warren, S. T., & Bear, M. F. (2002). Altered synaptic plasticity in a mouse model of fragile X mental retardation. *Proceedings of the National Academy of Sciences of the United States of America*, *99*(11), 7746–7750. https://doi.org/10.1073/pnas.122205699

Huber, K. M., Kayser, M. S., & Bear, M. F. (2000). Role for rapid dendritic protein synthesis in hippocampal mGluR- dependent long-term depression. *Science*, *288*(5469), 1254–1256. https://doi.org/10.1126/science.288.5469.1254

Hunt, D. L., & Castillo, P. E. (2012). Synaptic plasticity of NMDA receptors: Mechanisms and functional implications. *Current Opinion in Neurobiology*, Vol. 22, pp. 496–508. https://doi.org/10.1016/j.conb.2012.01.007

Hutten, S., Sharangdhar, T., & Kiebler, M. (2014). Unmasking the messenger. *RNA Biology*, Vol. 11, pp. 992–997. https://doi.org/10.4161/rna.32091

Jacobson, M., & Jacobson, M. (1991). Formation of Dendrites and Development of Synaptic Connections. In *Developmental Neurobiology* (pp. 223–283). https://doi.org/10.1007/978-1-4757-4954-0_6

Jahn, T. R., & Radford, S. E. (2008). Folding versus aggregation: Polypeptide conformations on competing pathways. *Archives of Biochemistry and Biophysics*, Vol. 469, pp. 100–117. https://doi.org/10.1016/j.abb.2007.05.015

Jiménez, J. L., Guijarro, J. I., Orlova, E., Zurdo, J., Dobson, C. M., Sunde, M., & Saibil, H. R. (1999). Cryo-electron microscopy structure of an SH3 amyloid fibril and model of the molecular packing. *EMBO Journal*, *18*(4), 815–821. https://doi.org/10.1093/emboj/18.4.815

Johnson, S. C., Rabinovitch, P. S., & Kaeberlein, M. (2013). MTOR is a key modulator of ageing and age-related disease. *Nature*, Vol. 493, pp. 338–345. https://doi.org/10.1038/nature11861

Kang, H., & Schuman, E. M. (1996). A requirement for local protein synthesis in neurotrophin-induced hippocampal synaptic plasticity. *Science*, *273*(5280), 1402–1406. https://doi.org/10.1126/science.273.5280.1402

Kennedy, M. B. (2000). Signal-processing machines at the postsynaptic density. *Science*, Vol. 290, pp. 750–754. https://doi.org/10.1126/science.290.5492.750

Kettenmann, H., & Ransom, B. R. (2013). Neuroglia. In *Neuroglia*. https://doi.org/10.1093/acprof:oso/9780195152227.001.0001

Koenig, E., & Adams, P. (1982). Local Protein Synthesizing Activity in Axonal Fields Regenerating In Vitro. *Journal of Neurochemistry*, *39*(2), 386–400. https://doi.org/10.1111/j.1471-4159.1982.tb03960.x

Koppers, M., Cagnetta, R., Shigeoka, T., Wunderlich, L. C. S., Zhao, S., Minett, M. S., … Holt, C. E. (2019). Receptor-specific interactome as a hub for rapid cue-induced selective translation in axons. *BioRxiv*. https://doi.org/10.1101/673798

Korn, H., & Faber, D. S. (1991). Quantal analysis and synaptic efficacy in the CNS. *Trends in Neurosciences*, *14*(10), 439–445. https://doi.org/10.1016/0166-2236(91)90042-S

Le Hir, H., Gatfield, D., Izaurralde, E., & Moore, M. J. (2001). The exon-exon junction complex provides a binding platform for factors involved in mRNA export and nonsense-mediated mRNA decay. *EMBO Journal*, *20*(17), 4987–4997. https://doi.org/10.1093/emboj/20.17.4987

Leemans, R., Asrar, G., Busalacchi, A., Canadell, J., Ingram, J., Larigauderie, A., … Young, O. (2009). Developing a common strategy for integrative global environmental change research and outreach: the Earth System Science Partnership (ESSP). *Current Opinion in Environmental Sustainability*, Vol. 1, pp. 4–13. https://doi.org/10.1016/j.cosust.2009.07.013

Li, H., Handsaker, B., Wysoker, A., Fennell, T., Ruan, J., Homer, N., … Durbin, R. (2009). The Sequence Alignment/Map format and SAMtools. *Bioinformatics*, *25*(16), 2078–2079. https://doi.org/10.1093/bioinformatics/btp352

Li, M., Cui, Z., Niu, Y., Liu, B., Fan, W., Yu, D., & Deng, J. (2010). Synaptogenesis in the developing mouse visual cortex. *Brain Research*, *81*(1), 107–113. https://doi.org/10.1016/j.brainresbull.2009.08.028

Liao, Y., Wang, J., Jaehnig, E. J., Shi, Z., & Zhang, B. (2019). WebGestalt 2019: gene set analysis toolkit with revamped UIs and APIs. *Nucleic Acids Research*, *47*(1), 199–205. https://doi.org/10.1093/nar/gkz401

Liu, Q. R., Lu, L., Zhu, X. G., Gong, J. P., Shaham, Y., & Uhl, G. R. (2006). Rodent BDNF genes, novel promoters, novel splice variants, and regulation by cocaine. *Brain Research*, *1067*(1), 1–12. https://doi.org/10.1016/j.brainres.2005.10.004

Liu, Q. R., Walther, D., Drgon, T., Polesskaya, O., Lesnick, T. G., Strain, K. J., … Uhl, G. R. (2005). Human brain derived neurotrophic factor (BDNF) genes, splicing patterns, and assessments of associations with substance abuse and Parkinson's disease. *American Journal of Medical Genetics - Neuropsychiatric Genetics*, *134 B*(1), 93–103. https://doi.org/10.1002/ajmg.b.30109

Liu, Y., Beyer, A., & Aebersold, R. (2016). On the Dependency of Cellular Protein Levels on mRNA Abundance. *Cell*, Vol. 165, pp. 535–550. https://doi.org/10.1016/j.cell.2016.03.014

López-Otín, C., Blasco, M. A., Partridge, L., Serrano, M., & Kroemer, G. (2013). The hallmarks of aging. *Cell*, *153*(6), 1194–1217. https://doi.org/10.1016/j.cell.2013.05.039

Love, M. I., Huber, W., & Anders, S. (2014). Moderated estimation of fold change and dispersion for RNA-seq data with DESeq2. *Genome Biology*, *15*(12), 550. https://doi.org/10.1186/s13059-014-0550-8

Lowe, R., Shirley, N., Bleackley, M., Dolan, S., & Shafee, T. (2017). Transcriptomics technologies. *PLoS Computational Biology*, *13*(5). https://doi.org/10.1371/journal.pcbi.1005457

Luo, W., Friedman, M. S., Shedden, K., Hankenson, K. D., & Woolf, P. J. (2009). GAGE: Generally applicable gene set enrichment for pathway analysis. *BMC Bioinformatics*, *10*.

https://doi.org/10.1186/1471-2105-10-161

Lury, D. A., & Fisher, R. A. (1972). Statistical Methods for Research Workers. *The Statistician*, *21*(3), 229. https://doi.org/10.2307/2986695

Mann, M., Hendrickson, R. C., & Pandey, A. (2001). Analysis of Proteins and Proteomes by Mass Spectrometry. *Annual Review of Biochemistry*, *70*(1), 437–473. https://doi.org/10.1146/annurev.biochem.70.1.437

Margeta, M. A., & Shen, K. (2010). Molecular mechanisms of synaptic specificity. *Molecular and Cellular Neuroscience*, Vol. 43, pp. 261–267. https://doi.org/10.1016/j.mcn.2009.11.009

Martin, K. C., & Ephrussi, A. (2009). mRNA Localization: Gene Expression in the Spatial Dimension. *Cell*, Vol. 136, pp. 719–730. https://doi.org/10.1016/j.cell.2009.01.044

McAllister, A. K. (2002). Conserved cues for axon and dendrite growth in the developing cortex. *Neuron*, Vol. 33, pp. 2–4. https://doi.org/10.1016/S0896-6273(01)00577-3

McClatchy, D. B., Liao, L., Lee, J. H., Park, S. K., & Yates, J. R. (2012). Dynamics of subcellular proteomes during brain development. *Journal of Proteome Research*, *11*(4), 2467–2479. https://doi.org/10.1021/pr201176v

Meredith, R. M. (2015). Sensitive and critical periods during neurotypical and aberrant neurodevelopment: A framework for neurodevelopmental disorders. *Neuroscience*, Vol. 50, pp. 180–188. https://doi.org/10.1016/j.neubiorev.2014.12.001

Middleton, S. A., Eberwine, J., & Kim, J. (2019). Comprehensive catalog of dendritically localized mRNA isoforms from sub-cellular sequencing of single mouse neurons. *BMC Biology*, *17*(1). https://doi.org/10.1186/s12915-019-0630-z

Moczulska, K. E., Pichler, P., Schutzbier, M., Schleiffer, A., Rumpel, S., & Mechtler, K. (2014). Deep and precise quantification of the mouse synaptosomal proteome reveals substantial remodeling during postnatal maturation. *Journal of Proteome Research*, *13*(10), 4310–4324. https://doi.org/10.1021/pr500456t

Morrison, J. H., & Baxter, M. G. (2012). The ageing cortical synapse: Hallmarks and implications for cognitive decline. *Nature Reviews Neuroscience*, Vol. 13, pp. 240–250. https://doi.org/10.1038/nrn3200

Nagy, A., & Delgado-Escueta, A. V. (1984). Rapid Preparation of Synaptosomes from Mammalian Brain Using Nontoxic Isoosmotic Gradient Material (Percoll). *Journal of Neurochemistry*, *43*(4), 1114–1123. https://doi.org/10.1111/j.1471-4159.1984.tb12851.x

Nimchinsky, E. A., Sabatini, B. L., & Svoboda, K. (2002). Structure and Function of Dendritic Spines. *Annual Review of Physiology*, *64*(1), 313–353. https://doi.org/10.1146/annurev.physiol.64.081501.160008

O'Connell, J. D., Zhao, A., Ellington, A. D., & Marcotte, E. M. (2012). Dynamic Reorganization of Metabolic Enzymes into Intracellular Bodies. *Annual Review of Cell and Developmental Biology*, *28*(1), 89–111. https://doi.org/10.1146/annurev-cellbio-101011-155841

Okabe, S. (2007). Molecular anatomy of the postsynaptic density. *Molecular and Cellular Neuroscience*,

Vol. 34, pp. 503–518. https://doi.org/10.1016/j.mcn.2007.01.006

Ori, A., Toyama, B. H., Harris, M. S., Bock, T., Iskar, M., Bork, P., … Beck, M. (2015). Integrated Transcriptome and Proteome Analyses Reveal Organ-Specific Proteome Deterioration in Old Rats. *Cell Systems*, *1*(3), 224–237. https://doi.org/10.1016/j.cels.2015.08.012

Ouwenga, R., Lake, A. M., O'Brien, D., Mogha, A., Dani, A., & Dougherty, J. D. (2017). Transcriptomic analysis of ribosome-bound mRNA in cortical neurites in vivo. *Journal of Neuroscience*, *37*(36), 8688–8705. https://doi.org/10.1523/JNEUROSCI.3044-16.2017

Palay, S. L. (1956). Synapses in the central nervous system. *The Journal of Biophysical and Biochemical Cytology*, *2*(Suppl. 4).

Pathak, B. K., Mondal, S., Banerjee, S., Ghosh, A. N., & Barat, C. (2017). Sequestration of Ribosome during Protein Aggregate Formation: Contribution of ribosomal RNA. *Scientific Reports*, *7*. https://doi.org/10.1038/srep42017

Peleg, S., Sananbenesi, F., Zovoilis, A., Burkhardt, S., Bahari-Javan, S., Agis-Balboa, R. C., … Fischer, A. (2010). Altered histone acetylation is associated with age-dependent memory impairment in mice. *Science*, *328*(5979), 753–756. https://doi.org/10.1126/science.1186088

Perea, G., Navarrete, M., & Araque, A. (2009). Tripartite synapses: astrocytes process and control synaptic information. *Trends in Neurosciences*, *32*(8), 421–431. https://doi.org/10.1016/j.tins.2009.05.001

Peters, A., Sethares, C., & Luebke, J. I. (2008). Synapses are lost during aging in the primate prefrontal cortex. *Neuroscience*, *152*(4), 970–981. https://doi.org/10.1016/j.neuroscience.2007.07.014

Petrova, O. E., Garcia-Alcalde, F., Zampaloni, C., & Sauer, K. (2017). Comparative evaluation of rRNA depletion procedures for the improved analysis of bacterial biofilm and mixed pathogen culture transcriptomes. *Scientific Reports*, *7*. https://doi.org/10.1038/srep41114

Poggio, T., & Koch, C. (1987). Synapses that compute motion. *Scientific American*, *256*(5), 46–52. https://doi.org/10.1038/scientificamerican0587-46

Purves, D. (2004). Neuroscience Third Edition. In *Vascular* (Vol. 3). https://doi.org/978-0878937257

Reis-Rodrigues, P., Czerwieniec, G., Peters, T. W., Evani, U. S., Alavez, S., Gaman, E. A., … Hughes, R. E. (2012). Proteomic analysis of age-dependent changes in protein solubility identifies genes that modulate lifespan. *Aging Cell*, *11*(1), 120–127. https://doi.org/10.1111/j.1474-9726.2011.00765.x

Rice, D., & Barone, S. (2000). Critical periods of vulnerability for the developing nervous system: Evidence from humans and animal models. *Environmental Health Perspectives*, *108*(Suppl. 3), 511–533.

Ritchie, M. E., Phipson, B., Wu, D., Hu, Y., Law, C. W., Shi, W., & Smyth, G. K. (2015). Limma powers differential expression analyses for RNA-sequencing and microarray studies. *Nucleic Acids Research*, *43*(7). https://doi.org/10.1093/nar/gkv007

Rueden, C. T., Schindelin, J., Hiner, M. C., DeZonia, B. E., Walter, A. E., Arena, E. T., & Eliceiri, K. W. (2017). ImageJ2: ImageJ for the next generation of scientific image data. *BMC Bioinformatics*, *18*(1), 529. https://doi.org/10.1186/s12859-017-1934-z

Rybak-Wolf, A., Stottmeister, C., Glažar, P., Jens, M., Pino, N., Hanan, M., … Rajewsky, N. (2014). Circular RNAs in the Mammalian Brain Are Highly Abundant, Conserved, and Dynamically Expressed. *Molecular Cell*, *58*(5), 870–885. https://doi.org/10.1016/j.molcel.2015.03.027

Sacramento, E. K., Kirkpatrick, J. M., Mazzetto, M., Sanzo, S. Di, Caterino, C., Sanguanini, M., … Ori, A. (2019). Reduced proteasome activity in the aging brain results in ribosome stoichiometry loss and aggregation. *BioRxiv*. https://doi.org/10.1101/577478

Sandberg, R. (2014). Entering the era of single-cell transcriptomics in biology and medicine. *Nature Methods*, *11*(1), 22–24. https://doi.org/10.1038/nmeth.2764

Schratt, G. (2009). MicroRNAs at the synapse. *Nature Reviews Neuroscience*, Vol. 10, pp. 842–849. https://doi.org/10.1038/nrn2763

Schrimpf, S. P., Meskenaite, V., Brunner, E., Rutishauser, D., Walther, P., Eng, J., … Sonderegger, P. (2005). Proteomic analysis of synaptosomes using isotope-coded affinity tags and mass spectrometry. *Proteomics*, *5*(10), 2531–2541. https://doi.org/10.1002/pmic.200401198

Shen, D., Coleman, J., Chan, E., Nicholson, T. P., Dai, L., Sheppard, P. W., & Patton, W. F. (2011). Novel Cell- and Tissue-Based Assays for Detecting Misfolded and Aggregated Protein Accumulation Within Aggresomes and Inclusion Bodies. *Cell Biochemistry and Biophysics*, *60*(3), 173–185. https://doi.org/10.1007/s12013-010-9138-4

Shepherd, G. M. (2004). The Synaptic Organization of the Brain. In *The Synaptic Organization of the Brain*. https://doi.org/10.1093/acprof:oso/9780195159561.001.1

Smyth, G. K. (2005). limma: Linear Models for Microarray Data. In *Bioinformatics and Computational Biology Solutions Using R and Bioconductor* (pp. 397–420). https://doi.org/10.1007/0-387-29362-0_23

Stahley, S. N., Bartle, E. I., Atkinson, C. E., Kowalczyk, A. P., & Mattheyses, A. L. (2016). Molecular organization of the desmosome as revealed by direct stochastic optical reconstruction microscopy. *Journal of Cell Science*, *129*(15), 2897–2904. https://doi.org/10.1242/jcs.185785

Stefani, M., & Dobson, C. M. (2003). Protein aggregation and aggregate toxicity: New insights into protein folding, misfolding diseases and biological evolution. *Journal of Molecular Medicine*, Vol. 81, pp. 678–699. https://doi.org/10.1007/s00109-003-0464-5

Steward, O., & Falk, P. M. (1985). Polyribosomes under developing spine synapses: Growth specializations of dendrites at sites of synaptogenesis. *Journal of Neuroscience*, *13*(1–2), 75–88. https://doi.org/10.1002/jnr.490130106

Steward, Oswald, & Schuman, E. M. (2003). Compartmentalized synthesis and degradation of proteins in neurons. *Neuron*, *40*(2), 347–359.

Strimmer, K. (2008). fdrtool: A versatile R package for estimating local and tail area-based false discovery rates. *Bioinformatics*, *24*(12), 1461–1462. https://doi.org/10.1093/bioinformatics/btn209

Sutton, M. A., & Schuman, E. M. (2006). Dendritic Protein Synthesis, Synaptic Plasticity, and Memory. *Cell*, Vol. 127, pp. 49–58. https://doi.org/10.1016/j.cell.2006.09.014

Takai, D., Inoue, K., Shisa, H., Kagawa, Y., & Hayashi, J. I. (1995). Age-associated changes of mitochondrial translation and respiratory function in mouse brain. *Biochemical and Biophysical Research Communications*, *217*(2), 668–674. https://doi.org/10.1006/bbrc.1995.2826

Tang, J., Maximov, A., Shin, O. H., Dai, H., Rizo, J., & Südhof, T. C. (2006). A Complexin/Synaptotagmin 1 Switch Controls Fast Synaptic Vesicle Exocytosis. *Cell*, *126*(6), 1175–1187. https://doi.org/10.1016/j.cell.2006.08.030

Taylor, A. M., Wu, J., Tai, H. C., & Schuman, E. M. (2013). Axonal translation of β-catenin regulates synaptic vesicle dynamics. *Journal of Neuroscience*, *33*(13), 5584–5589. https://doi.org/10.1523/JNEUROSCI.2944-12.2013

Thomas, P. J., Qu, B. H., & Pedersen, P. L. (1995). Defective protein folding as a basis of human disease. *Trends in Biochemical Sciences*, Vol. 20, pp. 456–459. https://doi.org/10.1016/S0968-0004(00)89100-8

Thomson, A. M. (2000). Facilitation, augmentation and potentiation at central synapses. *Trends in Neurosciences*, Vol. 23, pp. 305–312. https://doi.org/10.1016/S0166-2236(00)01580-0

Toyama, B. H., Savas, J. N., Park, S. K., Harris, M. S., Ingolia, N. T., Yates, J. R., & Hetzer, M. W. (2013). Identification of long-lived proteins reveals exceptional stability of essential cellular structures. *Cell*, *154*(5), 971–982. https://doi.org/10.1016/j.cell.2013.07.037

Tsumoto, T., & Suda, K. (1979). Cross-depression: an electrophysiological manifestation of binocular competition in the developing visual cortex. *Brain Research*, *168*(1), 190–194. https://doi.org/10.1016/0006-8993(79)90138-0

Vanderklish, P. W., & Edelman, G. M. (2005). Differential translation and fragile X syndrome. *Genes, Brain and Behavior*, Vol. 4, pp. 360–384. https://doi.org/10.1111/j.1601-183X.2005.00134.x

Venable, J. D., Dong, M. Q., Wohlschlegel, J., Dillin, A., & Yates, J. R. (2004). Automated approach for quantitative analysis of complex peptide mixtures from tandem mass spectra. *Nature Methods*, *1*(1), 39–45. https://doi.org/10.1038/nmeth705

Vendruscolo, M. (2012). Proteome folding and aggregation. *Current Opinion in Structural Biology*, Vol. 22, pp. 138–143. https://doi.org/10.1016/j.sbi.2012.01.005

Vukoja, A., Rey, U., Petzoldt, A. G., Ott, C., Vollweiter, D., Quentin, C., … Haucke, V. (2018). Presynaptic Biogenesis Requires Axonal Transport of Lysosome-Related Vesicles. *Neuron*, *99*(6), 1216–1232. https://doi.org/10.1016/j.neuron.2018.08.004

Walther, D. M., Kasturi, P., Zheng, M., Pinkert, S., Vecchi, G., Ciryam, P., … Hartl, F. U. (2015). Widespread proteome remodeling and aggregation in aging C. elegans. *Cell*, *161*(4), 919–932. https://doi.org/10.1016/j.cell.2015.03.032

Ward, M., McEwan, C., Mills, J. D., & Janitz, M. (2015). Conservation and tissue-specific transcription patterns of long noncoding RNAs. *Journal of Human Transcriptome*, *1*(1), 2–9. https://doi.org/10.3109/23324015.2015.1077591

Wei, Y. N., Hu, H. Y., Xie, G. C., Fu, N., Ning, Z. Bin, Zeng, R., & Khaitovich, P. (2015). Transcript and protein expression decoupling reveals RNA binding proteins and miRNAs as potential modulators of human aging. *Genome Biology*, *16*(1). https://doi.org/10.1186/s13059-015-0608-2

Whittaker, V. P., Michaelson, I. A., & Kirkland, R. J. (1964). The separation of synaptic vesicles from nerve-ending particles ('synaptosomes'). *The Biochemical Journal*, *90*(2), 293–303.

Williams, C., Shai, R. M., Wu, Y., Hsu, Y. H., Sitzer, T., Spann, B., … Miller, C. A. (2009). Transcriptome analysis of synaptoneurosomes identifies neuroplasticity genes overexpressed in incipient Alzheimer's disease. *PLoS ONE*, *4*(3). https://doi.org/10.1371/journal.pone.0004936

Winden, K. D., Oldham, M. C., Mirnics, K., Ebert, P. J., Swan, C. H., Levitt, P., … Geschwind, D. H. (2009). The organization of the transcriptional network in specific neuronal classes. *Molecular Systems Biology*, *5*. https://doi.org/10.1038/msb.2009.46

Wu, W. W., Wang, G., Baek, S. J., & Shen, R. F. (2006). Comparative study of three proteomic quantitative methods, DIGE, cICAT, and iTRAQ, using 2D gel- or LC-MALDI TOF/TOF. *Journal of Proteome Research*, *5*(3), 651–658. https://doi.org/10.1021/pr050405o

You, X., Vlatkovic, I., Babic, A., Will, T., Epstein, I., Tushev, G., … Chen, W. (2015). Neural circular RNAs are derived from synaptic genes and regulated by development and plasticity. *Nature Neuroscience*, *18*(4), 603–610. https://doi.org/10.1038/nn.3975

Zappulo, A., Van Den Bruck, D., Ciolli Mattioli, C., Franke, V., Imami, K., McShane, E., … Chekulaeva, M. (2017). RNA localization is a key determinant of neurite-enriched proteome. *Nature Communications*, *8*(1). https://doi.org/10.1038/s41467-017-00690-6

Zhao, W., He, X., Hoadley, K. A., Parker, J. S., Hayes, D. N., & Perou, C. M. (2014). Comparison of RNA-Seq by poly (A) capture, ribosomal RNA depletion, and DNA microarray for expression profiling. *BMC Genomics*, *15*(1). https://doi.org/10.1186/1471-2164-15-419

Zoidl, G., & Dermietzel, R. (2002). On the search for the electrical synapse: A glimpse at the future. *Cell and Tissue Research*, Vol. 310, pp. 137–142. https://doi.org/10.1007/s00441-002-0632-x